Modélisation des actionneurs piézoélectriques pour le contrôle des systèmes complexes

Abdou-Fadel Boukari

ParisTech
INSTITUT DES SCIENCES ET TECHNOLOGIES
PARIS INSTITUTE OF TECHNOLOGY

ARTS ET MÉTIERS ParisTech

2010-ENAM-0030

École doctorale n° 432 : Sciences des Métiers de l'Ingénieur

Doctorat ParisTech

T H È S E

pour obtenir le grade de docteur délivré par

l'École Nationale Supérieure d'Arts et Métiers

Spécialité " Conception "

présentée et soutenue publiquement par

Abdou-Fadel BOUKARI

le 23 Septembre 2010

Piezoelectric actuators modeling for complex systems control

Modélisation des actionneurs piézoélectriques pour le contrôle des systèmes complexes

Directeur de thèse : **Jean-Claude CARMONA**

Co-encadrement de la thèse : **George MORARU et François MALBURET**

Jury

M. Thierry POINOT, Professeur des Universités, Unité de recherche ESIP (France)	Président
M. Marc KAMLAH, P.U, Institute for Materials Research II Karlsruhe Institute of Technology (Germany)	Rapporteur
M. Laurent LEBRUN, Professeur des Universités, LGEF-Equipe Matériaux Electro-actifs et Procédés d'Elaboration, INSA de Lyon (France)	Rapporteur
M. Ali CHAABA, Maître de Conférences HDR, Département Génie Mécanique et Structure ENSAM-Meknès (Maroc)	Examinateur
M. Jean-Claude CARMONA, P.U, LSIS-INSM, Arts et Metiers ParisTech (France)	Directeur
M. George MORARU, Maître de conférences, LSIS-INSM, Arts et Metiers ParisTech (France)	Co-encadrant
M. François MALBURET, Maître de conférences, LSIS-INSM, Arts et Metiers ParisTech (France)	Co-encadrant

T H È S E

Arts et Métiers ParisTech - Centre d'Aix-en-Provence
Laboratoire des Sciences de l'Information et des Systèmes, Projet INSM

All my family
A ma chère famille

'All models are wrong. Some are useful'
George E. P. Box, Robustness in the strategy of scientific model building, 1979

'Ce qui est simple est toujours faux. Ce qui ne l'est pas est inutilisable'
Paul Valéry, Mauvaises pensées et autres, 1942

Acknowledgements

As a PhD candidate enrolled in Doctoral School 432 SMI (Engineering Sciences) of Arts et Metiers ParisTech, I performed my work in Arts et Metiers ParisTech campus Aix-en-Provence, within the research team INSM (Numerical Engineering of Mechanical Systems) of LSIS (Laboratory of Information and Systems Sciences) and in collaboration with ARTS (Association for Research and Technological Sciences).

I am thankful to Professors Marc Kamlah and Laurent Lebrun who reviewed my PhD-thesis and enable a better analysis of the work. I thank Professor Thierry Poinot and Doctor Ali Chaaba who examined the work.

I am grateful to Professors Jean-Paul Hautier and Pierre-Jean Barre respectively Head Manager of Arts et Metiers ParisTech and Aix-en-Provence Campus of Arts et Metiers ParisTach. They and their staff provided me the necessary comfort in the school.

I am also grateful to Mr Gerard Coffignal in charge of Doctoral School 432 SMI and his associates Florence Dumard and Claude Leroy, for their support despite the number of students they have to manage. They were involved in my cultural and scientific development during these three years.

I acknowledge Mr. Joachim Rams CEO of ARTS and all his associates. Especially M. Gerard Barreau and Mrs Weider Freiderick in Aix-en-Provence, Mrs Christine Vaisset and Cecile Dunand in Paris.

I am thankful to Professor Jean-Claude Carmona, principal supervisor of my thesis. Not to mention Professor Daniel Brun-Picard. I am also grateful to Doctors George Moraru and François Malburet, all co-advisers of the thesis and also good partners at work. Moreover they four provided me sustained support during these years.

I should not fail to mention Mr. Lionel Roucoule the INSM Team Leader, Mr. Philippe Veron Head of CIRD department, Mrs. Aline Cauvin, Messrs Jean-Philippe Pernot, Lionel Martin, Julien Gomand, Matthias Kleiner, Jean Vincenti, INSM team members and teachers at Arts et Metiers ParisTech, Mrs. Michelle Richard the secretary of the team.

I should also mention my colleagues and former colleagues Mrs. Minica Panchetti, Miss Anne Brindejonc , Camille Deleuze, Maud Rio and Soumia Mejd, Messrs Ruding Lou, Frederic Segond, Radouane Djeredi, Christophe Corbier, Antoine Sancelier, Gwenole Lemoel, Mikael Martin, Arnaud Tremollet, Pierre Renaud, and Nejeh Djemal, Etienne Roger and Frederic Depasse.

I also thank Cecile Pecheur, Sabine Hours and Emilie Veronne officials of Arts et Metiers ParisTech Aix-en-Provence library.

I thank Messrs. Philippe Saint-Armoux, Remy Debarnot and William Rock, Mrs. Dominique Angel all in charge of IT of the school.

I also thank all the technicians and coordinators of machining, plastic deformations, mechanics and electrotechnics laboratories of Arts et Metiers ParisTech Aix-en-Provence. They were helpful for the realization of various experimental setups.

I am grateful to Mr. Mohammed Douimi, teacher in ENSAM-Meknès for his contribution in the performed work.

I should mention all my friends at Arts et Metiers ParisTech and ENSAM-Meknès.

Especially, I am grateful to my family and our friends in Benin and Morocco. They are dedicated the best of this work.

Remerciements

Inscrit à l'Ecole Doctorale 432 SMI (Sciences des Métiers de l'Ingénieur) des Arts et Métiers ParisTech, j'ai réalisé cette thèse aux Arts et Métiers ParisTech d'Aix-en-Provence, au sein de l'Équipe INSM (Ingénierie Numérique des Systèmes Mécaniques) du LSIS (Laboratoire des Sciences de l'Information et des Systèmes), en collaboration avec ARTS (Association pour la Recherche Technologique et Scientifique).

Je commence par remercier sincèrement les Professeurs Marc Kamlah et Laurent Lebrun qui ont rapporté cette thèse. Je remercie aussi le Professeur Thierry Poinot et le Docteur Ali Chaaba qui l'ont examiné.

Je tiens à remercier Messieurs Jean-Paul Hautier et Pierre-Jean Barre, respectivement Directeur Général des Arts et Métiers ParisTech et Directeur de centre des Arts et Métiers ParisTech d'Aix-en-Provence, ainsi que tout leur personnel.

Je suis aussi reconnaissant à Monsieur Gérard Coffignal, Directeur de l'école doctorale 432 SMI et ses assistants Florence Dumard et Claude Leroy pour leur compréhension et leurs aides, malgré le nombre considérable de doctorants qu'ils ont à gérer.

Je remercie également Monsieur Joachim Rams Directeur Général de ARTS et tous ses associés en l'occurence Monsieur Gerard Barreau et Madame Freiderick Weider à Aix-en-Provence, Mesdames Christine Vaisset and Cecile Dunand à Paris.

Je suis reconnaissant à Monsieur Jean-Claude Carmona, non seulement parce qu'il a été le directeur de ma thèse, mais aussi pour son aide continue dans mes démarches administratives. Sans oublier Monsieur Daniel Brun-Picard. Je suis tout aussi reconnaissant à Messieurs George Moraru et Francois Malburet, bons encadrants de thèse et partenaires de travail.

Je ne saurais oublier Messieurs Lionel Roucoule Chef de l'équipe INSM, Philippe Veron Chef du département CIRD, Madame Aline Cauvin, Messieurs Jean-Philippe Pernot, Lionel Martin, Julien Gomand, Mathias Kleiner, Jean Vincenti et Madame Michelle Richard, membres de l'équipe.

Je pense aussi à mes actuels et anciens collègues, Madame Minica Panchetti, Mesdemoiselles Anne Brindejonc, Camille Deleuze, Maud Rio et Soumia Mejd, Messieurs Ruding Lou, Frederic Segond, Radouane Djeredi, Christophe Corbier, Antoine Sancelier, Gwenole Lemoel, Mikael Martin, Arnaud Tremollet, Pierre Renaud et Nejeh Djemal, Etienne Roger et Frédéric Depasse.

Je remercie aussi les responsables du centre de documentation: Cecile Pecheure, Sabine Hours et Emilie Veronne. Ainsi que les informaticiens Messieurs Philippe Saint-Armoux, Remy Debarnot et William Rock, Madame Dominique Angel.

Je remercie aussi tous les responsables et techniciens des laboratoires d'usinage, des déformations plastiques, de mécanique, d'électrotechnique du CER Aix-en-Provence des Arts et Métiers ParisTech. Ils m'ont été d'une aide précieuse pour la réalisation de divers montages expérimentaux.

Par ailleurs , je remercie Monsieur Mohammed Douimi enseignant à l'ENSAM-Meknès.

Je pense également à tous mes amis des Arts et Metiers ParisTech et de l'ENSAM-Meknès avec qui j'ai partagé des bons moments durant ces années.

Enfin je suis constament reconnaissant à ma famille et amis au Bénin et au Maroc pour leur soutien inconditionnel. Je leur dédie le meilleur de ce travail.

Abstract

The last discoveries and technology advances in understanding materials and in computation have contributed in the proliferation of the so-called smart materials with a wide applications scope. This thesis enrolls in the frame of piezoelectric actuators rather than pure material considerations. We aim to enhance their models' libraries in order to ease their integration in complex systems design. These models should take into account as more as possible the nonlinear effects (such as hysteresis) while remaining easy to handle. For this purpose we make a link between materials specialists and the field of engineers. We firstly analyze the constitutive equations of piezoelectricity with respect to operating conditions. This allows us to deduce a first analog model. This is then translated into bond graph. The obtained models are translated in block-diagrams. The established models in this step differ from those proposed by commercial package in such a way that they better integrate the dynamic nature of the actuator independently of the other parts of the structure. In fact we proposed two types of models. The first one only takes into account the first resonance mode while the second one takes into account two resonances. Thereafter, we suggested models taking into account nonlinearities and hysteresis. The Preisach approach was adopted for static hysteresis. Then we adapted Voigt approach in order to account for dynamic hysteresis. The two approaches were then merged in order to have a complete model.

Key words

Piezoelectricity, Magnetostriction, Lumped-parameters approach, Nonlinearities, Hysteresis, User oriented models, Complex and smart systems

Résumé

Les récentes découvertes et avancées technologiques dans la compréhension des matériaux ainsi que l'essor des outils informatiques d'aide au calcul ont contribué à la prolifération de matériaux intelligents avec un champ d'applications très large. Cette thèse s'inscrit dans le contexte d'utilisation des actionneurs piézoélectriques plutôt qu'une vision purement matériau. Le but est d'enrichir les bibliothèques de modèles de ces types d'actionneurs afin de faciliter leur prise en compte dans les phases de conception des systèmes complexes les intégrant. Le cahier des charges est que ces modèles incluent le plus possible les non-linéarités tout en restant aisés d'utilisation. Pour atteindre ces objectifs, nous proposons de faire un pont entre le domaine des experts des matériaux et celui de l'ingénieur en suivant une méthodologie claire. Dans un premier temps nous passons en revue les approches existantes dans la littérature ainsi que les solutions offertes par certains logiciels commerciaux. Une analyse des équations constitutives de la piézoélectricité associées aux conditions de fonctionnement de l'actionneur nous permet d'en déduire un premier modèle analogique. Ce dernier est ensuite traduit en bond graph pour en déduire des modèles blocs-diagramme. En plus de cet effort de formalisation, ces premiers modèles se distinguent de ceux proposés par les logiciels commerciaux en prenant mieux en compte la dynamique propre à l'actionneur. Nous proposons deux types de modèles. L'un rend uniquement compte du premier mode de résonance alors que le second rend compte de deux modes de résonance. Ensuite nous

proposons des modèles prenant en compte les non-linéarités : l'approche de Preisach pour la modélisation de l'hystérésis statique et l'approche de Voigt dans le cas dynamique. Ces deux approches sont ensuite fusionnées dans le but d'avoir un modèle plus complet.

Mots clés

Piézoélectricité, Magnétostriction, Approche des paramètres concentrés, Non-linéarités, Hystérésis, Modèles utilisateur, Systèmes complexes et intelligents

Contents

List of Figures

List of Tables

Glossary

LSIS: Laboratoire des Sciences de l'Information et des Systèmes
INSM: Ingénierie Numérique des Systèmes Mécaniques (projet du LSIS)

Principal notations

Symbols	Signification	Units
S	Strain	
T	Constraint	$N.\mu m^{-2}$
D	Electric induction	$C.\mu m^{-2}$
E	Electric field	$V.\mu m^{-1}$
u	Displacement of the piezoelectric moving face	μm
F	Applied force	N
q	Electric charge on the piezoelectric electrode	μC
Q	Material's quality factor	
V	Piezoelectric driving voltage	V
I	Electric current	A
H	Magnetic field	$A.m^{-1}$
B	Magnetic induction	$Tesla$
s	Flexibility constant	$\mu m^2.N^{-1}$
d	Piezoelectric coefficient	$\mu m.V^{-1}$
ε	Permittivity coefficient	$\mu C.V^{-1}.\mu m^{-1}$
k	Electromechanical coupling coefficient	
σ	Device section surface	m^2
ρ	Mass density	$kg.m^{-3}$
M	Device total mass	kg
m	Device moving mass	kg
L	Device length	m
Z	Generalized impedance	Ω
K, K_m, K_m^D	Device's stiffness	$N.\mu m^{-1}$
C, C_e, C_e^S	Device's capacitance	μF
R	Generalized resistance	Ω
W	Energy density	$J.m^{-3}$
P	Power density	$watt.m^{-3}$

f	Excitation or signal frequency	Hz
ω	Pulsation	$rad.s^{-1}$
v_{33}^{D}	Wave propagation speed at constant D	$m.s^{-1}$
α_{33}	Wave number	m^{-1}

Chapter 1

General Introduction

1.1 Introduction

1.1.1 Materials play role in development

Most periods of technological development have been linked to changes in the use of materials: the stone, bronze and iron ages. Some are available commercially but most of them can only be found in research laboratories [7]. The last discoveries and technology advances in materials science and in computation have contributed in the proliferation of so-called smart or intelligent, active, adaptive, or functional materials [16]. Smart materials can significantly change their mechanical properties (such as shape, stiffness and viscosity), their thermal, optical or electromagnetic properties, in a predicable or controllable manner in response to their environment [8]. However, in this thesis we especially deal with electro-active materials (piezoelectric and magnetostrictive).

The emergence of such materials made it possible to reconsider actuation and sensing functions thanks to their interesting principle of electromechanical energy conversion. Devices made of these materials are useful in many advanced and complex mechanical structures design and their machining process. Their application scope includes all fields [17]. This requires the participation of scientists and engineers from diverse fields, mechanical, electrical, control, computing, etc.

1.1.2 Context

1.1.2.1 Problem specific to drilling

Assembling is a process that may require drilling thousands of holes. This is the case in aeronautics at the assembly of the fuselage and the wings and others parts. The holes are specified as to be of diameter ϕ much smaller than the depth h: $\frac{\phi}{h} < 0.2$. The main difficulty with such a process is about shattering and evacuating the chips. There are many risks with this. Some are illustrated in Figure 1.1. The drilling tool could be stuck or broken in the hole.

The first and classical solution consists of stripping cycles. Its main drawback concerns time consuming and poor finish.

Therefore, smart solutions were proposed. The typical one consists of *gun drill* (Figure 1.2). Gun drill cutting edges form thin, curled chips that are carried away from the bore by

Figure 1.1: Problems with deep drilling [EADS corporation]

high pressure lubricant. The off-center design of the cutting edges creates pressure within the bore that is carried by pads behind the drill tip. The coolant that flushes the chips also lubricates these pads, which burnish the surface and develop the fine finish for which deep hole gun drilling is known [1, 2].

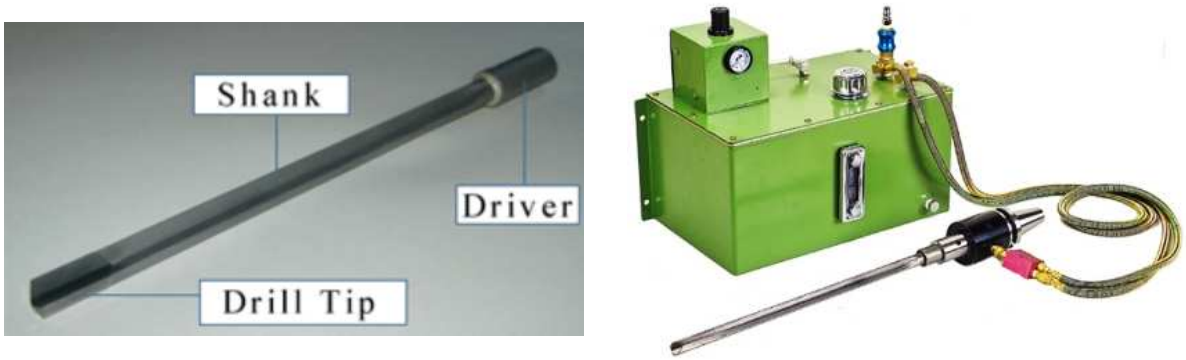

Figure 1.2: Gun drill bit [1, 2]

Although gun drills eliminate stripping phases and allow to obtain excellent surface, they set low manufacturing rates because of their unique edge. Moreover, they require a high pressure source and still exhibit chip digging problems despite this pressure. Moreover, in some case such as embedded systems, it is not possible to instal the pressure source.

Therefore, researchers and manufacturers introduced vibration drilling. Micro-vibrations are generated and transmitted either to the workpiece either to the drill bit. One of the first techniques in vibration drilling is based on self-maintained systems as shown in Figure 1.3. This technic takes benefits from a cutting process instability by introduction of controlled low stiffness suspension in the tool-holder [3].

Inherent changes in real cutting forces (depending on the tool wear for example) can be dramatic and eventually stop the resonance. Therefore, once the user changes the cutting parameters, the excitation system has to be reconsider.

The drawbacks of this technique are therefore its lack of robustness and its non-adaptability. Hence an alternative could consist of replacing the self-exciting system by an electro-active actuator. This offers a controllable solution since the generated vibrations are electrically driven.

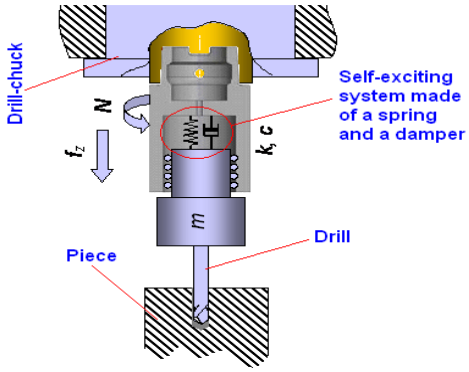

Figure 1.3: Self-exciting vibration drilling operation [3, 4]

1.1.2.2 Machining in general

Cutting process in general is very sensitive to changes in parameters and imbalances. These are the origin of chatter, the most undesirable phenomenon in cutting process. Chatter effects include undesirable noise, poor surface finish of the sample, reduced dimensional accuracy and reduced machine tool life [18]. Several techniques are known for enhancing dynamic stiffness and stability for chatter-resistance. In [19] (Minimizing vibration tendencies in machining), the four widely used and most universal approaches are enumerated: the use of anisotropic bars with specifically assigned orientations of the stiffness axes, the use of Young's modulus and/or high damping materials, the use of passive dynamic vibration absorbers (DVA) and the use of **active vibration control means**. The last technique requires vibration sensors and actuators generating forces that oppose the deflections of the tool during the vibratory process.

For this purpose, conceptual studies performed at INSM (see Glossary) validated that the best solutions are offered by intelligent materials such as piezoelectric and magnetostrictive. Other studies also revealed the interest of rheological damping substances.

1.1.3 An enthusiasm but lots of obstacles

The interesting properties of smart materials are recognized in all fields. During these last years, the techniques evolve from the step of laboratories concepts and experiences to industrial applications. Everyone is enthusiastic but lots of obstacles do not ease their usage.

As a matter of fact, the complex phenomena taking place into these materials are under investigation for years. However, the existing literature shows that researchers mostly care about meticulous description of the phenomena in atomistic or nano scales. One can refer to [20, 21, 22].

The diffusion of the science-based knowledge for technological realizations was largely ignored up to recently. There is a gap between materials specialists and engineers who are supposed to be the final users of devices made of such materials (Figure 1.4).

However users need at their disposal simple tools to handle these devices and integrate them into systems. The availability of models could be of great aid in design. Indeed, they allow dimensioning, simulation of interaction between the device and the others parts of the system, not to say optimization of the system [23].

Figure 1.4: Gap to be filled between materials scientists and engineers

For example, in the case of vibration drilling, the availability of efficient models would allow simulation in order to check the actuator choice, to ensure its capability to generate the vibration with good accuracy upon taking into account the whole machining process. In addition, some possible resonances could be easily avoided.

Moreover, these models help for knowledge capitalization. However they should be appropriate to the context and established in accessible formalisms for the user.

As a matter of fact, models construction implies many choices: the approach, the tools and details level. Especially in the case of smart materials, multi-physics tools are required.

1.1.4 User oriented modeling

The lack of models concerns many scientists and industrialists. In this vein, piezoelectric and magnetostrictive materials models are more than more included in engineering software.

1.1.4.1 Finite Elements Analysis (FEA) codes

For a realistic and detailed study of physical systems involving partial differential equations, a numerical method must be used to solve the problem [24]. Finite-element methods are often found to be the most appropriate.

As recalled in [25], the pioneers of FEA application to piezoelectric materials and structures are Lloyd and RedWood [26], Holland [27], Tiersten [28], Eerniess [29], Allik and Hugues [30]. Since then many improvements have be yielded.

Nowadays, many commercial FEA packages include piezoelectric coupling. Many codes have been implemented in ANSYS [31]. One can also refer to the work of Kamlah and al. In [32] they implemented in a public domain non-linear multipurpose finite element code PSU (For more information see the web page http://www.isd.uni-stuttgart.de /arbeitsgruppen/psu-www/index.html) of the constitutive law.

The effectiveness of FEA approach is well accepted. However, FEA models are positioned at a high level of details in design process. In order to illustrate our statement, let us consider the V cycle generally used in mechatronic design (Figure 1.5).

By contrast, we are concerned with the upper part of the design cycle. This part is difficult because at this level, decisions are made in an environment where few elements are defined. Therein, high level details are not useful.

Moreover, FEA models require high computation effort and they are not usable for real time control design. One single simulation could take hours to be computed.

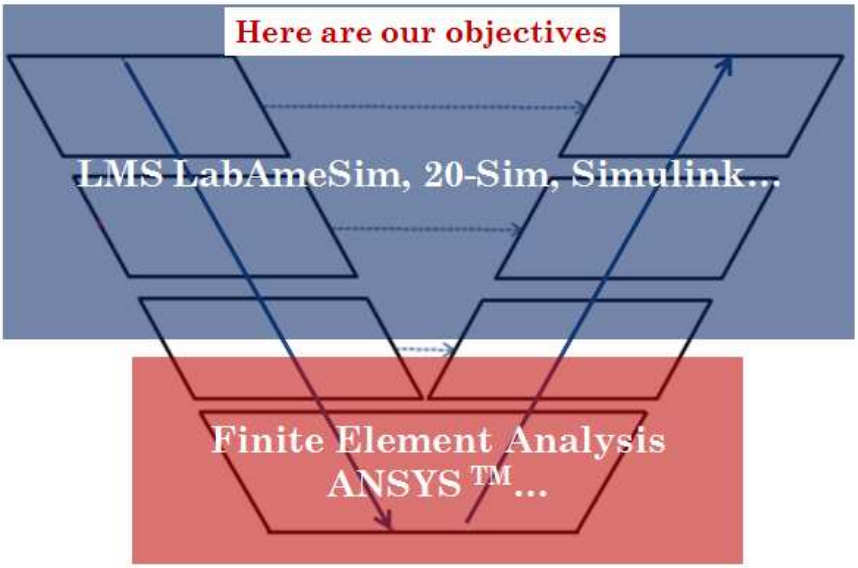

Figure 1.5: Position of software with respect to required details level

These are the reasons for not using FEA approaches, when only low level of details are necessary.

1.1.4.2 Lumped-parameters approach

Lumped-parameters modeling consists in developing electrical and mechanical components that are analogous to the concerned system under certain conditions.

More generally, a lumped-parameters approach consists of assumptions and approximations which minimize computation efforts while achieving good accuracy as long as the assumptions made are satisfied. This makes it possible to simulate the response of the system, quantify the influence of design parameters and make tradeoffs between them.

Many lumped-parameters system models exist that have provided satisfaction. For example the reader can refer to [33, 34, 35] where lumped-parameters approaches were applied to fluids systems.

Thereafter, these approaches have been extended to piezoelectric systems [36, 37]. One can also refer to other works [38, 39, 40, 41, 42].

All those efforts are formalized in user friendly way. Thus, one finds commercial packages such as 20-Sim [6] and LabAmesim [5] including piezoelectric modulus for mechatronic design.

In our case, we adopt this philosophy while bringing some improvements in comparison with existing models.

1.1.4.3 LMS Imagine.Lab AMESim suite

LMS Imagine.Lab AMESim offers a complete 1D simulation suite to model and analyze multi-domain, intelligent systems and predict their multi-disciplinary performance [5].

To create a system simulation model, all the user has to do, it is to use the various dedicated tools to access the required pre-defined components from validated libraries covering

different physical domains. LMS Imagine.Lab AMESim can work with a variety of libraries in order to create a physics-based system model [5].

One finds in the electromechanical library of Lab AMESim, models of piezoelectric actuator (Figure 1.6): EMPA01, EMPA02, EMPA03, EMPA01A, EMPA02A, EMPA03A, EMPA11, EMPA12, EMPA13 etc. They differ from each other only in the variables associated with each port. Some of the models use input displacements whereas the others use input velocities. Input displacements make the model more robust for stabilizing runs.

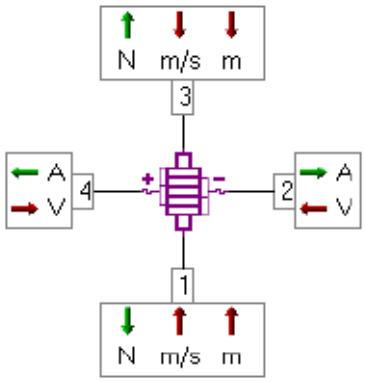

Figure 1.6: Lab AMESim integrated linear piezo actuator [5]

However, the integrated models are based on linear description accepted by IEEE Standard on piezoelectricity [43]. This is in contrast with nonlinear and complex phenomena observed in electro-active materials. In addition to be linear, the proposed models are static. LMS Lab AMESim suggests to include in the load, the effective inertia of the device, considered as to be ms/3, where ms is the mass of the device (Figure 1.7). However, in such a way the openness of the model is lost.

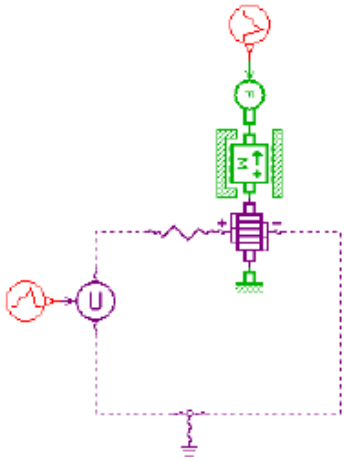

Figure 1.7: Lab AMESim: solution for including dynamic aspects [5]

1.1.4.4 Controllab 20-Sim suite

20-sim fully supports graphical modeling, allowing to design and analyze dynamic systems in a intuitive and user friendly way, without compromising power. 20-sim supports the use

of components. This allows the user to enter models as in an engineering sketch: by choosing components from the library and connecting them [6].

The modeling principle is the similar to Lab AMESim. However, 20-Sim allows to easily modify the constitutive equations of the elements.

In 20-Sim there are piezoelectric elements such as *CMABender* and *CMAStretcher* located in the folds *Library/ Iconic Diagrams/ Electric/ Actuators* and *Library/ Iconic Diagrams/ Mechanical/ Translation/ Actuators*: Figure 1.8.

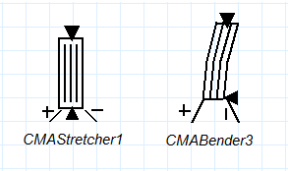


```
parameters
    real C = 1.7e-6 {electrical capacitance,F};     // capacitance
    real KF = 1.75 {N/V};     // voltage to force conversion factor
    real m = 0.2e-3 {mass,kg};   // equivalent mass
    real k = 1.3e7 {stiffness,N/m};     // stiffness
    real B = 0.07 {magnitude,none};  // relative damping ratio
    real KB = 0.076 {V/N};   // force to voltage conversion factor
variables
    real v {m/s}; // velocity difference between both translation ports
    real x {m};         // deflection
equations
    p1.i = C * ddt(p1.u) - KB*C*k*v;
    // mass: works on p3 only
    p3.v = (1/m)*int(p2.F - p3.F);
    // spring-damper-force: between p2 and p3
    v = p2.v - p3.v;
    x = int(v,0);
    p2.F = k*x + 2*B*sqrt(k*m)*v + KF*p1.u;
```

Figure 1.8: 20-Sim piezo elements and modifiable equations [6]

The integrated models in 20-Sim are also based on only linear descriptions.

1.2 Thesis contribution

After the analysis of smart materials domain, we came up with the necessity to continue the task of formalizing models until the field maturity. Nevertheless, the need for user oriented models should not omit efficiency and scientific rigor.

All these motivate our work. Our objective is to take part in the improvement process of electro-active devices' models libraries. These models must include as well as possible the materials nonlinearities while remaining understandable on the final user point of view.

To achieve our goal we make a link between the developments of materials specialists and engineering field [44]. We follow a traditional and clear methodology (Figure 1.9).

Prior to all, we retranslate the existing models in our language, using bond graph and block diagram formalisms. This task in compulsory since its outcome should be the basis for our developments.

Moreover, we should emphasize on the fact that the performed work should not be limited to formalization. It is only the final outcome. As one could remark in this report, great care has been taken for nonlinearities modeling.

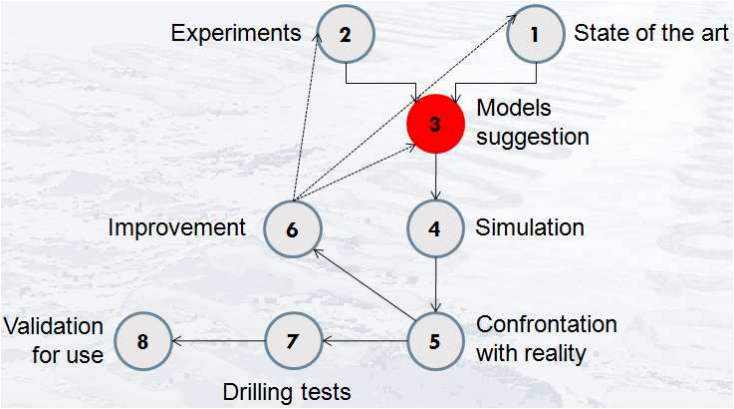

Figure 1.9: Classical Methodology and method adopted

Following are the contents of this report.

Chapter 2 gives a short review of smart materials and devices. Its purpose is to facilitate the reading to non-experts. Many definitions and examples of applications are given. Then a comparison between technologies is given.

Chapter 3 recalls the basis of piezoelectric devices. Then, techniques and experiments for piezo-bars characterization are presented. Thereafter we go for static formalization.

In chapter 4 we deal essentially with modeling and use of piezo-bar devices in dynamics. We adopt lumped-parameter approach. This allows us to depict the first vibration mode. Thereafter, we suggest a distributed parameters model in order to depict the second mode. The results are compared to existing approaches and experimental measurements are performed to validate the models.

Then chapter 5 presents the main contribution of this thesis in comparison to existing commercial packages. Piezoelectric nonlinearities are analyzed and taken into account. We firstly distinguish static and dynamic operating cases. Preisach and Voigt approach are used. Then we combine them to obtain a complete model.

In chapter 6 we show the outcome of our proposal models. For this purpose, examples of our challenging applications are given. We show how the proposal models could be integrated into mechatronic systems. Then an extension is made for magnetostrictive bar devices.

Finally we summarize the achieved work and propose perspectives.

This report is both in English and French. 25% of the content is translated in French at the beginning of each chapter.

1.3 Introduction en langue française

1.3.1 Le rôle des matériaux dans le développement

Tout développement technologique ou presque est associé à l'avènement de nouveaux matériaux: l'âge de la pierre, du bronze, du fer etc. On trouve souvent ces derniers sur le marché alors que d'autres sont encore au stade de recherche en laboratoire [7]. Récemment, les découvertes et avancées technologiques dans l'appréhension des matériaux ainsi que l'essor des outils informatiques d'aide au calcul ont contribué à la prolifération de matériaux qualifiés d'intelligents, d'actifs, d'adaptatifs, de fonctionnels, etc [16]. Ils peuvent se définir comme des matériaux capables de modifier leurs propriétés intrinsèques ou extrinsèques (mécaniques, thermiques, optiques ou électromagnétiques) d'une manière plus ou moins contrôlable en réponse aux variations de leurs environnements [8]. Le champ d'application de ces matériaux est assez large voire total [17]. Cela implique scientifiques et ingénieurs de divers domaines: mécanique, électrique, automatique, informatique etc. Toutefois, dans le cadre de notre thèse nous nous limiterons aux matériaux électrostrictifs (piézoélectriques et magnétostrictifs).

L'avènement des matériaux électrostrictifs a permis de repenser les fonctions d'actuation et mesure grâce à leur intéressant principe de conversion électromécanique de l'énergie. Les composants faits à base de ces matières sont prisés dans la conception des structures complexes et avancées ainsi que dans les processus de fabrication. Cela nécessite le concours des scientifiques et ingénieurs de divers horizons.

1.3.2 Contexte

L'assemblage est un processus qui peut nécessiter le perçage de milliers de trous. C'est le cas dans l'aéronautique lors de la jonction du fuselage aux autres parties de l'avion. Ces trous sont de diamètres ϕ beaucoup plus faibles que la profondeur h: $\frac{\phi}{h} \ll 1$. La principale difficulté d'un tel processus est la fragmentation et l'évacuation des copeaux. Les risques liés à cela sont illustrés en Figure 1.1. L'outil peut se retrouver coincé ou cassé dans le trou.

Les premières solutions consistaient en des cycles de débourrages avec comme principal inconvénient un manque à gagner en temps et en état de surface.

D'autres solutions ont été alors proposées . En l'occurence, la technique de perçage au foret 3/4 (Figure 1.2). L'outil est conçu de telle façon à ce que les copeaux soient évacuées à l'aide d'un système de pression. Ceci élimine les cycles de débourrage et améliore l'état de surface [1, 2].

L'inconvénient majeur de cette approche est la nécessité d'un système de pression. Une autre alternative a été d'injecter des micro-vibrations soit à l'outil, soit à la pièce. Celles-ci aident alors à l'obtention de copeaux fins. Les premiers systèmes du genre étaient purement mécaniques. Leur inconvénient est que lorsqu'on change sensiblement les conditions de coupes, il faut changer le système de vibration.

Dans cette situation, les matériaux électro-actifs sont les meilleurs candidats en ce sens qu'ils sont plus flexibles et contrôlables.

Par ailleurs, de façon générale, le processus d'usinage est très sensible aux changements des paramètres de coupe et aux déséquilibres à l'origine de broutements. Ces derniers sont les plus problématiques dans le processus de coupe. Leurs effets indésirables incluent notamment le bruit, le mauvais état de surface, la médiocre précision et ils réduisent aussi la durée de vie des outils [18]. Plusieurs techniques dont quatre citées dans [19] (Minimizing

vibration tendencies in machining), sont utilisées pour améliorer la rigidité dynamique et la stabilité du processus: utilisation de barres anisotropes à axes spécifiques de rigidité, agissement sur du module d'Young ou utilisation des matériaux à fort amortissement, utilisation d'amortisseurs dynamiques mais passifs de vibrations et utilisation des moyens de contrôle actif des vibrations.

Cette dernière requiert des capteurs et des générateurs de vibrations en contre sens du bruit. Certains utilisent alors des matériaux piézoélectriques, magnétostrictifs ou des fluides rhéologiques. Ils ont fait leur preuve.

1.3.3 Un enthousiasme, mais plein d'obstacles

L'intérêt des matériaux intelligents est reconnu par tous. On passe progressivement des études de concept en laboratoires aux implémentations industrielles. L'on est enthousiaste mais confronté à certains obstacles ne facilitant pas l'utilisation de ces matériaux.

En effet, les phénomènes complexes dont ces matériaux sont généralement le siège, font l'objet de plusieurs études ces trois dernières décennies. Cependant, l'état de l'art nous montre que le plus important effort est plutôt fourni dans la description minutieuse de ces phénomènes à l'échelle atomique ou nanométrique. La question de transfert des connaissances scientifiques pour des réalisations technologiques n'est pas suffisamment posée. Ce qui explique le fossé entre les spécialistes des matériaux et les ingénieurs utilisateurs de composants faits de ces matériaux (figure 1.4).

Il est pourtant d'une grande importance que l'utilisateur dispose de moyens simples pour manipuler ces actionneurs et les intégrer dans des systèmes. Dans ce contexte la disposition de modèles peut constituer un véritable outil d'aide à la conception en permettant par exemple de simuler son fonctionnement en interaction avec les autres éléments du système, d'optimiser le système [23]. Mieux, ces modèles participent aussi à la capitalisation des connaissances. Mais faudra-t-il que ces modèles collent au contexte et sous les formes les plus accessibles à l'utilisateur.

1.3.4 Modélisation orienté utilisateur

Dans ce contexte, certains logiciels proposent des modèles d'actionneurs piézoélectriques.

Parmi eux les logiciels d'Analyse par Eléments Finis. Même si ces outils sont très utiles dans le dimensionnement de système, ils interviennent plutôt à un niveau plus avancé de la conception. La Figure 1.5 illustre très bien nos propos. En plus ces outils ne peuvent pas être utilisés pour l'élaboration des boucles de contrôle ou de commande temps réel.

Dans notre cas, nous nous situons sur la partie haute du cycle. Dans ce sens, d'autres éditeurs de logiciels de simulation tels que 20-Sim [6] et LabAmesim [5] par exemple intégrent des modules d'actionneurs piézoélectriques aux bibliothèques de modèles. Pour 20-Sim nous trouvons les composants *CMABender* et *CMAStretcher* répertoriés dans les dossiers *Library/ Iconic Diagrams/ Electric/ Actuators*, *Library/ Iconic Diagrams/ Mechanical/ Translation/ Actuators*. Dans le cas de LabAmesim nous trouvons des composants dans le module *Mechatronic*.

Cependant ces modèles sont basiques et limités aux lois de comportements linéaires voire statiques (LabAmesim) admises par le standard IEEE sur la piézoélectricité [43]. Or, les matériaux électro-actifs sont le siège de phénomènes non-linéaires complexes.

1.3.5 Contribution de la thèse

Les efforts de formalisation doivent se poursuivre jusqu'à maturité du domaine. Toutefois le besoin de modèles simples d'utilisation ne devrait pas omettre la nécessité d'efficacité et de rigueur scientifique.

Cette thèse s'inscrit dans cette optique. Nous visons à alimenter ces bibliothèques de modèles de composants électro-actifs. Ces modèles doivent inclure le plus possible les non-linéarités de ces matériaux mais aussi ils doivent être faciles de compréhension par l'ingénieur. Pour atteindre ces objectifs nous proposons de faire un pont entre le domaine des experts des matériaux et celui de l'ingénieur [44] en suivant une méthodologie classique mais claire (Figure 1.9).

Toutefois la tâche de formalisation ne représente qu'une partie du travail réalisé dans cette thèse. Comme le montre le contenu de ce rapport, la majeure partie porte sur la modélisation. Car, si les phénomènes complexes sont maîtrisés par les experts en matériaux, leur modélisation reste d'actualité. Il n'existe pas aujourd'hui pour ces actionneurs, un modèle complet faisant l'unanimité des communautés scientifiques. Nous apportons des améliorations, surtout en ce qui concerne la modélisation de l'hystérésis.

Dans le chapitre 2 nous proposons un aperçu du monde des matériaux et composants intelligents. Tout d'abord, cela permettra aux non-spécialistes de se familiariser au vocabulaire du domaine. Plusieurs exemples d'applications sont aussi présentés. Ensuite ce chapitre permet de montrer les challenges relatifs à l'utilisation des actionneurs intelligents.

Dans le chapitre 3 nous rappelons les équations basiques de la piézoélectricité ainsi que les techniques usuelles pour la caractérisation de ces matériaux.

Dans le chapitre 4 nous traitons essentiellement des aspects dynamiques. Nous adoptons les méthodes de masse concentrée et de distribution des paramètres. Les résultats obtenus sont comparés aux mesures expérimentales ainsi qu'aux travaux existants.

En continuité, dans le chapitre 5, nous proposons des modèles prenant en compte les non-linéarités. L'approche de Preisach pour la modélisation de l'hystérésis statique et l'approche de Voigt dans le cas dynamique. Ces deux approches sont ensuite fusionnées dans le but d'avoir un modèle plus complet.

Dans le chapitre 6 nous montrons la valeur ajoutée de notre travail. Des cas d'applications sont ainsi présentés. Mieux, à travers ce chapitre nous visons à montrer comment les modèles proposés s'articulent avec les autres éléments d'un système global. Ensuite une adaptation au cas des actionneurs magnetostrictifs est proposée.

Enfin nous concluons et proposons des perspectives.

Ce rapport est écrit en anglais. Mais chaque chapitre est résumé en français dans une proportion d'environ 25% du texte. Les figures et certaines équations ne sont pas répétées.

Chapter 2

Generalities on smart materials/devices and applications

2.1 Résumé du chapitre en Francais

Le qualificatif *intelligent* est couramment associé à tous matériaux ayant une capacité non-négligeable à convertir de l'énergie d'une forme à une autre, sans pour autant se distinguer des matériaux traditionnels. Cependant les scientifiques s'accordent sur le fait qu'il n'existe pas de définition claire [45, 46]. Nous donnons dans cette section un aperçu d'une terminologie assez large.

Pour Z.L. Wang and al [47], les matériaux qui physiquement ou chimiquement sont sensibles à la température, la pression, le champ électromagnétique, les ondes optiques, la valeur du pH de leur environnement, sont qualifiés de *matériaux fonctionnels* puis qu'ils peuvent être utilisés pour assurer des fonctions biologiques, chimiques ou mécaniques. Ils sont plus intéressants s'ils sont maîtrisables. Ailleurs, ces mêmes matériaux sont appelés *matériaux actifs* en raison de leur capacité à récupérer des informations de leur environnement et à y apporter des changements. Par antagonisme aux passifs, les matériaux actifs stockent, convertissent ou manipulent de l'énergie comme par exemple les matériaux piézoélectriques. On les qualifie d'*adaptatifs* du fait qu'ils activent leurs fonctions selon l'état de l'environnement. Lorsqu'ils peuvent être associés à la construction d'une structure on parle de *matériaux structurels*. La consolidation de ces capacités dans un même matériau fait de lui *un matériau intelligent*, parce que l'on y retrouve certaines caractéristiques de l'intelligence des systèmes naturels. Selon George Akhras [8] les matériaux intelligents ont des capacités intrinsèques et extrinsèques, à d'une part répondre aux stimuli et modifications de l'environnement et, d'autre part, à activer leurs fonctions conformément à ces changements.

Dans *Smart Materials Bulletin of September 2002* on rapporte que l'on peut subdiviser les matériaux intelligents en deux catégories. Le premier groupe concerne les matériaux qui, en réponse aux stimuli, changent de forme à une entrée, correspond une déformation. Ils sont utilisés dans la conception des structures complexes. La deuxième catégorie concerne les matériaux qui répondent en modifiant leurs propriétés telles que la conductivité, la viscosité etc.

Parmi les matériaux intelligents, nous pouvons citer les matériaux piézoélectriques, les matériaux magnétostrictifs, les alliages à mémoire de forme, les fluides rhéologiques, les matériaux chromogéniques, les matériaux halo-chromiques, les polymères sensibles au pH

etc.

Les matériaux intelligents sont pour la plupart polyvalents. L'intégration de ces dispositifs dans les aéronefs permettrait l'autocontrôle de leurs performances et la réduction des maintenances préventives. Ce qui diminuerait alors le temps d'indisponibilité des appareils.

Les matériaux intelligents sont aussi utilisés dans le suivi des infrastructures. Ils permettent d'augmenter la sécurité pendant leur durée de vie en fournissant des alertes concernant d'éventuels problèmes structurels. En outre, ils permettent de réduire les coefficients de sécurité généralement utilisés en conception, ce qui réduit le coût de vie de ces structures.

Par ailleurs il existe d'autres matériaux utilisés dans l'industrie textile. Alors que les fonctions d'isolation thermique des vêtements peuvent être traditionnellement assurées par du textile épais à faible densité, ils affectent la liberté de mouvement et génèrent un inconfort physiologique. L'avènement des textiles capables de gérer intelligemment l'énergie thermique offre alors de nouvelles perspectives. Ils s'utilisent dans la fabrication des combinaisons spatiales, des gants, des gants de planche à neige, des sous-vêtements, pour divers sports améliorant ainsi le confort [9].

En qui concerne le processus d'usinage qui nous intéresse le plus, il est généralement l'objet de vibrations pouvant affecter la qualité requise du produit final. On peut alors utiliser des matériaux actifs pour amortir ces vibrations. Toutefois, plutôt que de chercher à amortir ces vibrations, on peut les mettre à profit si elles sont contrôlées. Elles peuvent intervenir positivement dans la formation et l'évacuation des copeaux [3]. L'utilisation des actionneurs intelligents offre alors des moyens flexibles de génération de vibrations, contrairement au système auto-entretenu en Figure 1.3.

L'avènement des matériaux intelligents suscite donc un certain engouement dans les communautés scientifiques, industrielles et universitaires dont l'équipe INSM dans laquelle s'est déroulée la présente thèse.

2.1.1 Piézoélectricité

La découverte de la piézoélectricité est généralement attribuée aux frères Curie même si on doit sa première observation à René Just Hauy. Ce phénomène se caractérise par le fait qu'un matériau initialement neutre, se polarise sous l'action d'une pression mécanique. Inversement, il se déforme sous l'action d'un champ électrique. Les premières études théoriques et expérimentales de l'effet direct sont cependant dues aux frères Curie en 1880. L'effet inverse quant-à-lui a été vérifié par Gabriel Lippmann en 1881.

Certains matériaux piézoélectriques possèdent des propriétés pyroélectriques. Parmi ces derniers, il y en a qui sont ferroélectriques, selon leur classe cristallographique. La composition chimique ainsi que l'état thermique du matériau influencent aussi ces propriétés. La température au-delà de laquelle le matériau perd toute propriété piézoélectrique est appelée *température de Curie*.

D'un point de vue macroscopique, la piézoélectricité est l'interaction entre des grandeurs électriques et mécaniques auxquelles on doit ajouter l'influence thermique. Dans le cas où cette dernière est négligée, on obtient la Figure 2.9.

Les matériaux piézoélectriques sur le marché sont en général faits de céramiques. Mais les fabricants communiquent très peu à ce sujet. Toutefois, on sait que les céramiques les plus utilisées sont à base de zirconate et de titanate de plomb [12].

Les piézo-céramiques sont obtenues par cuisson (élaboration sous haute température)

suivie d'abrasion. Il en résulte des plaquettes (appelées stacks) de l'ordre de 100 à 300μm. Ensuite, on crée des électrodes en utilisant une mince couche d'argent.

Un stack contient une multitude de dipôles électriques orientés aléatoirement. Un processus d'alignement sous fort champ électrique est alors nécessaire à température de Curie. Les stacks sont ensuite associés afin d'obtenir des dimensions importantes (figure 2.11).

2.1.2 Magnétostriction

Les matériaux magnétostrictifs sont sous influence d'un champ magnétique. Mais à l'inverse de la piézoélectricité inverse (déformation proportionnelle au champ électrique), dans le cas de la magnétostriction, la déformation est proportionnelle au carré du champ magnétique appliqué. La découverte de l'effet magnétostrictif est due à James Joules en 1842. L'effet inverse est appelé effet de Villary.

Comme dans le cas des piézoélectriques, les matériaux magnétostrictifs nécessitent une phase d'homogénéisation de l'orientation des micro-domaines. Le plus commercialisé est TERFENOL-D.

2.1.3 Autres matériaux et phénomènes

Les alliages à mémoire de forme se déforment à faible température. Mais exposés à une température élevée, ils retrouvent leur forme initiale. On distingue deux types d'alliages à mémoire de forme. Ceux pouvant revenir à leur forme initiale uniquement par réchauffement (1 sens de mémoire) et ceux qui peuvent aussi se déformer par refroidissement (2 sens de mémoire).

Quand aux substances chromogéniques, elles changement de couleur en réponse aux changements électriques, optiques ou thermiques de leur milieu. Elles sont utilisées dans l'automobile, l'architecture, les aéronefs, et les écrans d'affichage.

Parmi les autres matériaux intelligents on peut citer les polymères sensibles au pH. On peut aussi citer les matériaux halochromiques qui changent de couleur selon le pH. Par ailleurs les fluides rhéologiques modifient leur viscosité lorsqu'on leur applique un champ électrique ou magnétique. De ce fait, ils pourraient être utiles dans la conception des systèmes d'amortissement.

2.1.4 Choix de matériaux

Plusieurs aspects doivent être pris en compte lors du choix du type de matériaux. La fonction à assurer (stocker ou convertir de l'énergie), le type d'énergie utilisé... Matériaux structurels ou pas. La contrôlabilité constitue aussi un critère de choix. Par rapport à ces critères, les matériaux piézoélectriques et magnétostrictifs apparaissent plus adéquats dans le cas de nos applications.

Par ailleurs nous pouvons utiliser la notion d'énergie volumique comme critère complémentaire de choix. Par définition, il s'agit de l'énergie disponible dans les parties utiles du composants [48]. Elle est homogène à une pression.

L'énergie volumique d'un actionneur électrostatique est d'environ $W_{es} = 4.10^1 J/m^3$. Pour les actionneurs électromagnétiques, on peut atteindre $W_{em} = 4.10^5 J/m^3$. Pour les

actionneurs hydrauliques on atteint facilement $W_h = 4.10^7 J/m^3$. Pour les actionneurs piézoélectriques, c'est de l'ordre de $W_{pi} = 3,8.10^7 J/m^3$. Pour les actionneurs magnétostrictifs, $W_{mg} = 7.10^7 J/m^3$.

Un autre critère, non négligeable, est la fréquence maximale f de déplacement. Ce critère combiné avec l'énergie volumique donne la densité de puissance $P = W * f$. Par rapport à cette dernière, les actionneurs piézoélectriques et magnétostrictifs l'emportent sur les actionneurs électriques classiques.

D'autres critères tels que la fiabilité, la durabilité, la fragilité devraient être par la suite intégrés.

The objective of this chapter is to outline the wide panel of smart materials. While remaining general, we shall stress on the particularities of each of them and their processing. We shall also highlight their potential applications and especially show up in which way devices and systems made of these materials could be a good alternative to the classical and common devices/systems. However, we shall begin by clarifying the huge number of adjectives that usually accompany the term material.

2.2 Discussion on terminologies

The concept of intelligent materials is of rather recent origin [49]. It is usual in popular language to associate the term *smart* with materials that allow the conversion of one form of energy into another in useful quantities. Following this logic, several types of materials would be included in the category of smart materials even though they do not present any particularity in comparison to traditional materials. Such a definition does not make consensus. The differentiation becomes even less clear when in literature, one frequently meets many adjectives associated to materials. Thus, apart from the term *smart* we also meet the words *advanced, active, functional, adaptive, structural, ...* interchangeably used. And, all authors seem to agree that there is no clear definition of these terms [45, 46]. However in such a field that is wide ranging and stile developing [7], it is important to dwell on the terminologies.

Literally, *functional* materials are materials which own certain properties serving specified application needs. Z.L. Wang and al. defined functional materials as materials of which the physical and chemical properties are sensitive to a change in the environment such as temperature, pressure, electric field, magnetic field, optical wavelength, adsorbed gas molecules and the pH value [47]. However one should emphasize the necessity that this sensitivity be usable to achieve specific biological, chemical or mechanical functions. They can sense and response, through functions directly built into their microstructure, to environmental stimulus in a predetermined fashion, and go back to their original state when the stimulus is removed, not according to usual laws of physics or mechanics, but rather optimized towards a given goal dictated by the application [50]. Therefore these materials arouse more interest if their stated native properties are controllable. Some even qualify these materials as multi-functional because of their ability of coupling functions.

Elsewhere, these materials are called *active* because of their capacity to take action or effectuate change in a system. They stock, convert or handle energies by antagonism to 'passive' materials. This aptitude makes it possible to use them as actuators, sensors or both. Their presence in certain systems modifies compulsory the effect of the other components of these systems like for example piezoelectric materials that activate a damping function in presence of vibrations in their environment.

So, these materials could have several functions that they activate with respect to their environment state, where would the term *adaptive* probably come from. In this sense, V. K. Wadhawan and al. who cited [51] and [52], noticed in [53] that the concerned materials can be defined as materials with an ability to respond in a pre-designed useful and efficient manner to changing environmental conditions, including any changes in their own condition. This contrast with 'dumb' materials which are preprocessed and/or designed to offer only a limited set of responses to external stimuli

On the other hand, a material is called *structural* if it has an ability to withstand external

forces and therefore it can be integrated in the construction of structures. The notion of structure here is very wide including mechanical, chemical and biological forces. This allows therefore to include the above cited materials in the category of structural materials as soon as their functions in a system involve forces. This category of materials include also traditional materials which are used in mechanical or civil structures such as steels, cooper, and bricks.

However the target materials present peculiar properties in comparison to traditional materials. They are *advanced* because they represent advances over the traditional materials that have been used for years. In this way, they refer to all new materials and modifications to existing materials to obtain superior performance in one or more characteristics that are critical for the application under consideration.

The consolidation of these abilities in certain materials lead to qualify them *smart*, because one found in them certain characteristics of natural systems intelligence. Indeed the materials involved in natural systems have the capability to sense their environment, process this data, and respond. We found a satisfying definition given by G. Akhras [8] according to who *smart/intelligent* materials are materials that have intrinsic and extrinsic capabilities, first to respond to stimuli and environment changes and, second, to activate their functions according to these changes. But Vinod K. Wadhawan and al. emphasized on the adaptability which must be the main characteristic of smart materials [53].

Nevertheless, we should not fail to mention other opinions according to which the supposed smart materials are not actually smart. For, S. Hurlebaus and al. [54], the materials can all be used to design and develop structures that can be called smart. However, the materials themselves are not smart. E. Flint and al. outright saying that in order to be smart these materials have to have a way of 'deciding' how to react to the sensed environment [7], whereas this is currently only achieved by control hardware and algorithms. Therefore, "Smartness" should refer to the exploitation of these materials properties to better serve a design function than would be possible through conventional structural design. Accordingly, the term smart should refer to the integration of actuators, sensors in structural components, and the usage of some kind of control unit or enhanced signal processing with a material or structural component. The goal of this integration would be the creation of a material system having enhanced structural performance, but without adding too much mass or consuming too much power.

However, we accept the definition of G. Akhras (see above) because in spite of the clarification brought by S. Hurlebaus and al. or E. Flint and al., the so called smart materials can inherit the smartness from what they allow to achieve in comparison to traditional materials.

In *Smart Materials Bulletin of September 2002* they report the ideas of Frost and Sullivan Joseph Constance who divided smart materials into two groups. The first group comprises materials which, upon application of a stimulus, they respond with a change in shape or in length of the material. Input is always transformed into strain, used to introduce motion or dynamics into a system. They are the most widely used in the design of smart structures. They could be integrated into a mechanical host structure, such as an airplane wing or automotive suspension system. The second family of smart materials, includes materials that respond to stimuli and a change occurring in a property of those materials. Such a property may be electrical conductivity or viscosity. These are less frequently integrated into mechanical structures. Instead, researchers use them to design complex modules, for example clutches, fasteners, valves or various switches and in sensing systems. Although

materials in this group do not produce strain when an external stimulus is applied to them, they are sometimes also referred to as actuator systems. Examples of these include the electro-rheological (ER) and magneto-rheological (MR) fluids and smart hydrogels, which respond with an increase in viscosity upon application of an external electrical or magnetic field.

A smart system is composed of sensing, processing, actuating, feedback, self-diagnosing and self-recovering subsystems. It uses the functional properties of advanced materials to achieve high performances with capabilities of recognition, discrimination, and adjustification in response to a change of its environment [47].

There exists a huge number of smart materials. New ones continue to be discovered or synthesized thanks to advances in science so that we can not give an entire list of them. However we should enumerate the most known: piezoelectric materials, magnetostrictive materials, shape-memory alloys, rheological fluids, chromogenic materials, halochromic materials, ph-sensitive polymers...

2.3 The world of smart materials

The British Office of Science and Technology Foresight Programme (see [55]) expects an increasing range of smart materials applications and the underlying science in this area. They guesses that smart materials must solve engineering problems with up to now unachievable efficiency, and provide an opportunity for new wealth creating products. Current and potential applications of smart materials are widely presented and illustrated in [56].

2.3.1 Smart materials in Aerospace and transport in general

Smart materials are most of them versatile. Some can be used for sensing their environment and generating data for the health and usage monitoring systems. The integration of such smart devices in aircrafts could allow the self-monitoring of their performance to a high level and could considerably reduce preventive maintenance occurrences. This would obviously limit the aircrafts out of service duration.

E.M. Flint and al. well summarize the potential use of smart materials especially in small satellites but their conclusions also apply to every type of transport means. In [7], they showed through Figure 2.1 these applications where the smart materials are expected to provide reduced weight, to allow new functionalities and to provide performance that are hitherto met with extremely costly passive structures.

2.3.2 Smart materials in Civil Engineering

In the same way, smart materials are used in monitoring civil structures. They can enhance the safety during the life of the infrastructures since they can provide early warning of structural problems at a stage where minor repairs should improve durability. Moreover because they would allow reduced safety factors in initial design, this would impact the life costs of such structures by reducing upfront construction costs. Nowadays because of the continuous diminution of land space in cities, it is no longer a fashion but a necessity to develop underground infrastructures. This is even a brain teaser because underground structures require huge resources for construction and maintenance, and any collapse could

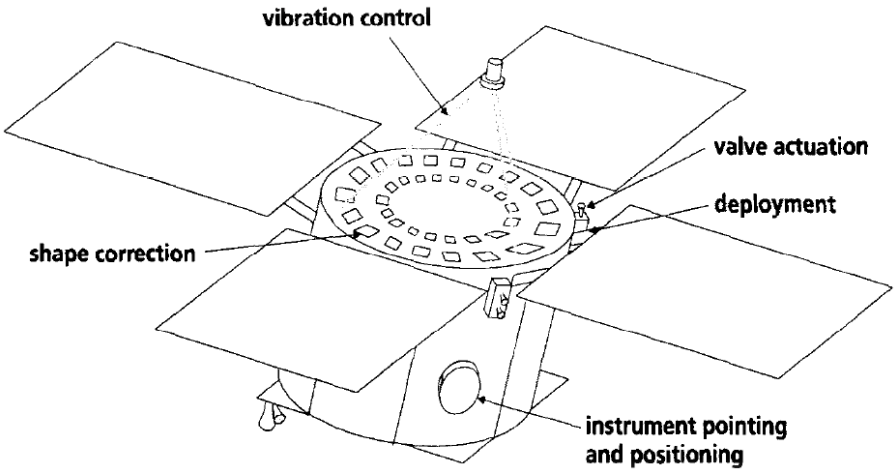

Figure 2.1: Potential applications of smart materials to sample satellite [7]

be detrimental to the nation in terms of economy, lives and properties. Y.W. Yang and al. in [57] demonstrated the feasibility of using smart materials in monitoring of rocks. They showed the assets of fibre optic and piezo-transducers in such applications in comparison to conventional devices like vibration wire strain gauges and electrical strain gauges. Figure 2.2 drawn from [8] presents an example of smart bridge.

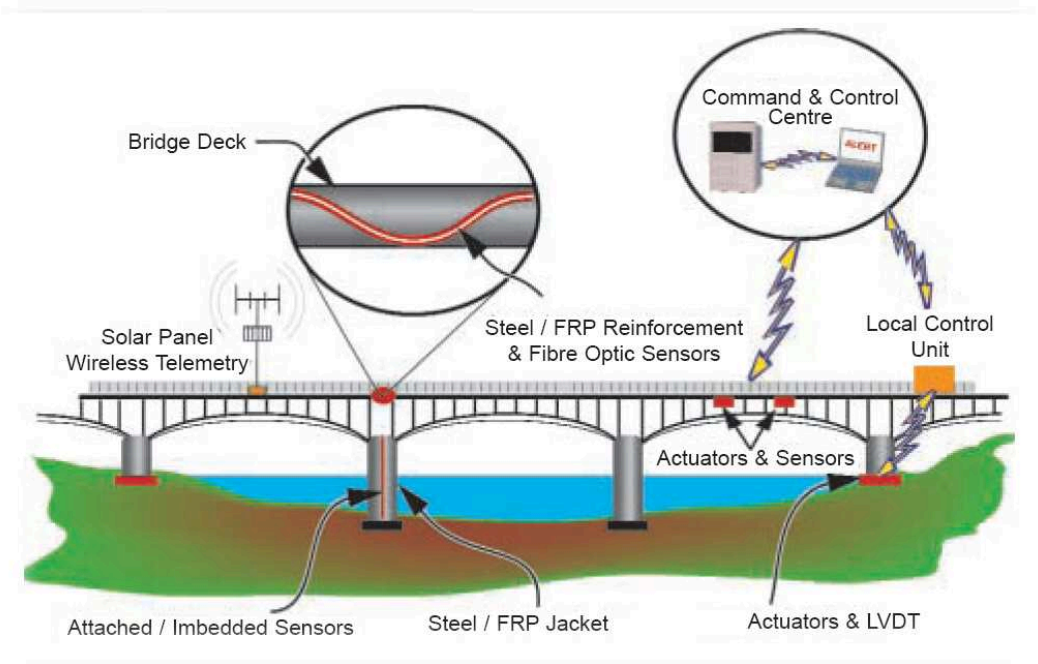

Figure 2.2: Schematic example of a smart bridge [8]

2.3.3 Smart materials in medicine and health in general

Smart materials applications concern also human and animal well being. In [9], the authors deal with the required thermal insulation of clothing systems for the human's body. Traditionally, the improvement of clothes insulation functions goes by the use of high thickness and low density textiles because of their lots of air gaps. however their major inconvenient is their greater weight that affects the freedom of movement of the wearer and generates physiological uncomfort.

The advent of smart textiles able to handle heat energy thus opens a novel era. They act as temperature regulators allowing to use them for active garments. Figure 2.3 shows the example of Phase Change Materials (PCMs) which regulate temperature through a phase change solid-liquid. They could potentially apply to space suits and gloves, snowboard gloves, underwear, ice climbing and underwear for cycling and running, footwear, etc. They would then ensure better comfort for human in their rest or in their activities [9]. Furthermore , smart materials present great interest for clinical and hygienic applications. They could be potentially used in surgical apparel, patient bedding materials, bandages and products to regulate patient temperatures in intensive care units [58].

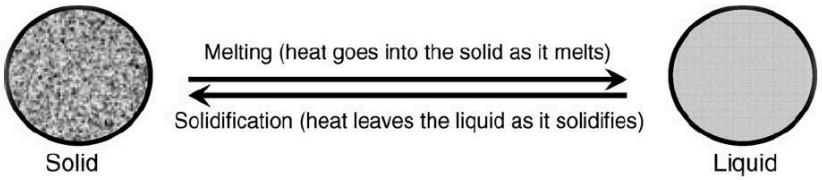

Figure 2.3: Schematic representation of phase change materials behaviour [9]

Other smart materials are used in osteosynthesis, a surgical procedure that stabilizes and joins the ends of fractured bones by mechanical devices. In Figure 2.4, shape-memory alloys (in red) are utilized.

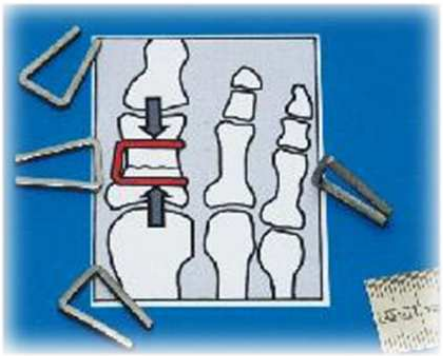

Figure 2.4: Smart osteosynthesis (From:Courtesy Forschengszentrum Julcih, Germany)

2.3.4 The place of our laboratory

The event of smart materials draws the interest of several communities: scientists, industrialists and academics. The INSM (see Glossary) team of LSIS (see Glossary) is not a reference in smart materials studying. However, it develops an axle in smart structures in collaboration with many industries and organisms, especially EADS Group and CETIM. The favourite topics of this axle concern machining and aircrafts, for which innovative concepts are proposed, tested and validated by researchers of the team. A real interest in the use of smart materials is observed. This raises the need of ready-to-use models of devices made of such materials.

2.4 Examples of smart materials

2.4.1 Piezoelectric materials

The term piezoelectricity comes from Greek "Piézein" for "pressure electricity". Its discovery is generally associated to Curie brothers. However, according to Michel Brissaud, the first qualitative observation of the phenomenon is due to René Just Hauy, a French mineralogist, in 1817 [59]. The theory and experimental study of the phenomenon is then undertaken by the brothers Pierre and Jacques Curie in 1880 who realized that a quartz crystal (SiO_2) initially neuter becomes polarized when subjected to mechanical pressure. One year later, Gabriel Lippmann predicted the converse effect which had been proven later. The converse effect is called "electrostriction". Nowadays there exist both natural and synthetic piezo-materials.

Microscopically, the piezoelectric phenomenon is mainly due to the presence of positive and negative electric charges in the material and secondly the non-symmetry of those charges [60]. In the absence of external mechanical and electrical solicitations on the material, the positive charges and negative charges centers of gravity coincide (figures 2.5 and 2.6). Then, if a mechanical force is applied to the material, one can remark that in figure 2.5 the gravity centers remain combined because of the symmetry. On the contrary, in figure 2.6 the gravity centers separate and polarize the material because the charges distribution was not symmetric.

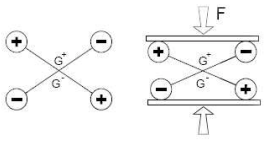

Figure 2.5: Material with symmetry center

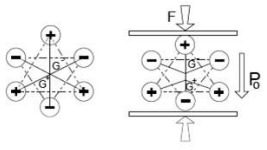

Figure 2.6: Material without symmetry center

Some piezoelectric materials exhibit pyroelectric effect i.e. their polarization can be modified by radiations. Pyroelectric materials include a category of materials called ferroelectric. They own an internal polarization which varies with the external electric field. So, as one could imagine it, materials properties depend on their crystallographical class.

In addition, materials properties vary with their chemical compositions and their thermal state. B. Jaffe and al. performed in [10] a study on an alloy of $PbZr_3$ and $PbTiO_3$ for which they depicted in Figure 2.8 the phase diagram.

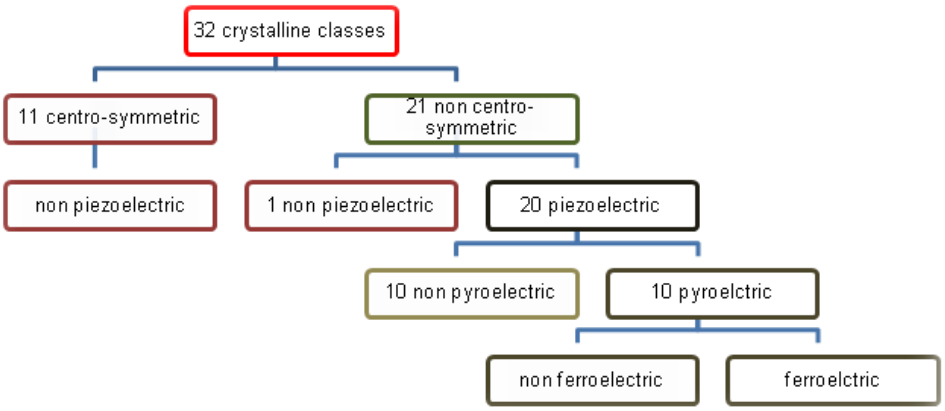

Figure 2.7: Crystallographic classification

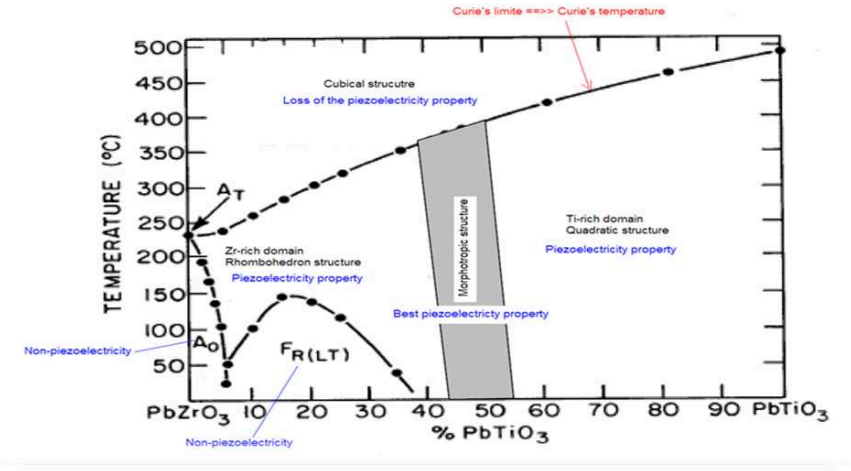

Figure 2.8: Alloy $PbZr_3$ - $PbTiO_3$ [10]

As one can remark, there is a temperature up to which the material looses its piezo-electricity. This temperature is called *Curie's temperature*. It depends on the alloy ingredients rates. Concerning the $PbZr_3$-$PbTiO_3$ (PZT) alloy, the curie's temperature goes from $240\,^\circ C$ to $475\,^\circ C$. There also exist a temperature down to which the material looses its piezo-properties. However, this temperature does not present any concern in comparison to curie's temperature. This could explain the absence of references on it.

Elsewhere, we should look at the phenomena in macroscopical point of view, notably in terms of physical interactions. In piezoelectric materials electrical and mechanical quantities interact. To this we may add the contribution of pyroelectricity if the materials are exposed to their sensitive radiations. This is well clarified in [59] in Figure 2.9 where T is the constraint tensor $(6,1)$, S the deformation tensor $(6,1)$, E the electric field tensor $(3,1)$ and D the electric induction tensor $(3,1)$. Here the pyro-effect is assumed to be negligible.

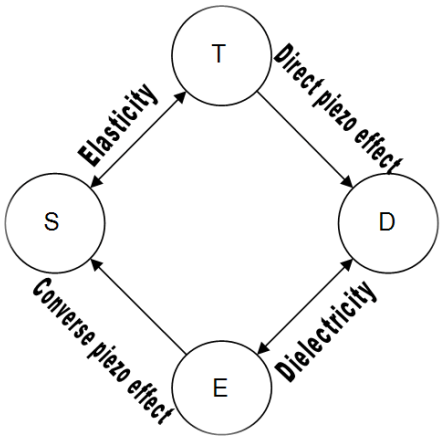

Figure 2.9: Physical explanation of piezoelectricity

Elaboration process

Commercial piezoelectric materials are in general made of ceramics. Ceramics are inorganic nonmetallic materials with obligatory a crystalline structure. There is wide panel of ceramics but the materials suppliers are too disinclined to give their composition. There is a hard competition in the market. However, the most important piezoelectric ceramics are based on the oxide mixed crystals system lead zirconate and lead titanate [12].

So, as all ceramics, piezo-ceramics are obtained through a firing process: elaboration under high-temperature [12]. Ceramics' elaboration process is well described in [61] (pg.47-325). The first step for piezo-ceramics's elaboration is about alloy PZT powder obtention: the raw materials are mixed in their solid-state at about 850 $^\circ$C; the solute particles fit into the space between solvent particles. This step leads to a solid-state solution. Next, the solid solution is mixed with a sociable and sintered at high temperature though under the melting point. Then another step (conditioning) allows to obtain wafers with dimension on the order of a few centimeters with two sides and thickness in the range of 100 to 300μm. Then, according to their thickness, wafers can be assembled in order to form what one call *stack* in technical language [62]. Then electrodes are created on the stacks faces by painting on them a thin silver layer.

A stack is composed of multitude crystals containing dipoles. Up to this time, the dipoles are randomly oriented. The row material in that form is not sufficiently piezoelectric. Consequently, the process requires an important step of poling during which the dipoles are oriented with respect to one another. The poling step can take place at ambient temperature (soft ceramics) or at high temperature (hard ceramics). A strong electric field is thereby applied ($2 - 3kV/mm$) leading thus in combination with the temperature effect, to the free motions of the dipoles. The poling process is generally performed in silicone oil in order to avoid air breakdown phenomenon. The dipoles therefore align along the electric field direction. This direction corresponds to the so-called *Poling axis* of the piezo-stack. The temperature is then quickly reduced and the electric field is removed. Thereafter, the material dipoles are aligned and then the piezoelectricity is enhanced. It should be noticed that not all the domains become exactly aligned, some of the domains only partially align and some are not aligned at all (Figure 2.10). This could leads to a phenomenon called

creep.

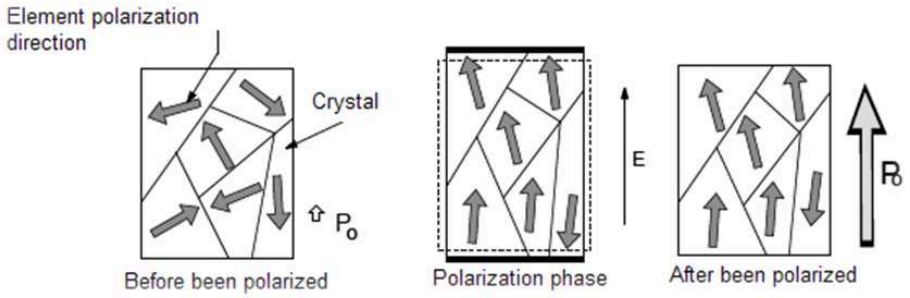

Figure 2.10: Poling process

The stacks are then joined with others in order to obtain important dimensions (Figure 2.11). They are mechanically in series and electrically in parallel.

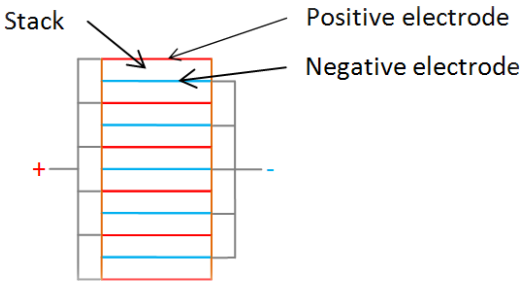

Figure 2.11: Multi-layers piezoelectric device

One reason for preferring a multi-layers device to a one-layer device of the same dimension could be related to the total elongation of the device. Indeed, the junction of several stacks allows theoretically to increase the piezoelectric coefficient. Another reason could be related to the poling process. Above, we noticed that about $2-3kV/mm$ is required to pole a wafer of $300\mu m$ thickness. Therefore, for a tube of $30000\mu m$ (for example) or more the poling process would require a high voltage.

2.4.2 Magnetostrictive materials

Magnetostrictive materials are similar to piezoelectric materials in terms of macroscopical behaviour, except the fact that instead of an electric field, magnetostrictive materials involve a magnetic field. Hence, one can define magnetostrictive effect as a reversible exchange of energy form mechanical form to magnetic form. Magnetostriction is the change in shape occurring in some materials submitted to an external magnetic field.

Magnetostrictive effect was discovered more earlier than piezo-effect. It is a discovery of James Joules in 1842. Magnetostrictive effect is therefore sometimes called Joule effect. The converse effect is called Villary effect who verified it.

Microscopically, magnetostrictive materials contain magnetic micro-domains which tend to align themselves to the external magnetic field; they rotate and this rotation causes

internal strains in the material [63]. A region constituted of micro-magnetic domains of the same orientation is called *Weiss Region* (Figure 2.12).

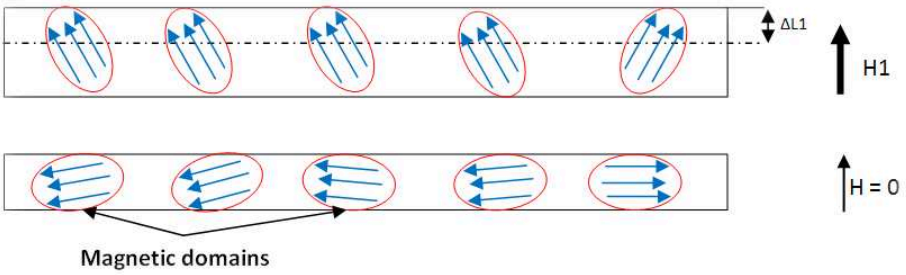

Figure 2.12: Weiss region in magnetostrictive material

But not all the regions have naturally the same orientation. A step of homogenization is therefore necessary at high temperature. Magnetostrictive materials elaboration process is similar to that of piezoelectric materials. And, as said above concerning piezo-materials, magneto-materials' properties also depend on their chemical constitution and they also possess Curie temperature up to which they loose those properties.

The most commercialized magneto-material is TERFENOL-D. The name comes from Terbium (TER), iron (FE) and Naval Ordinance Labs (NOL) and Dysprosium (-D). The material has first been developed by the Navy.

2.4.3 Shape-memory alloys

They are thermo-responsive materials that remember their geometry. Such materials can be plastically deformed at some relatively low temperature and, upon exposure to some relatively higher temperature recover their original shape (Figure 2.13). This behavior is due to a martensitic-austenic phase transition and, at low temperature, to martensitic twinning [11].

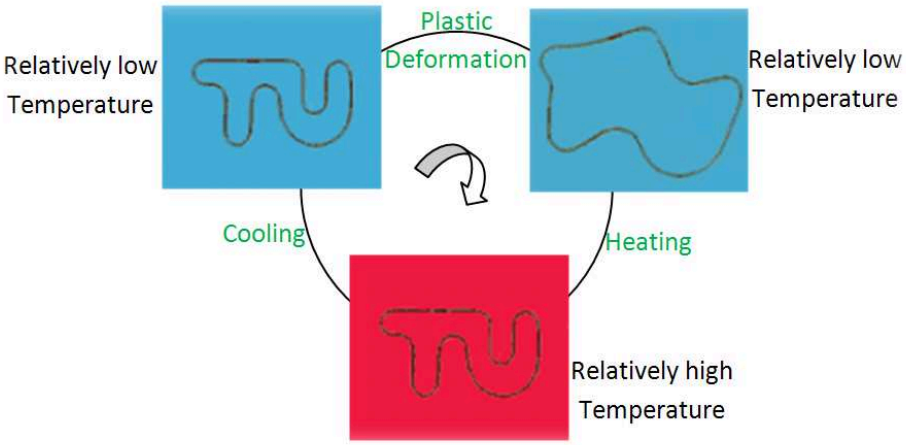

Figure 2.13: Thermomechanical behaviour of Shape Memory Alloys [11]

One distinguishes two kinds of shape-memory phenomenon: materials that can memory their shape only upon heating (one-way shape-memory) and materials that can also undergo a change in shape upon recooling (two-way shape-memory). This kind of materials is so called ordinary shape-memory alloys or temperature driven shape memory (TSM) alloys. These properties are made possible through a solid state phase change that is molecular rearrangement which is due to temperature change. A temperature change of only 10řC is sufficient to initiate this phase change. The two phases which occur in shape-memory alloys are martensite and austenite.

Some of the main advantages of shape memory alloys include their bio-compatibility. They have diverse Fields of Application. However, they are relatively expensive to manufacture and machine compared to other materials such as steel and aluminum.

2.4.4 Chromogenic materials

Chromogenic substances change color in response to electric, optical or thermal changes. Chromogenic materials are used especially in automotive, architectural, aircraft, and information display. In automotive field, electrochromic materials, which reversely change their optical properties in response to an electric field, involve in dynamic antiglare automotive mirrors. In aerospace, there is an interest in developing visors and windows that can control glare for pilots and passengers. The topic of chromogenic technology and market is amply exposed in [64].

Figure 2.14 shows an example for thermochromic materials. When the teacup is empty or if the content is cold, the teacup is dark. On the other hand, it becomes bright when filled with hot content. In sum, thermochromic materials get their color changed at a determined temperature.

Figure 2.14: Thermochromic material (from [12])

2.4.5 Other smart materials

We can enumerate ph-sensitive polymers which respond to a change in their surrounding medium ph by swelling or collapsing. This is due to the presence of certain functional groups (acidic or basic groups) in the polymer chain. These materials are being extensively used in controlled drug delivery systems and biomimetics.

We can also cite halochromic materials which behave as pH-sensitive ones but instead of changing their dimensions they change their color according to the pH of the medium.

These substances are very useful in environments where pH changes occur frequently, or places where pH changes are extreme.

Elsewhere some fluids vary their viscosity when applied to electric field (electro-rheological fluid) or magnetic field (magneto-rheological fluid). This feature permits to use these fluids in advanced damping systems.

Fibre optics respond to a change in transmitted light. This change could be in intensity, phase, frequency, polarization, wavelength or mode. They are highly sensitive, can detect minuscule variations.

The list of smart materials is in expansion; it is impossible to cite them exhaustively.

2.5 Choice criteria

Many criteria should be considered in order to choose a device. One could base on the function to achieve: stock or convert energy. The type of energy handled and the reversibility of the phenomenon could also be important. The X-Mechanical conversions are strongly appreciated especially in industrial applications. Piezo, magneto, shape-memory and X-rheological materials are in these conditions the best candidates.

Another qualifying parameter could be the possibility for the material to serve as structural component. Effort transmission with contact is valued. Piezo and magneto materials have the exceptional capability to bear high efforts with very small strains.

Moreover the controllability constitutes an important criterion of choice. Devices controllable via electrical quantities are preferred.

All those requirements are listed in the types of our applications. Consequently piezo and magneto devices correspond better to our needs than devices made of the other smart materials. Their phenomena are reversible making it possible to use them both as actuators and sensors.

In next section we compare classical electro-devices and piezo or magneto devices.

2.5.1 Piezo and magneto actuators Vs classical hydro and electro actuators

The ratio energy/dimensions (energy density) is a fundamental criterion for the comparison between actuators. We have studied and used these concept in the past during a project on mechatronics deployment in a renowned company [65].

By definition, the energy density is the disposal energy in the useful area of the device and it is identified to a pressure [48]. Let us compare then electrostatic, electromagnetic, hydraulic, piezo and magneto actuators basing on [48].

The maximal energy density of electrostatic actuators is $W_{es} = 4.10^1 J/m^3$. Concerning electromagnetic actuators, one can reach $W_{em} = 4.10^5 J/m^3$.

For hydraulic actuators one reaches easily $W_h = 4.10^7 J/m^3$. Piezo-bar actuators can bear up to $380bar$. This corresponds to an energy density of $W_{pi} = 3,8.10^7 J/m^3$. Magneto-bar actuators bear easily $700bar$ corresponding to $W_{mg} = 7.10^7 J/m^3$.

The energy density gives an idea on the range of force that an actuator can develop. In static applications this criterion could be sufficient. For example in applications where

one is concerned with clamping forces (high force and small volume change), magneto-actuators are the best choice instead of hydraulic actuators and piezo-actuators. Then come electromagnetic actuators.

In the energy density criterion, one only considers the useful area of the device. However, the total sizes of the devices and their casing are parameters not to be neglected. In this sense, piezo actuators constitute the best option.

On the other hand, if one is interested in the displacement instead of the clamping force, hydraulic and electromagnetic actuators would take the advantage. Piezo and magneto actuators are only capable of micro-displacements.

Another criterion, not negligible, which complete the above energy density criterion, is the maximal frequency f of the displacements. This is important in dynamical applications since one is concerned with the response rapidity of the device. This criterion combined with energy density lead to define the power density $P = W * f$.

The maximal frequency for electrostatic actuators is $f_{es} = 10^6 Hz$, leading to $P_{es} = 4.10^7 Watt/m^3$. With electromagnetic actuators, one has $f_{em} = 10^5 Hz$, leading to $P_{em} = 4.10^{10} Watt/m^3$. Hydraulic actuators allow to reach $f_h = 10^2 Hz$, leading to $P_h = 4.10^9$ $Watt/m^3$. Piezo actuators allow easily $f_{pi} = 10^4 Hz$, leading to $P_{pi} = 3,8.10^{11} Watt/m^3$. And magneto actuators allow easily $f_{mg} = 10^3 Hz$, leading to $P_{es} = 7.10^{10} Watt/m^3$.

Accordingly, piezo and magneto actuators offer the best options.

One could consider other criteria such as reliability, durability or shelf life, fragility. However the field of smart materials is not mature yet. We still are in lack of sufficient statistical data.

Finally we should notice that the benefits of the materials often come though at the cost of increased design complexity and requirements for additional signal conditioning, power amplification and controller hardware subsystems [7]. This increase in complexity has been described by Hiroaki Yanagida as the *spaghetti syndrome*.

2.5.2 Piezoelectric actuators Vs and magnetostrictive actuators

CEDRAT Technologies S.A, a supplier of smart technologies, conducted a comparative study of piezoelectric and magnetostrictive actuators [66]. Accordingly, the choice between these two technologies could be based on many criteria. It could be related to their sizes, their physical output quantities or their driving techniques. Table 2.1, provides an overview of such a comparison.

Criteria	Piezoelectric	Magnetostrictive
Size	Small	Very large
Physical quantities		
Unloaded-device displacement (u_F)	1000-1400 ppm	$>$ 1600 ppm
Blocked-device force (F_b)	Very large	Less important
Elastic energy ($E_e = \frac{u_F.F_b}{2}$)	Important	Less important
Output energy/mass unit	Very large	Small
Dynamic strain at resonance	1600-2000 ppm	3000-4000 ppm
Driving techniques		
Control	Voltage or Charge	Electric current
Frequency	Wide range	Small frequencies

Table 2.1: Piezoelectric Vs Magnetostrictive Actuators

2.6 Conclusion and challenges

Advanced materials reduce weight, eliminate sound, reflect more light, dampen vibration and handle more heat. They lead to smart structures and systems which will definitively enhance our quality of life [8]. Piezo and magneto devices impress the more in relation to their high power density. Moreover the whole system weight and volume can be lighted by coupling functions such as structural support and vibration control.

Due to its nature, the field of smart structures depends on inter-disciplinary research since numerous disciplines (e.g. material science, applied mechanics, control theory, etc.) are involved in the design of a smart structure system solution.

First of all, understanding and controlling their composition and microstructure must be ultimate objectives of research in this field. It is crucial to the production of good smart materials.

Another challenge is to model short-term micro-scale material behavior through the meso-scale and macro-scale behavior into long-term structural system performance. The availability of models will then allow to take up an additional challenge concerning the method of their application, the durability in repeated use.

Chapter 3

Basis, characterization of piezo-bar devices, trade rules

3.1 Résumé du chapitre en Francais

L'objectif premier de ce chapitre est de présenter les équations de base de la piézoélectricité. Ensuite nous procéderons à la caractérisation fréquencielle de deux actionneurs afin d'en déduire certains paramètres. Enfin nous présenterons un cas d'application en statique.

L'équation 3.1 acceptée par la norme IEEE-ANSIS [43] constitue le point départ des développements sur les dispositifs piézoélectriques.

$$\begin{array}{rcl} S & = & \left[s^E\right].T + [d]^t.E \\ D & = & [d].T + \left[\varepsilon^T\right].E \end{array} \tag{3.1}$$

$\left[s^E\right]$ est le tenseur de flexibilité. L'exposant E dans $\left[s^E\right]$ signifie que le tenseur est à champ électrique constant. $\left[\varepsilon^T\right]$ est le tenseur de permittivité. L'exposant T dans $\left[\varepsilon^T\right]$ signifie que le tenseur est à contrainte constante. $[d]$ est le tenseur des coefficients piézoélectriques. L'exposant t fait référence à l'opération de transposition des matrices.

On remarque que les coefficients électriques dépendent des conditions aux limites mécaniques. Et inversement les coefficients mécaniques dépendent des conditions électriques. Ils dépendent aussi de l'axe de polarisation et de la structure microstructure (Conf. Annexes A). Ces équations peuvent être simplifiées selon le mode utilisé [59].

Dans notre cas, nous utilisons le mode barreau. Les matériaux sont des céramiques de la classe cristallographique ∞mm. Ainsi nous retiendrons l'Equation suivante.

$$\begin{array}{rcl} S_3 & = & s_{33}^E.T_3 + d_{33}.E_3 \\ D_3 & = & d_{33}.T_3 + \varepsilon_{33}^T.E_3 \end{array} \tag{3.2}$$

Par la suite on définit le coefficient de couplage électromécanique comme suit.

$$k = \frac{d_{33}}{\sqrt{s_{33}^E.\varepsilon_{33}^T}} \tag{3.3}$$

Dans la section 3.3, nous choisissons une procédure de caractérisation. Toutefois, le lecteur pourrait se référer aux documents [67, 68, 69, 70, 13] pour d'autres détails.

En Figure 3.2, sont présentés les types d'actionneurs utilisés: des barreaux à section rectangulaire ou circulaire. Il a été vérifié que le type de section n'influence pas les résultats

[59]. Le plus important est que la longueur soit 5 à 10 fois supérieur aux dimensions latérales. Soit L, σ et ρ respectivement la longueur, la section et la masse volumique.

Nous choisissons de faire la caractérisation sur un actionneur non-contraint c'est-à-dire libre à ses deux extrémités. Nous l'excitons avec une tension sinusoidale. Il en résulte une propagation d'onde progressive longitudinale à travers le barreau.

En appliquant le principe fondamental de la dynamique et la loi de conservation des charges électriques, par transformations des équations il vient:

$$Z_{El} = \frac{1}{j\omega.C_e^0}\left[1 - k^2.\left(\frac{\tan\left(\frac{\omega.L}{2v_b^D}\right)}{\frac{\omega.L}{2v_b^D}}\right)\right] \tag{3.4}$$

$$k^2 = \frac{\pi}{2}.\frac{f_r^0}{f_a^0}.\cot\left(\frac{\pi}{2}.\frac{f_r^0}{f_a^0}\right) \tag{3.5a}$$

$$\varepsilon_{33}^T = \frac{C_e^0.L}{(1-k^2).\sigma} \tag{3.5b}$$

$$s_{33}^E = \frac{1}{\rho(1-k^2)\left(2f_a^0.L\right)^2} \tag{3.5c}$$

$$d_{33} = \sqrt{k^2.s_{33}^E.\varepsilon_{33}^T} \tag{3.5d}$$

$$Q_M = \frac{1}{2\pi\left(f_r^0\right)Z_rC_e^1}\left(\frac{\left(f_a^0\right)^2}{\left(f_a^0\right)^2 - \left(f_r^0\right)^2}\right) \tag{3.5e}$$

$$k_{31}^2 = \frac{A}{1+A} \tag{3.5f}$$

$$A = \frac{\pi}{2}\left(1 + \frac{f_a^0 - f_r^0}{f_r^0}\right)\tan\left(\frac{\pi\left(f_a^0 - f_r^0\right)}{2f_r^0}\right) \tag{3.5g}$$

$$s_{11}^E = \frac{1}{\left(2f_r^0.a\right)^2} \tag{3.5h}$$

$$d_{31} = \sqrt{k_{31}^2.s_{11}^E.\varepsilon_{33}^T} \tag{3.5i}$$

Plus loin en section 3.4 deux cas pratiques sont présentés. En Figure 3.3, nous avons le montage générique pour la caractérisation fréquencielle. Dans notre cas, notre dispositif expérimental est composé d'un multimètre, d'un générateur de fonctions à balayage fréquenciel, d'un shunt de précision et d'une carte d'acquisition de signaux (Voir Annexes B). Les éléments piézoélectriques utilisés sont le HPSt 1000/35-25/80 de Piezomechanik [71] et le P-885.90 de Physik Instrumente [62].

Dans un premier temps on mesure la capacité à basse fréquence de l'actionneur non-contraint. Ensuite, on réalise le montage (Figure 3.4) équivalent à la Figure 3.5. On mesure les tensions V_{GFG} et V_S respectivement à la sortie du générateur de fonction et aux bornes de la résistance de précision R_S.

L'impédance électrique est alors donnée par l'équation 3.6. Les tracés d'impédances (Figures 3.6 et 3.7) nous permettent de relever les premières fréquences de résonance f_r^0 et d'anti-résonance f_a^0.

$$Z_{El} = \frac{(V_{GFG} - V_S) * R_S}{V_S} \tag{3.6}$$

Ces trois mesures nous permettent de calculer les paramètres de l'actionneur selon les expressions 3.5.

Les limites de cette démarche sont liées aux cartes d'acquisition utilisées. Leurs fréquences d'échantillonage sont limitées à 140 kHz. Pour y remedier on pourrait utiliser des analyseurs d'impédances que l'on peut trouver sur le marché.

Dans la section 3.6, nous passons des paramètres physiques (coefficients de rigidité et de permittivité) à des paramètres macroscopiques que nous appelons paramètres ingénieur (Equations 3.7 et 3.8): raideur et capacité. La raideur dépend des conditions électriques et la capacité dépend des conditions mécaniques. Ces paramètres varient entre deux positions extrèmes comme nous le montrons dans le tableau 3.3.

$$K = \frac{\sigma}{s.L} \tag{3.7}$$

$$C = \frac{\varepsilon.\sigma}{L} \tag{3.8}$$

Nous pouvons déplorer l'absence de ces précisions dans les données techniques des fournisseurs de ces actionneurs. Mais en comparant nos calculs à leurs données et suite à une enquête téléphonique au près des techniciens de Piezomechanik en France, nous concluons que par défaut, les fournisseurs donnent la raideur de l'actionneur en circuit ouvert et sa capacité à vide.

Dans la section 3.6.1 nous traitons des cas d'utilisation en régime statique. Dans la section 3.6.2 nous proposons des règles de choix d'un actionneur. Ces règles sont dictées par des considérations très pratiques. Le choix se fait selon le déplacement nominal désiré, la charge nominale à supporter, l'effort de blockage ainsi que la fréquence de résonance d'actionneur non-contraint.

The content of this chapter is useful in the sense that it firstly recalls the main basis of piezoelectricity. It is a compulsory starting point of any study. In this vain, we discuss the general assumptions under which the basic equations are valid. Moreover we present a simple and prompt way to characterize any piezo-bar device and determine what we name engineer's parameters. A comparison can then be done between the determined parameters and those provided by devices'suppliers. Finally, static use case of a piezo-bar device is presented. This is important for ideational studies in design process. The background in structures dimensioning shows that as often as not, this task takes place in static.

3.2 Preliminaries

Woldemar Voigt, a German physicist, introduced in 1910 the tensorial notion to describe piezoelectric behaviour of some crystals under the assumption neglecting temperature influence. Accordingly, piezoelectricity involves two couples of variables: mechanical ones (T, S) (Stress, Strain) and electrical ones (E, D) (Electric field, Electric induction).

The widely accepted mathematical description basing on the assumption of linearity is the one given by IEEE-ANSIS Standards [43] in Equation 3.9:

$$\begin{array}{rcl} S & = & \left[s^E\right].T + [d]^t.E \\ D & = & [d].T + \left[\varepsilon^T\right].E \end{array} \tag{3.9}$$

$\left[s^E\right]$ is a 6x6 symmetrical matrix called mechanical matrix of flexibility. The superscript E in $\left[s^E\right]$ indicates that either the electrical field is zero or it is a constant. $\left[\varepsilon^T\right]$ is a 3x3 symmetrical matrix called electrical permittivity of the material. The superscript T in $\left[\varepsilon^T\right]$ indicates that either the stress is zero or it is a constant. $[d]$ is a 3x6 matrix named matrix of piezoelectric coefficients. The superscript t refers to matrix transposition.

In Equation 3.9, the choice of (E, T) as independent variables instead of (D, S) is motivated by the device controlling techniques. Indeed, since we are mainly dealing with actuating function, (E, T) are the stimuli and (D, S) are the outputs. However, in literature, one justifies the choice according to frequency domain [72]. When the device is used near its anti-resonance frequency, the good independent variables choice is (D, S). If it is used near the resonance frequency, the good choice would be (E, T).

Equation 3.9 could be written in three other manners as one could notice it in literature. This leads to four definitions of piezoelectric coefficients. However the most important is that a piezoelectric coefficient links mechanical quantities to electrical ones. In all this report d refers to the piezoelectric coefficient.

Development of Equation 3.9 depends on the device polling axis. Conventionally one sets the polling axis to be z-axis.

Moreover, operating modes are defined with respect to the device polling axis, its geometry and boundaries conditions [59].

General applications deal with bar operating mode (Figure 3.2) since it allows important displacements.

In this case one has: $D_1 = D_2 = 0 \;\; D_3 \neq 0$, $E_1 = E_2 = 0 \;\; E_3 \neq 0$, $T_1 = T_2 = 0 \;\; T_3 \neq 0$, $S_1, S_2, S_3 \neq 0$.

Piezo-bar devices could be of rectangular cross-section, powders, or tubes. However, one could verify that according to the equations of transition from cartesian base to cylindrical,

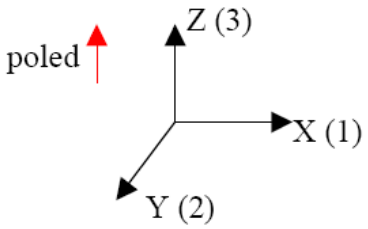

Figure 3.1: Standard axis nomenclature

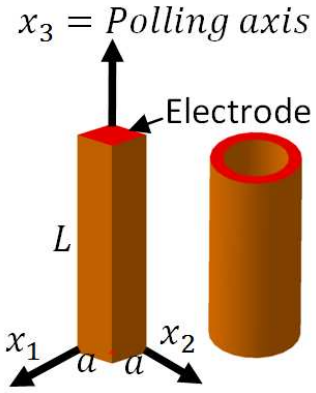

Figure 3.2: Piezo-bar devices particularities

the physical tensors do not change. Therefore the theory and results for rectangular section elements are also valid for circular cross-section elements and vice-versa.

Equation 3.9 reduction depends not only on the operating mode but also on the physical matrix structures. The matrix structures depend in their turn on the concerned material's crystallographic system. We invite readers to look at Annexes A where we recall some crystallographic systems and their corresponding matrix. It could therefore be noticed that not all kinds of piezo-materials are interesting for bar operating mode. As a matter of fact, the choice of a particular crystallographic system piezo-material should depend on the application goal and the operating modes. Examples of interesting crystallographic systems for bar operating mode include hexagonal $6mm$, hexagonal 6, monoclinic 2 and orthorhombic $2mm$.

The devices we deal with in our studies and applications, as well as general industrial piezo-devices, crystallize in hexagonal $6mm$ system for which one has:

$$\left[s^E\right] = \begin{bmatrix} s_{11}^E & s_{12}^E & s_{13}^E & 0 & 0 & 0 \\ s_{12}^E & s_{11}^E & s_{13}^E & 0 & 0 & 0 \\ s_{13}^E & s_{13}^E & s_{33}^E & 0 & 0 & 0 \\ 0 & 0 & 0 & s_{44}^E & 0 & 0 \\ 0 & 0 & 0 & 0 & s_{44}^E & 0 \\ 0 & 0 & 0 & 0 & 0 & s_{66}^E \end{bmatrix}$$

$$\left[\varepsilon^T\right] = \begin{bmatrix} \varepsilon_{11}^T & 0 & 0 \\ 0 & \varepsilon_{11}^T & 0 \\ 0 & 0 & \varepsilon_{33}^T \end{bmatrix}$$

$$[d] = \begin{bmatrix} 0 & 0 & 0 & 0 & d_{15} & 0 \\ 0 & 0 & 0 & d_{15} & 0 & 0 \\ d_{31} & d_{31} & d_{33} & 0 & 0 & 0 \end{bmatrix}$$

Thanks to the so-evolved elaboration process of piezo-device, we can consider the above physical coefficients as constants. Indeed a piezo-bar device is a stacking up of thin elements from 100 to 300μm.

In bar operating mode Equation 3.9 are reduced as follows:

$$\begin{array}{rcl} S_1 & = & s_{13}^E.T_3 + d_{31}E_3 \\ S_2 & = & s_{13}^E.T_3 + d_{31}E_3 \\ S_3 & = & s_{33}^E.T_3 + d_{33}E_3 \\ D_3 & = & d_{33}.T_3 + \varepsilon_{33}^T E_3 \end{array} \tag{3.10}$$

However, since in actuation applications, the lateral faces are not functional (they are free of deformation) the two first lines of equation 3.10 can be omitted. In this case, the basic reduced equations governing the piezoelectricity in the device are:

$$\begin{array}{rcl} S_3 & = & s_{33}^E.T_3 + d_{33}.E_3 \\ D_3 & = & d_{33}.T_3 + \varepsilon_{33}^T.E_3 \end{array} \tag{3.11}$$

Thereby, in theory only three coefficients are needed d_{33}, ε_{33}^T and s_{33}^E. From these three coefficients another one is deducted. It is the electromechanical coupling coefficient denoted k. It is the main parameter which express the coupling character of piezoelectric materials. It indicates the aptitude of a piezoelectric material to convert reciprocally the elastic energy to electric energy. Its expression varies from one operating mode to another.

Let us consider the elementary energy of a piezoelectric material subjected to T and E in Equation 3.12

$$\delta U = [T]^t.\delta[S] + [E]^t.\delta[D] \tag{3.12}$$

According to Equation 3.11 it comes:

$$\delta U = T_3.(s_{33}^E \delta T_3 + d_{33}\delta E_3) + E_3.(d_{33}\delta T_3 + \varepsilon_{33}^T \delta E_3) \tag{3.13}$$

Then

$$\delta U = s_{33}^E.T_3\delta T_3 + d_{33}.(T_3\delta E_3 + E_3\delta T_3) + \varepsilon_{33}^T.E_3\delta E_3 \tag{3.14}$$

And

$$\delta U = s_{33}^E.T_3\delta T_3 + d_{33}.\delta(T_3.E_3) + \varepsilon_{33}^T.E_3\delta E_3 \tag{3.15}$$

Finally

$$U = \frac{1}{2}.s_{33}^E.(T_3)^2 + d_{33}.T_3.E_3 + \frac{1}{2}.\varepsilon_{33}^T.(E_3)^2 \tag{3.16}$$

Or

$$U = U_{Me} + 2U_C + U_{El} \tag{3.17}$$

where $U_{Me} = \frac{1}{2}.s_{33}^E.(T_3)^2$ denotes the pure mechanical energy, $U_{El} = \frac{1}{2}.\varepsilon_{33}^T.(E_3)^2$ the pure electrical energy, and $U_C = \frac{1}{2}.d_{33}.T_3.E_3$ the electromechanical coupling energy.

The electromechanical coupling coefficient is defined as the ratio of coupling energy and driving energy: $k = \frac{U_C}{\sqrt{U_{Me}.U_{El}}}$

Thus

$$k = \frac{d_{33}}{\sqrt{s_{33}^E.\varepsilon_{33}^T}} \tag{3.18}$$

3.3 Piezo-material and piezo-device characterization approaches

Methods for piezoelectric materials characterization are widely reported in literature [67, 68] and in academic laboratories so be it easy or not, expensive or not, efficient or simply approximative. One could also refer to IEEE Standard [69] on piezoelectric measurements. Practice aspects and required setup are reported in [70, 13] and exposed in many web sites. However, depending on the disposal means, one improves the accuracy of the measurements.

Characterization procedures are generally based on resonance measurements. Thanks to piezoelectric material versatility, unique electrical measurements allows to determine both mechanical and electrical coefficients and vice-versa. In the current report we use electrical measurements.

Although these procedures are widely accessible for anonymous public, we cannot overlook the minimum comprehension of their philosophy.

Firstly we should note that electrical coefficients depend on mechanical conditions and mechanical coefficients depend on electrical conditions. However the measurements under a given condition allow to deduct all the other parameters.

Let us consider a piezoelectric bar in Figure 3.2. We denote L the bar's length, σ its cross-sectional area and ρ its mass density.

We study the propagation of a longitudinal wave within the bar (see [59]). The study is yielded for free device i.e. the two bases of the bar are free (Equation 3.19). This mechanical condition is simply realized.

$$T_3(x_1, x_2, 0) = T_3(x_1, x_2, L) = 0 \tag{3.19}$$

Moreover, the lateral dimensions are so smaller than the longitudinal dimension so that the physical quantities are independent of x_1 and x_2.

We excite the piezo-device with an harmonic electric voltage i.e. an harmonic electric field. This results in the propagation of a traveling longitudinal wave in the bar.

The mechanical equilibrium states:

$$\rho \frac{\partial^2 u_3}{\partial t^2} = \frac{\partial T_3}{\partial x_3} \tag{3.20}$$

where u_3 denotes the displacement of the considered point. Under the assumption of small deformations ($< 10^{-2}$ [73]), one has:

$$S_3 = \frac{\partial u_3}{\partial x_3} \tag{3.21}$$

A non validity of small deformation assumption would lead to what one calls nonlinearities of deformation (different from nonlinearities of constitutive law) [74]. In this case one would have:

$$S_3 = \frac{\partial u_3}{\partial x_3} + \frac{1}{2}\left(\frac{\partial u_3}{\partial x_3}\right)^2 \tag{3.22}$$

This assumption is valid since piezoelectric devices are subject to micro/nano scale displacements. Table 3.1 drawn from piezoelectric devices manufacturers data sheets could provide a quick appreciation of commercialized piezo-devices.

Ref	Length (mm)	Maximal displacement (mm)	Corresponding deformation [%]
P-882.10	9	0.008	$0.9 * 10^{-1}$
P-882.30	13.5	0.013	$0.96 * 10^{-1}$
P-882.50	18	0.018	10^{-1}
P-885.90	36	0.038	$1.06 * 10^{-1}$
P-010.80	107	0.120	$1.12 * 10^{-1}$

Table 3.1: General deformation of piezo-bars

We can see that small deformation assumption is valid for all of them.
Elsewhere the electrical conservation law states:

$$\frac{\partial D_3}{\partial x_3} = 0 \Rightarrow D_3 = D_0 . \exp^{j\omega t} \tag{3.23}$$

Therefore the electric charges collected at one electrode are:

$$q = D_0 . \sigma . \exp^{j\omega t}$$

And the electric current is:

$$I = \frac{\partial q}{\partial t} = j\omega . D_0 . \sigma . \exp^{j\omega t} \tag{3.24}$$

t is the time variable.
Equation 3.11 combined with Equation 3.20 and 3.23 lead to:

$$\rho \frac{\partial^2 u_3}{\partial t^2} = \frac{1}{(1-k^2) s_{33}^E} . \frac{\partial^2 u_3}{\partial x_3^2} \tag{3.25}$$

The coefficient $s_{33}^D = (1-k^2) s_{33}^E$ corresponds to the flexibility coefficient at constant electric induction. It comes:

$$\frac{\partial^2 u_3}{\partial t^2} = \frac{1}{\left(v_b^D\right)^2} . \frac{\partial^2 u_3}{\partial x_3^2} \tag{3.26}$$

Equation 3.26 is the classical known bar-vibration equation in mechanics. $v_{33}^D = \sqrt{\frac{1}{\rho . s_{33}^D}}$ denotes the wave propagation speed.
Solutions of this equation yield:

$$u_3(x_3, t) = (A_1 . \exp^{-j\alpha_3 . x_3} + A_2 . \exp^{j\alpha_3 . x_3}) . \exp^{j\omega t} \tag{3.27}$$

where α_3 is the wave number:

$$\alpha_3 = \frac{\omega}{v_{33}^D}$$

The constants A_1 and A_2 are determined with respect to boundaries conditions (Equation 3.19). It comes:

$$u_3(x_3, t) = \frac{v_{33}^D . d_{33} . D_0}{\varepsilon_{33} \omega} . \left[\sin(\alpha_3 . x_3) - \tan\left(\frac{\omega . L}{2 v_{33}^D}\right) . \cos(\alpha_3 . x_3) \right] . \exp^{j\omega t} \tag{3.28}$$

Elsewhere:

$$E_3 = -\frac{\partial V}{\partial x_3} \tag{3.29}$$

where V denotes the electrical potential. It comes:

$$\Delta V = \frac{L}{j\omega.(1-k^2).\varepsilon_{33}^T.\sigma}\left[1 - k^2.\left(\frac{\tan\left(\frac{\omega.L}{2v_{33}^D}\right)}{\frac{\omega.L}{2v_{33}^D}}\right)\right].j\omega.D_0.\sigma.\exp^{j\omega t} \tag{3.30}$$

where ΔV denotes the potential difference between the two electrodes. Hence, the electrical impedance of the stack is:

$$Z_{El} = \frac{\Delta V}{I} = \frac{L}{j\omega.(1-k^2).\varepsilon_{33}^T.\sigma}\left[1 - k^2.\left(\frac{\tan\left(\frac{\omega.L}{2v_{33}^D}\right)}{\frac{\omega.L}{2v_{33}^D}}\right)\right] \tag{3.31}$$

Expression 3.31 reveals resonance and anti-resonance frequencies (f_r^0 and f_a^0). The superscript 0 refers to the mechanical boundaries condition ($T_3(0) = T_3(L) = 0$). Theoretically the resonance frequency corresponds to $Z_{El} = 0$ and the anti-resonance frequency corresponds to $Z_{El} = \infty$. However in practice, the impedance only reaches local minimum and maximum respectively at these frequencies. A quality factor Q_M should therefore be attributed to the piezo-bar device. Another factor relative to electrical dissipations is called losses angle $\eta = \tan(\delta)$. It is determined at low frequencies.

The expression:

$$C_e^0 = \frac{(1-k^2).\varepsilon_{33}^T.\sigma}{L} \tag{3.32}$$

corresponds to the free-device capacitance at $2f_a^0$ i.e. it can be measured at $2f_a^0$. However, in practice it could be difficult to measure the capacitance at $2f_a^0$. Common equipments enable capacitance measurements for some hertz to about ten (10) kilo hertz.

Recalling power series development of $\frac{\tan x}{x} \simeq 1$ around 0, it comes that at low frequency one measures

$$C_e^1 = \frac{\varepsilon_{33}^T.\sigma}{L} = \frac{C_e^0}{1-k^2} \tag{3.33}$$

C_e^1 corresponds to the free-device capacitance at low frequency.

Hence:

$$Z_{El} = \frac{1}{j\omega.C_e^0}\left[1 - k^2.\left(\frac{\tan\left(\frac{\omega.L}{2v_b^D}\right)}{\frac{\omega.L}{2v_b^D}}\right)\right] \tag{3.34}$$

According to literature [59, 70, 13], one can deduce:

$$k^2 = \frac{\pi}{2}.\frac{f_r^0}{f_a^0}.\cot\left(\frac{\pi}{2}.\frac{f_r^0}{f_a^0}\right) \tag{3.35a}$$

$$\varepsilon_{33}^T = \frac{C_e^0.L}{(1-k^2).\sigma} \tag{3.35b}$$

$$s_{33}^E = \frac{1}{\rho(1-k^2)\left(2f_a^0.L\right)^2} \tag{3.35c}$$

$$d_{33} = \sqrt{k^2.s_{33}^E.\varepsilon_{33}^T} \tag{3.35d}$$

$$Q_M = \frac{1}{2\pi\left(f_r^0\right)Z_r C_e^1}\left(\frac{\left(f_a^0\right)^2}{\left(f_a^0\right)^2-\left(f_r^0\right)^2}\right) \tag{3.35e}$$

$$k_{31}^2 = \frac{A}{1+A} \tag{3.35f}$$

$$A = \frac{\pi}{2}\left(1+\frac{f_a^0-f_r^0}{f_r^0}\right)\tan\left(\frac{\pi\left(f_a^0-f_r^0\right)}{2f_r^0}\right) \tag{3.35g}$$

$$s_{11}^E = \frac{1}{\left(2f_r^0.a\right)^2} \tag{3.35h}$$

$$d_{31} = \sqrt{k_{31}^2.s_{11}^E.\varepsilon_{33}^T} \tag{3.35i}$$

where Z_r denotes the impedance at resonance.

In practice, in order to ensure the admitted assumptions, the measurements should be performed on piezo-bars of which the length is $= 5-10$ times higher than the lateral dimensions.

3.4 Experiments on samples: practical aspects

One usually find in literature generic setup for determining the frequencies of minimum and maximum impedance of piezo-bar samples and their corresponding magnitude. It is illustrated in Figure 3.3 drawn from [13].

First, the switch is set to position 1 (piezo line). Then, the oscillator frequency is varied until the multi-meter indicates a particular value (minimum or maximum). The corresponding frequencies and meter indications are noticed. Next, the switch is set to position 2. The calibrated resistor is adjust in order to obtain the previous noticed meter indication for the same frequency. This is the impedance magnitude at this frequency.

This setup could require a precision from the experimenter that general human does not have. Moreover this procedure is manual and that being so, it becomes quickly useless if one wants to plot the impedance. Automated acquisition and analysis tools are therefore required.

It is possible in certain conditions to realize a circuit for automatic impedance analysis. For this purpose we need a multi-meter, a function generator with frequency sweeping command, a precision shunt resistance, and acquisition cards with associated monitoring software. Figure 3.4 gives the references of the equipment that we use for experiments performed on HPSt 1000/35-25/80 a piezo-bar element supplied by Piezomechanik [71]. See Annexes B.

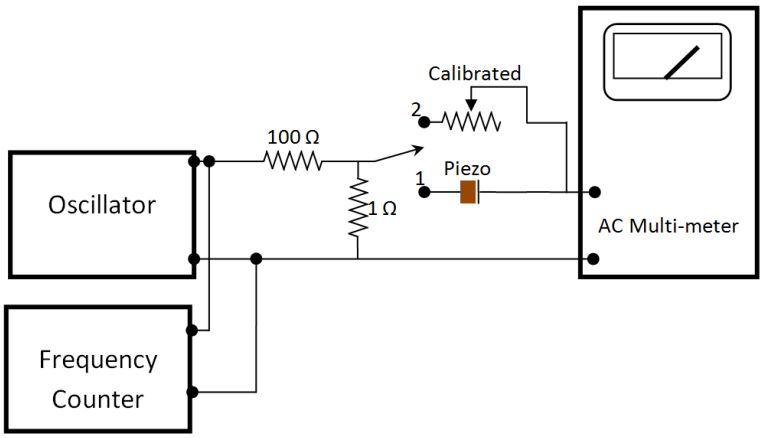

Figure 3.3: Piezo-bar characterization principle [13]

The multi-meter is used for capacitance, resistance and inductance measuring. The measurements are performed with the unloaded-device ($T_3(0) = T_3(L) = 0$). Measures are noticed in Table 3.2.

Measurement frequency f	Capacity C_f (μF)	Inductance L_f (mH)	Resistance
100 Hz	2.135	1185.200	Unstable value
120 Hz	2.131	824.200	Unstable value
1 kHz	2.100	11.801	Unstable value
10 kHz	2.541	0.108	Unstable value

Table 3.2: Electrical characteristics of the free-piezo-device

One can remark that the values measured depend all on the multi-meter signal frequency as predicted by Z_{El} in Equation 3.31. The table gives us an idea of C_e^0 which should be the global minimum of the free-device capacitance with respect to excitation frequency. According to the table $C_e^0 < 2.100\mu F$.

Elsewhere the piezo-device is not purely capacitive. It presents some inductance and resistance varying with the frequency but also on the time.

Next, setup in Figure 3.4 is realized in order to plot the impedance of the piezo-device with respect to frequency.

The setup is equivalent to the scheme in Figure 3.5

By means of the function generator (GFG), a $3V$ sinusoidal signal with slow sweeping frequency from $0.1Hz$ to $25000Hz$ is generating. The measurement of the shunt resistance voltage allows to analyze the response of the piezo-bar in terms of current. The shunt resistance is of high precision and non-inductive. The acquisition cards allow to continuously measure the voltages and Labview [75] software determines continuously their magnitudes and frequencies. In this configuration, it comes:

$$Z_{El} = \frac{(V_{GFG} - V_S) * R_S}{V_S} \tag{3.36}$$

Figure 3.6 depicts the experimental resonance curve obtained for the HPSt 1000/35-25/80 (a multi-layers device).

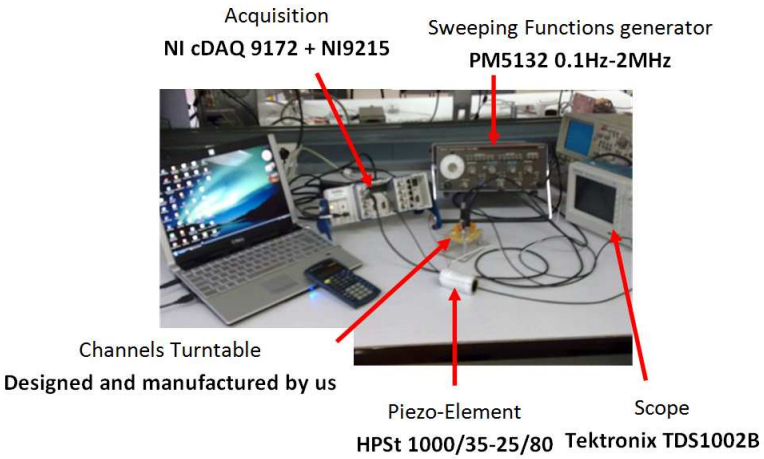

Figure 3.4: Frequencies measurements setup

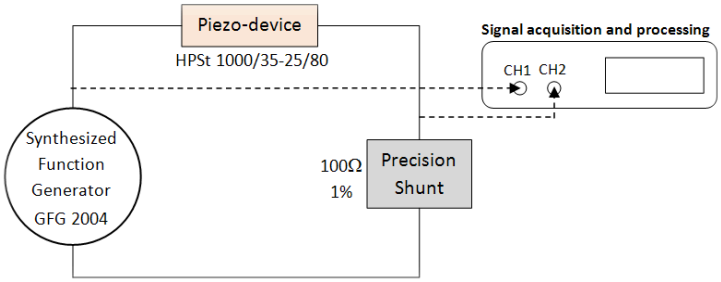

Figure 3.5: Frequencies measurements circuit

We then get:

$$\begin{aligned} f_r^0 &\simeq 12180Hz \\ f_a^0 &\simeq 14235Hz \end{aligned}$$

By means of a calliper and a digital weighing machine we measure $\sigma = 5.1 * 10^{-4}m^2$, $L = 0.072m$ and $M = 0.260kg$. So $\rho = 7.084 * 10^3 kg.m^{-3}$.

Then we deduct according to Equation 3.35:

$$k \simeq 0.55 \tag{3.37a}$$

$$s_{33}^E \simeq 48.694\mu m^2.N^{-1} \tag{3.37b}$$

At $2f_a^0 = 28470Hz$ we measure an impedance of $9.68dB$ and deduct

$$C_e^0 \simeq 1.84\mu F \tag{3.38}$$

And then

$$\varepsilon_{33}^T = \frac{C_e^0.L}{(1-k^2).\sigma} = 2.6 * 10{-}4\mu C\mu m^{-1}V^{-1} \tag{3.39a}$$

$$d_{33} = \sqrt{k^2.s_{33}^E.\varepsilon_{33}^T} = 0.06\mu mV^{-1} \tag{3.39b}$$

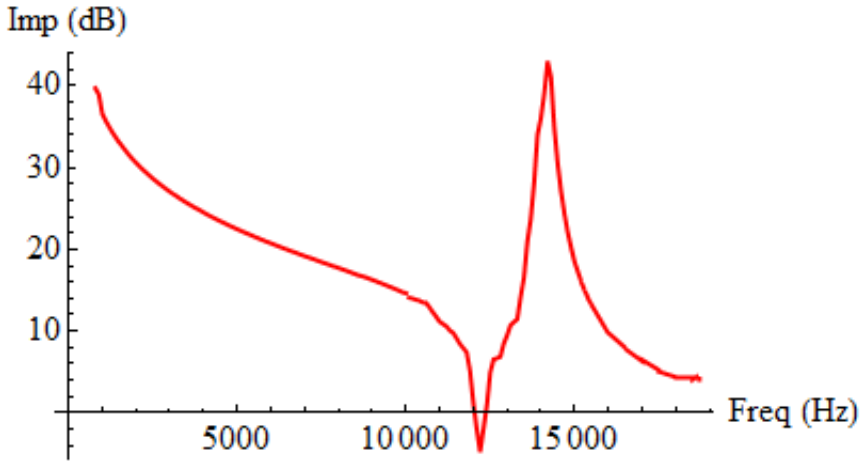

Figure 3.6: Electrical impedance evolution of HPSt 100/35-25/80

We should notice that the above suggested setup for the device characterizing shows its limit when the devices resonances frequencies are high. In this case high sampling frequency is required from the acquisition cards. Unfortunately these cards are generally limited around $140kHz$. For accurate analysis, in practice, it is recommended to sample above 10 times the maximal signal measured frequency [75]. However, for simple observation of resonances, we remark that Shanon's theorem is satisfying. Accordingly, at these frequency, at best one can measure signal of $70kHz$. Another limitation is observed when the magnitudes of minimum and maximum impedances greatly differ. In this case it is necessary that the analog measuring channels ($CH1$ and $CH2$) automatically adapt their resistances. However classical analog acquisition cards have fixed channels resistances.

Figure 3.7 gives an example of measurements performed on a small device P-885.90 (a multi-layers device) supplied by Physik Instrumente [62] with the same setup shown in Figure 3.4. One can remark that the resonance frequency is not roundly depicted while the anti-resonance frequency is.

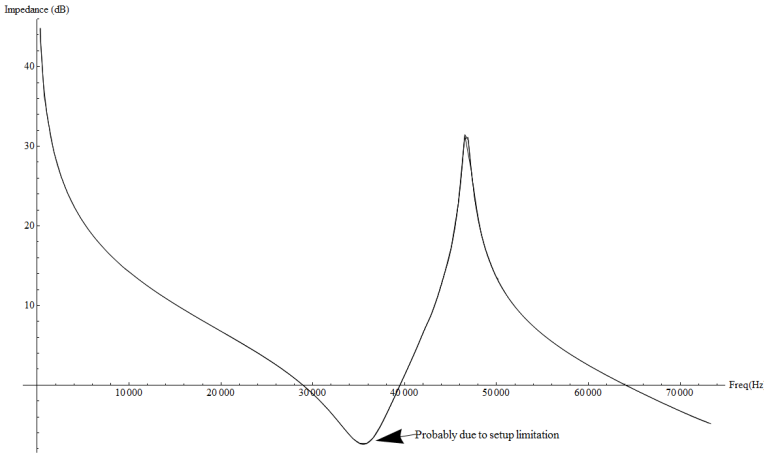

Figure 3.7: Electrical impedance evolution of P-885.90

All those difficulties encountered with the manual and the suggested automatic setups

(Figures 3.3 and 3.4) are sorted out by embedded electronic equipments. Precision impedance analyzers are nowadays commercialized. They can automatically adapt the analog inputs resistances and their sampling frequency can reach hundreds Mega Hertz. However, we do not have at our disposal such an instrument.

3.5 Constitution Vs Engineer parameters

The parameters in Equation 3.10 and 3.35 could be named *constitution parameters*. They are required when ordering custom-tailored device from piezoelectric manufacturers. By contrast, in trading there is another technical language. For example, in data sheets supplied by piezo-devices distributors, one deals with the device stiffness instead of the constitutive material flexibility coefficient. The parameters used in trading could be named *engineer parameters*. Constitution parameters and engineer parameters are linked by the device dimensions and density.

No matter with the superscripts and subscripts, a flexibility s (constitution parameter) allows to define a stiffness K (engineer parameter) as follows:

$$K = \frac{\sigma}{s.L} \tag{3.40}$$

where σ is the device cross-sectional area and L the device dimension in the same direction as s.

A dielectricity ε (constitution parameter) allows to deduct a capacitance C (engineer parameter) as follows:

$$C = \frac{\varepsilon.\sigma}{L} \tag{3.41}$$

Concerning piezoelectricity coefficient d, it can be assimilated to an electromechanical or mechanic-electrical capacitance because it links an electrical charge to a mechanical force or a displacement to an electrical force (voltage).

In bar operating mode, one is especially interested in the longitudinal behaviour of the piezo-device. However, not all the parameters used in Equation 3.10 and 3.35 step in this longitudinal movements. s_{11}, s_{13}, d_{31} and by the way k_{31} all step in Poisson's effect: lateral striction orthogonal to the polling axis. However this effect is so smaller that a classical assembly set takes them into account (Figure 3.8). Moreover it can constitute cooling channel for the piezo-device.

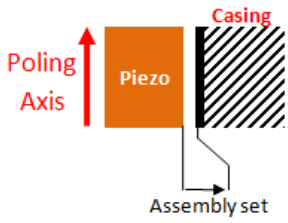

Figure 3.8: Assembly set of about 1 to 5μm for not considering Poisson's effect

Therefore we only need s_{33}, d_{33}, ε_{33}, k_{33}...

As we noticed it in above sections, the electric characteristics of the piezo-device depend on its mechanical boundaries conditions. Conversely, the mechanical characteristics depend

on the electrical conditions. For each of them one remarks two extremal configurations. We sum up these configurations in Table 3.3.

	Device capacitance	Device stiffness
Upper extreme	Free-device Maximal capacitance 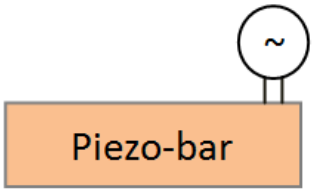 $C_e^T = \frac{\varepsilon_{33}^T.\sigma}{L}$	Opened-electrodes Maximal stiffness 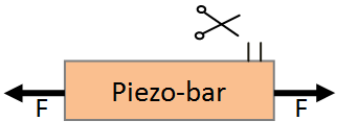 $K_m^D = \frac{\sigma}{s_{33}^D.L}$
Lower extreme	Blocked-device Minimal capacitance 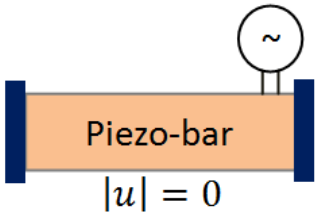 $C_e^S = \frac{\varepsilon_{33}^S.\sigma}{L}$	Short-circuit-electrodes Minimal stiffness 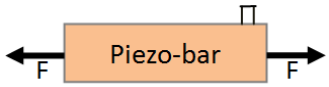 $K_m^E = \frac{\sigma}{s_{33}^E.L}$
Intermediary values	Between the two extremes $C_e^S < C < C_e^T$	Between the two extremes $K_m^E < K < K_m^D$

Table 3.3: Piezo-bar extremal configurations

According to experimental results in Section 3.4, for the HPSt 1000/35-25/80 device we have:

$$K_m^E = 165.165 N\mu m^{-1} \tag{3.42a}$$

$$K_m^D = \frac{K_m}{1-k^2} \tag{3.42b}$$

$$C_e^T = 1.84\mu F \tag{3.42c}$$

$$C_e^S = C_e(1-k^2) \tag{3.42d}$$

These should be compared to the data sheets provided by the device distributor (Table 3.4).

After a comparison of experimental values and data sheets, we could conclude that the supplier Piezomechanik has specified in the data sheets the opened-circuit stiffness and the blocked-device capacitance. This was not clear initially.

We then decide to perform other experiments on the P-885.90 device (Physik Instrumente). Table 3.5 compares experimental results to the supplier data.

According to Table 3.5 it seems that Physik Instrumente specify in their data the shorted electrodes device stiffness and the free-device capacitance, contrary to Piezomechanik. We check the information beside a technic representative of Physik Instrumente in France.

Concerned characteristic	Experiments	Data sheets
Resonant frequency	$f_r^0 = 12180Hz$ (Free device resonance)	$f_r^* = 12000Hz$
Anti-resonant frequency	$f_a^0 = 14235Hz$ (Free device anti-resonance)	
Mechanics	$K_m^E = 165.165N\mu m^{-1}$ $K_m^D = 211N\mu m^{-1}$	$K = 250N\mu m^{-1}$
Electrical	$C_e^T = 1.84\mu F$ $C_e^S = 1.27\mu F$	$C = 1.3\mu F$
Piezoelectric	(At about 3 V) $d = 0.06\mu mV^{-1}$	(At 1000 V) 0.08 to $0.105\mu mV^{-1}$

Table 3.4: HPSt 1000/35-25/80 (Piezomechanik): Experiments Vs Data sheets

Concerned characteristic	Experiments	Data sheets
Resonant frequency	$f_r^0 = 35000Hz$ (Free device resonance)	$f_r^* = 40000Hz \pm 20\%$
Anti-resonant frequency	$f_a^0 = 46500Hz$ (Free device anti-resonance)	
Mechanics	$K_m^E = 32.228N\mu m^{-1}$ $K_m^D = 62.445N\mu m^{-1}$	$K = 25N\mu m^{-1}$
Electrical	$C_e^T = 3.12\mu F$ $C_e^S = 1.61\mu F$	$C = 3.1\mu F \pm 20\%$
Piezoelectric	(At about 3 V) $d = 0.21\mu mV^{-1}$	(At 100 V) $0.32\mu mV^{-1} \pm 20\%$

Table 3.5: P-885.90 (Physik Instrumente): Experiments Vs Data sheets

The comparison highlights a lack of clearness in the data sheets provided by piezo-device suppliers. Is there any standard on parameters that should be given in data sheets?

Elsewhere, one can remark differences between the experimental K_m^D, C_e^S and the suppliers data K, C. Why this? Which of the experimental values or the suppliers data are the most realistic? Analysis of suppliers data, shows that they always specify a margin ($\pm 10 - 20\%$) for the blocked-device capacitance. By contrast, they do not specify a margin for the opened-circuit device stiffness. Would this mean that they are confident in their specified opened-circuit stiffness and less in the measured capacitance? So why do we find nearly the same capacitance but a different stiffness?

Answers could be found in the theory we followed in our approach. According to that, we set:

$$\begin{aligned} s_{33}^D &= \frac{1}{\rho(2f_a^0.L)^2} \\ s_{33}^E &= \frac{s_{33}^D}{1-k^2} \end{aligned}$$

This supposed that the anti-resonant point could be assimilated to an opened-electrodes configuration and the resonant point assimilated to shorted electrodes configuration. This

would be exact if the device's impedance were really infinite at anti-resonance and zero at resonance. However one can remark in Figure 3.6 that the impedance is in fact finite at anti-resonance and different from zero at resonance. Therefore the opened-electrodes stiffness deducted for HPSt 1000/35-25/80 (Table 3.4) is in fact at bit lower than the actual opened-circuit stiffness and the shorted electrodes stiffness deducted for P-885.90 (Table 3.5) is a bit higher than the actual device short-circuit stiffness.

Concerning the capacitance, it is technically impossible to ensure good accuracy for its measurement. This could explain why the supplier specify a margin for the capacitance but not for the stiffness.

The last observation concerns the piezoelectric coefficient. As one can deduct it from the comparison between the experimental values and the suppliers data, the piezoelectric coefficient varies with respect to the applied voltage (Table 3.4 and Table 3.5). The suppliers generally give the value at nominal voltage.

3.6 Trade rule for rapid choice of a piezo-device

It is useful to have a formalized trade-rule that can be used for quick piezo-device choice upstream from piezo-using-systems design cycle. In this stage of design, decision are made despite lack of specification [65, 76]. For that reason one could content themselves with basic model around a nominal operating point. Calculi could be performed in statics.

3.6.1 Static basic model

From now on, we only deal with piezo-bar devices in Figure 3.2. Since then, we can conscientiously omit the subscripts and superscripts used in Equation 3.11 without no risk of confusion. So, we shall simply write:

$$S = s.T + d.E \tag{3.43a}$$

$$D = d.T + \varepsilon.E \tag{3.43b}$$

The lower face ($x_3 = 0$) is supposed to clamped and we are interested in the displacement of the upper face ($x_3 = L$). In static one has:

$$\frac{\partial^2 u}{\partial t^2} = \frac{\partial T}{\partial x_3} \simeq 0 \tag{3.44}$$

where u denotes the longitudinal displacement of the upper face. In harmonics the condition 3.44 implies that the frequency must be too smaller than the resonant frequency of the device.

In this condition we have:

$$\int_0^L S(x_3)dx_3 = s\int_0^L T(x_3)dx_3 + d\int_0^L E(x_3)dx_3 \tag{3.45a}$$

$$\int\int_{x_3=L} Ddx_1dx_2 = d\int\int_{x_3=L} T(x_3 = L)dx_1dx_2 + \varepsilon\int\int_{x_3=L} E(x_3 = L)dx_1dx_2 \tag{3.45b}$$

T, E, S and D can only depend on x_3. Therefore it comes

$$D(x_3 = L)\sigma = d\sigma T(x_3 = L) + \varepsilon\sigma E(x_3 = L) \tag{3.46}$$

$q = D(x_3 = L)\sigma$ is the electric charges collected on the electrode, $F = T(x_3 = L)\sigma$ the force applied on the upper face, $V(x_3 = L) - V(x_3 = 0) = \int_0^L E(x_3)dx_3$ where V represents the potential of the face. We could fix without lost of generality $V(x_3 = L) = V$ and $V(x_3 = 0) = 0$.

According to Equation 3.44 the quantity T is constant. Then it comes:

$$\begin{array}{rcl} u & = & \frac{s.L}{\sigma}.F + d.V \\ q & = & d.F + \frac{\varepsilon.\sigma}{L}.V \end{array} \tag{3.47}$$

$\frac{\sigma}{s.L}$ is the short-circuit stiffness K_m and $\frac{\varepsilon.\sigma}{L}$ is the free-device capacitance C_e.

By making the ratio $\sqrt{\frac{d^2.K_m}{C_e}}$ one finds the above defined electromechanical coupling coefficient k.

$$\begin{array}{rl} u & = \frac{F}{K_m} + d.V \\ q & = d.F + C_e.V \end{array} \tag{3.48}$$

One could also use the opened electrodes stiffness K_m^D and the blocked-device capacitance C_e^S.

$$\begin{array}{rl} C_e & = \frac{C_e^S}{1-k^2} \\ K_m & = (1-k^2)K_m^D \end{array} \tag{3.49}$$

where:

$$k^2 = \frac{d^2.K_m}{C_e} \tag{3.50a}$$

$$k^{*2} = \frac{d^2.K_m^D}{C_e^S} \tag{3.50b}$$

$$k^2 = \frac{1 + 2k^{*2} - \sqrt{1 + 4k^{*2}}}{2k^{*2}} \tag{3.50c}$$

We denote k^* a pseudo coupling coefficient obtained directly from suppliers data.

A piezo-bar can be used as an actuator or as a sensor. In the first case the device converts an electric energy in order to act mechanically on a structure whereas in sensing case, the device converts a mechanical energy into electrical energy. It is also possible to use the device simultaneously as actuator or sensor. Regardless the configurations, one distinguishes an electrical port (Ep) and two mechanical ports (Mp_1 and Mp_2). The subscripts 1 and 2 refer respectively to the two faces of the piezo-bar. However in our case we clamp the lower face. So it remains only one mechanical port Mp.

Any physical port is constituted of two energy variables: a generalized effort variable and a generalized displacement variable. Hence, a notion of causality emerges too.

In actuating mode, one can control the piezo-bar either by voltage or by electric charge. However, the second option is difficult to realize because of piezo-devices small capacities. They hardly bear thousandth of coulombs whereas they easily support hundreds of volts. This explains the common adoption of voltage control. Therefore, the voltage (electric effort) is imposed at the electrical port of the device; in response, the device imposes the charge (electric displacement). Concerning the mechanical port, usually, the structure imposes the force (mechanical effort) to the piezo-bar which in its turn imposes to the structure a displacement. However, the inverse case exists.

In sensing mode there is no longer question of electrical control but rather electrical information acquisition. The device senses the force or the displacement and accordingly gives a voltage as output.

3.6.2 Methodology

Assuming that for a given mechatronic system design one firstly performed a benchmark and decided to use a piezo-bar device for actuating purpose. The requirements and specifications should provide:

1. The nominal displacement in the form $u_{nom} = \frac{u_{cc}}{2}(u_d + \sin(2\pi f_{nom}t + \phi))$, where u_{cc} denotes the desired displacement crete-to-crete amplitude, u_d refers to mean of the signal divided by u_{cc}, f_{nom} denotes the nominal operating frequency
2. The load to displace F_{Load} at u_{nom} and the blocked-force $F_{Blocked}$ $(u = 0)$
3. The desired resonance frequency f_r^0

From these specifications we can directly calculate the needed stiffness K_m. It is calculated for $u_d = 1$

$$K_m = \frac{F_{Blocked}}{u_{cc}} \tag{3.51}$$

Then we should choose the driving voltage $V_{nom} = \frac{V_{cc}}{2}(u_d + \sin(2\pi f_{nom}t + \phi))$ and the device capacitance C_e. For this purpose we can base on the potential energy stocked into the capacitor. This energy in ideal case equals the energy stocked in the a spring of stiffness K_m:

$$\frac{1}{2}.K_m.u_{rms}^2 = \frac{1}{2}.C_e.V_{rms}^2 = \frac{\xi}{2} \tag{3.52}$$

where the subscript rms means root mean square. One has:

$$\begin{aligned} u_{rms} &= \frac{u_{cc}\sqrt{(1+2u_d^2)}}{2\sqrt{2}} \\ V_{rms} &= \frac{V_{cc}\sqrt{(1+2u_d^2)}}{2\sqrt{2}} \end{aligned}$$

So:

$$C_e.V_{rms}^2 = \xi \tag{3.53}$$

The unique Equation 3.53 does not allow to make a decision. At least a second equation or choice function is necessary.

Elsewhere due to electrical losses angle $\tan(\delta)$, the required power to drive the piezo-device is:

$$Power = 2\pi \tan(\delta).f_{nom}.C_e.V_{rms}^2 \tag{3.54}$$

Equation 3.54 may help in the voltage generator choice.

Once V_{rms} is fixed, we can determine the nominal piezoelectric constant d:

$$d = \frac{u_{rms}}{V_{rms}} = \frac{u_{cc}}{V_{cc}} \tag{3.55}$$

Next, one has to choose the device's dimensions: L the bar length, a the lateral dimension. For some of the above equations validity and the device stability, it is recommended:

$$L = 5 \text{ to } 10\ a \tag{3.56}$$

Moreover one has to choose between circular or rectangular piezo-bar or tubular piezo-bar. The architecture choice is rather open-minded.

Lastly one has to determine the constitutive parameters

$$s_{33}^{E} = \frac{\sigma}{K_m.L} \tag{3.57a}$$

$$\varepsilon = \frac{C_e.L}{\sigma} \tag{3.57b}$$

σ is the device cross-section function of a.

3.7 Conclusion

Through this chapter, we saw that anyone could easily characterize a piezo-bar device; the measurements principle is almost common. However different equipments are utilizable. Elsewhere, two experimental cases (HPSt 1000/35-25/80 and P-885.90) were compared to information given by the devices distributors in their data sheets. This allows us to emphasize on the device parameters variability with respect to the boundaries mechanical and electrical conditions.

The exposed theory were based on simplifying assumptions which should be checked in the next chapters.

Chapter 4

Modeling of piezo-bar actuators dynamics

4.1 Résumé du chapitre en Francais

Dans ce chapitre ne traitons essentiellement que de l'utilisation des piézoelectriques en régime dynamique.

L'approche de Butterworth-Van Dyke admise par le standard IEEE [43] et illustrée par la Figure 4.1, vise à modéliser le comportement électrique d'un actionneur piézoélectrique. C_e représente la capacité électrique de l'actionneur et C_m-R_m-L_m la partie mécanique. Cette approche est valide autour d'une résonance mais ne prend pas en compte d'autres modes en ajoutant des branches mécaniques supplémentaire.

Cependant, d'une façon plus générale, un actionneur piézoélectrique comporte non seulement un port électrique (comme dans le cas de Butterworth-Van Dyke) mais aussi deux ports mécaniques.

C'est dans cette logique que le modèle de Mason est présenté (voir Figure 4.2). Il est construit à partir de l'étude de la propagation d'une onde progressive le long d'un barreau. Pour ce faire, on considère les équations 4.1.

$$\begin{array}{lcl} S_3 & = & s_{33}^E.T_3 + d_{33}.E_3 \\ S_3 & = & \frac{\partial u_3}{\partial x_3} \\ D_3 & = & d_{33}.T_3 + \varepsilon_{33}^T.E_3 \\ \frac{\partial D_3}{\partial x_3} & = & 0 \Rightarrow D_3 = D_0.\exp^{j\omega t} \\ \rho\frac{\partial^2 u_3}{\partial t^2} & = & \frac{\partial T_3}{\partial x_3} \end{array} \tag{4.1}$$

Ces dernières permettent d'établir l'équation de propagation 4.8, où A_1 et A_2 sont des constantes qui dépendent des conditions aux limites.

$$u(x_3,t) = (A_1.\exp^{-j\alpha_3.x_3} + A_2.\exp^{j\alpha_3.x_3}).\exp^{j\omega t} \tag{4.2}$$

Dans un premier temps nous supposons que l'actionneur est fixé à une table. Dans ce cas un seul port mécanique est à considérer. Ce qui nous permet d'obtenir l'équation 4.3.

$$\begin{array}{lcl} u_L & = & \frac{1-k^2}{1-k^2\frac{\tan(\alpha_3 L)}{\alpha_3 L}}.\frac{\tan(\alpha_3 L)}{\alpha_3 L}\left(\frac{F_L}{K_m} + d.V\right) \\ q & = & \frac{1-k^2}{1-k^2\frac{\tan(\alpha_3 L)}{\alpha_3 L}}\left(\frac{\tan(\alpha_3 L)}{\alpha_3 L}.d.F_L + C_e.V\right) \end{array} \tag{4.3}$$

On obtient alors le modèle de Mason de la Figure 4.5.

Le premier inconvénient de ce développement mathématique, est qu'il ne prédit les différentes résonances à des intervalles réguliers comme le montre la Figure 4.6, ce qui est en contradiction avec les observations effectuées sur le HPSt 1000/35-25/80 en Figure 4.7. Précisons que les expériences et simulations ont été réalisées sur l'actionneur non-contraint. Le montage expérimental est celui décrit dans la section 3.4. La génération du signal est faite directement par le générateur de fonction à une fréquence d'échantillonnage de 2 MHz. L'acquisition quant à elle est faite à une fréquence d'échantillonnage de 120 kHz.

Le second inconvénient vient du fait que ce modèle aura toujours besoin de connaître à l'avance la fréquence d'excitation, ce qui n'est pas pratique pour une modèle de contrôle de commande.

Ces constats nous ont poussés à utiliser l'approche des "paramètres concentrés". Cette dernière a été utilisée par [39, 40, 41].

Le schéma analogique correspondant est donné par la Figure 4.11. Ce dernier est alors traduit en bond graph, puis sera complèté par les éléments amortissants.

Ainsi, ce premier modèle permet de n'avoir que le premier mode de vibration. Afin d'avoir les modes suivants, nous adoptons la méthode de "distribution des paramètres" à l'instar de [41, 77]. Cette méthode est semblable aux méthodes d'analyse par éléments finis. Cependant, plutôt que d'avoir une distribution régulière de la masse, la distribution dans notre cas est calculée en accord avec les observations expérimentales. En effet, une distribution régulière de la masse entrainerait une apparition de résonances à interavalles réguliers, ce que nous avions déjà remis en cause.

L'application au piézoélectrique nous a permis d'obtenir (voir Figure 4.19) une réponse fréquentielle "collant" au mieux aux expériences.

Ensuite, nous avons proposé une prise en compte des systèmes de précharge dynamique (Figures 4.20, 4.21 et 4.22). Nous avons ensuite étudié l'influence de la précharge du piézo sur la dynamique de la structure. Nous faisons varier la précharge à l'aide de clinquants. La Figure 4.25 montre la variation de l'impédance du piézo-actionneur en fonction de la précharge. Nous pouvons remarquer qu'elle n'influence pas la fréquence de résonance mais plutôt l'intensité de celle-ci. En fait, plus la précharge augmente, plus la résonance est aigue.

In this chapter we shall deal essentially with modeling and use of piezo-bar devices in dynamics. In a first step, we shall begin by the configuration in which the device is fixed to a support. Thereby the device will be considered as a two ports device Ep and Mp as in Section 3.6.1. Next we shall treat the general case in which the device has three ports Ep, Mp_1 and Mp_2.

4.2 Piezo-device dynamics phenomenological models: an overview

In literature one finds various approaches for piezo-device dynamics analysis. Some of them are interested either in electric behaviour or in mechanical behaviour while others deal with electromechanical response.

Butterworth-Van Dyke approach in Figure 4.1 aims to depict the electric behaviour of any piezo-device.

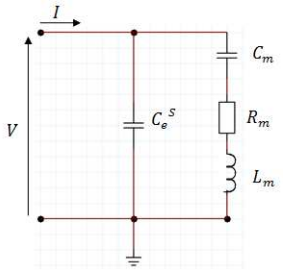

Figure 4.1: Butterworth-Van Dyke model

C_e^S represents the blocked-device capacitance. The stocked energy in this capacitance is not converted into mechanical energy but rather stocked into an electrostatic form. The branch C_m-R_m-L_m represents the mechanical part. This approach as well as many others suppose the piezo-device parameters to be independent of frequency. As mentioned in [78] in reference to [43], this model is valid near the resonance frequency and only if the device's vibration modes are isolated from each other. However in the case of several close vibration modes, one could connect in parallel additional branches C_m-R_m-L_m [79].

In the case that one needs to depict the piezo-device electromechanical character, it is mandatory to consider mechanical terminal (s).

Any electromechanical equivalent model is based on Mason's approach. It consists in applying traditional electromechanical analogies with the piezoelectric equations and Newton's laws of motion [80]. Any other analogical models are improvements of Mason's approach [40, 81], as developed in the Section bellow.

4.3 Mason modeling principle

Mason's approach consists in transforming the constitutive equations and the device boundaries limits in order to obtain a six-pole device shown in Figure 4.2 [59].

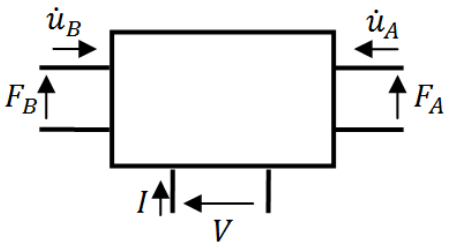

Figure 4.2: Mason modeling principle

In this figure, $\dot{u}$ denotes the velocity of the concerned face and I denotes the electric current. We recall that in harmonics one has:

$$\begin{aligned} \dot{u} &= j.\omega.u \\ I &= j.\omega.q \end{aligned}$$

In the case of clamped device we have:

$$\begin{aligned} \dot{u}_B &= 0 \\ \dot{u}_A &= \dot{u}_L \\ F_A &= F_L \end{aligned}$$

where u_L denotes the displacement of the upper face.
Therefore the Mason model is simplified as shown in Figure 4.3

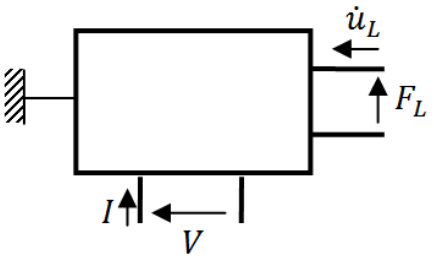

Figure 4.3: Mason modeling when one face is fixed

The matrix relations of Figure 4.3 is:

$$F_L = Z_u \dot{u}_L + Z_{uI} I \tag{4.4a}$$
$$V = Z_{uI} \dot{u}_L + Z_I I \tag{4.4b}$$

4.4 Basic dynamics equations

Basic laws for narrow description of piezo-bar devices is the one in Equation 4.5.

$$\begin{aligned} S_3 &= s_{33}^E.T_3 + d_{33}.E_3 \\ D_3 &= d_{33}.T_3 + \varepsilon_{33}^T.E_3 \end{aligned} \tag{4.5}$$

As noticed in the previous Chapter, the choice of (E, T) as independent variable instead of (D, S) is motivated by the type of the device control. Indeed, since we are mainly dealing with actuating function, (E, T) are the stimuli and (D, S) are the response.

It is sufficient in static or quasi-static functioning. However, in dynamics, it should be completed with Newton motion laws as follows:

$$\begin{array}{lcl} S_3 & = & s_{33}^E.T_3 + d_{33}.E_3 \\ S_3 & = & \frac{\partial u_3}{\partial x_3} \\ D_3 & = & d_{33}.T_3 + \varepsilon_{33}^T.E_3 \\ \frac{\partial D_3}{\partial x_3} & = & 0 \Rightarrow D_3 = D_0.\exp^{j\omega t} \\ \frac{\partial D_3}{\partial x_3} & = & 0 \Rightarrow \frac{\partial E_3}{\partial x_3} = -\frac{d_{33}}{\varepsilon_{33}^T}.\frac{\partial T_3}{\partial x_3} \\ \rho\frac{\partial^2 u_3}{\partial t^2} & = & \frac{\partial T_3}{\partial x_3} \end{array} \tag{4.6}$$

T_3 is no longer constant along the bar.

Afterwards in this chapter we conscientiously omit the superscripts as well as the subscripts. Further indications will be provided only when it is necessary to avoid any confusion.

4.5 Continuous mass approach

4.5.1 Assumption of continuous mass distribution

The multi-layers piezoelectric device is considered as a one bulk element with continuous and homogeneous mass distribution (Figure 4.4).

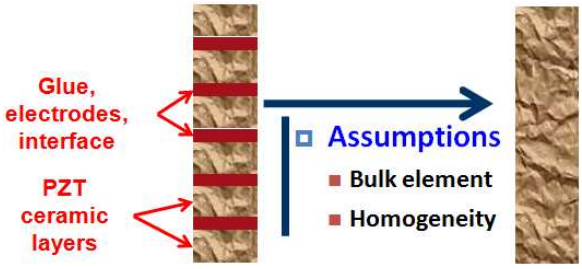

Figure 4.4: Mason modeling when one face is fixed

4.5.2 Wave propagation

Because of the electromechanical coupling character, a combination of wave propagation in elastic solids [82, 83, 84] with dielectricity and piezoelectricity laws is necessary to determine mathematical dynamic model of the piezo-bar device [85].

From Equation 4.6 one gets 4.7 describing the propagation of linear longitudinal wave [86] in the piezo-solid.

$$\frac{\partial^2 u}{\partial t^2} = \frac{1}{\rho s_{33}^E(1-k^2)}.\frac{\partial^2 u}{\partial x_3^2} \tag{4.7}$$

Let us denote:

$$k^2 = \frac{d^2}{\varepsilon.s}$$

Since $s_{33}^E(1-k^2) = s_{33}^D$, the expression $\frac{1}{\rho s_{33}^E(1-k^2)}$ corresponds to the wave propagation speed at constant induction (v_{33}^D).

$$v_{33}^D = \sqrt{\frac{1}{\rho s(1-k^2)}}$$

Solution of Equation 4.7 takes the form:

$$u(x_3,t) = (A_1.\exp^{-j\alpha_3.x_3} + A_2.\exp^{j\alpha_3.x_3}).\exp^{j\omega t} \tag{4.8}$$

where ω denotes the angular frequency of the wave and α_3 the wave number:

$$\alpha_3 = \frac{\omega}{v_{33}^D}$$

Constants A_1 and A_2 depend on electromechanical boundaries conditions. To remain general as in [59] one could set:

$$T(0,t) = T_0 \tag{4.9a}$$
$$T(L,t) = T_L \tag{4.9b}$$

However, we assume that the bar is clamped at its lower face. So we can set:

$$u(0,t) = 0 \tag{4.10a}$$
$$T(L,t) = T_L \tag{4.10b}$$

In this last case, it comes:

$$A_2 = -A_1 \Rightarrow u(x_3,t) = A_1\left(\exp^{-j\alpha_3.x_3} - \exp^{j\alpha_3.x_3}\right).\exp^{j\omega t} \tag{4.11}$$

Conventionally one has [87]:

$$S = \frac{\partial u}{\partial x_3}$$
$$E = -\frac{\partial V}{\partial x_3}$$

where V denotes the electrical potential. One gets:

$$\frac{\partial u}{\partial x_3} = s.T - d.\frac{\partial V}{\partial x_3} \tag{4.12a}$$
$$D = d.T - \varepsilon.\frac{\partial V}{\partial x_3} \tag{4.12b}$$

Then:

$$T(x,t) = \frac{1}{s.(1-k^2)}\left[\frac{\partial u}{\partial x_3} - \frac{d}{\varepsilon}.D\right]$$

$k^2 = \frac{d^2}{\varepsilon.s}$; $s^D = (1-k^2)s$ corresponds to the material flexibility at constant electric induction.

So:

$$T(x,t) = \frac{\exp^{j\omega t}}{s.(1-k^2)} \left[-2j\alpha_3.A_1.\cos(\alpha_3.x_3) - \frac{d}{\varepsilon}.D_0 \right] \tag{4.13}$$

$\Rightarrow$

$$A_1 = \frac{1}{2j\alpha_3 \cos(\alpha_3 L)} \left[-\frac{d}{\varepsilon}.D_0 - \frac{s(1-k^2)}{\exp^{j\omega t}} T_L \right] \tag{4.14}$$

Since $D_0.\exp^{j\omega t} = D$.

$$u(x_3,t) = \frac{\sin(\alpha_3 x_3)}{\alpha_3 \cos(\alpha_3 L)} \left[s(1-k^2).T_L + \frac{d}{\varepsilon}.D \right] \tag{4.15}$$

Therefore the displacement $u(L,t) = u_L(t)$ of the upper face yields:

$$u_L(t) = \frac{\sin(\alpha_3 L)}{\alpha_3 \cos(\alpha_3 L)} \left[s(1-k^2).T_L + \frac{d}{\varepsilon}.D \right]$$

This leads to:

$$u_L(t) = \frac{\tan(\alpha_3 L)}{\alpha_3 L} \left[\frac{s(1-k^2).L}{\sigma}.\sigma T_L + d.\frac{L}{\varepsilon.\sigma}.\sigma.D \right] \tag{4.16}$$

where σ denotes the device's cross-sectional area.

One can recognize:

$K_m = \frac{\sigma}{s.L}$ the short-circuit device stiffness and $C_e = \frac{\varepsilon.\sigma}{L}$ the unloaded device capacity as defined in Section 3

$q = D\sigma$ is the electric charges collected at the electrode and $F_L = T_L\sigma$ the force applied on the upper face.

Then:

$$u_L(t) = \frac{\tan(\alpha_3 L)}{\alpha_3 L} \left[F_L.\frac{(1-k^2)}{K_m} + d.\frac{q}{C_e} \right] \tag{4.17}$$

Elsewhere, if we consider that the electric potential of the lower face is our reference ($V(0,t) = 0$), one can verify that:

$$V(t) = \frac{\tan(\alpha_3 L)}{\alpha_3 L}.\frac{1}{C_e}.d.F_L - \frac{q}{(1-k^2)C_e} \left(1 - k^2 \frac{\tan(\alpha_3 L)}{\alpha_3 L} \right) \tag{4.18}$$

where V is the electric potential of the upper face.

Finally:

$$\begin{aligned} u_L &= \frac{1-k^2}{1-k^2\frac{\tan(\alpha_3 L)}{\alpha_3 L}}.\frac{\tan(\alpha_3 L)}{\alpha_3 L} \left(\frac{F_L}{K_m} - d.V \right) \\ q &= \frac{1-k^2}{1-k^2\frac{\tan(\alpha_3 L)}{\alpha_3 L}} \left(\frac{\tan(\alpha_3 L)}{\alpha_3 L}.d.F_L - C_e.V \right) \end{aligned}$$

We should notice that in Chapter 3, we set $E = +\frac{\partial V}{\partial x_3}$ instead of $E = -\frac{\partial V}{\partial x_3}$. This explain the negative sign on V in Equation 4.19. This is only convention matter. However in order to avoid sign handling we shall adopt the first expression. This does not weaken our developments.

$$\begin{aligned} u_L &= \frac{1-k^2}{1-k^2\frac{\tan(\alpha_3 L)}{\alpha_3 L}}.\frac{\tan(\alpha_3 L)}{\alpha_3 L} \left(\frac{F_L}{K_m} + d.V \right) \\ q &= \frac{1-k^2}{1-k^2\frac{\tan(\alpha_3 L)}{\alpha_3 L}} \left(\frac{\tan(\alpha_3 L)}{\alpha_3 L}.d.F_L + C_e.V \right) \end{aligned} \tag{4.19}$$

4.5.3 Application to Mason's model

From Equation 4.19 we get:

$$F_L = \frac{\alpha_3 L}{\tan(\alpha_3 L)}.\frac{K_m}{1-k^2}.u_L - \frac{d.K_m}{(1-k^2).C_e}.q \tag{4.20a}$$

$$V = -\frac{d.K_m}{(1-k^2).C_e}.u_L + \frac{1}{(1-k^2).C_e}.q \tag{4.20b}$$

We then deduct:

$$F_L = \frac{\alpha_3 L}{\tan(\alpha_3 L)}.\frac{K_m}{1-k^2}.\frac{\dot{u}_L}{j\omega} - \frac{d.K_m}{(1-k^2).C_e}.\frac{I}{j\omega} \tag{4.21a}$$

$$V = -\frac{d.K_m}{(1-k^2).C_e}.\frac{\dot{u}_L}{j\omega} + \frac{1}{(1-k^2).C_e}.\frac{I}{j\omega} \tag{4.21b}$$

Therefore

$$Z_u = \frac{\alpha_3 L}{\tan(\alpha_3 L)}.\frac{K_m}{j\omega(1-k^2)} \tag{4.22a}$$

$$Z_I = \frac{1}{j\omega(1-k^2).C_e} \tag{4.22b}$$

$$Z_{uI} = -\frac{d.K_m}{j\omega(1-k^2).C_e} \tag{4.22c}$$

One recognizes in these equations $C_e^S = (1-k^2)C_e$ and $K_m^D = \frac{K_m}{1-k^2}$ defined in Chapter 3 respectively as the blocked-device capacitance and the opened electrode stiffness. Mason approach leads to the analogical model in Figure 4.5.

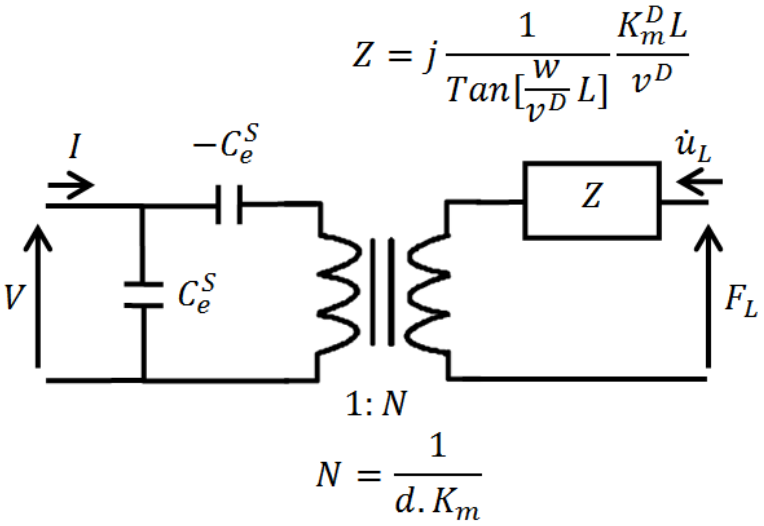

Figure 4.5: Analogical interpretation associated to Mason approach

Through a virtual transformer element, this analogical interpretation reveals the converting function of a piezo-device. It converts an electrical input into mechanical output and vice-versa. In addition the analogical interpretation is distinguishable from ordinary

electrical circuit. As a matter of fact, one can remark the appearance of a negative capacity in the scheme. This can present computation troubles [88].

Since $\alpha_3 = \frac{\omega}{v^D} = \omega\sqrt{\rho s^D}$, one can remark that the mechanical port impedance Z involves both the stiffness and the inertia (through ρ).

According to this model, the device frequency response with respect to an input voltage is depicted in Figure 4.6. The simulation has been performed using HPSt 1000/35-25/80 piezo-device characteristics (Chapter 3).

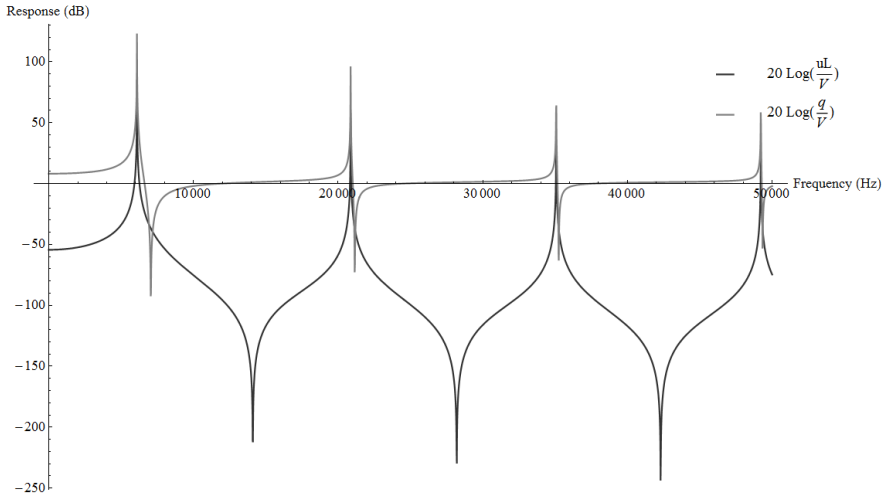

Figure 4.6: Frequency responses to an input voltage

The first limit of the continuous mass approach is that it predicts regular intervals resonances as we showed in Figure 4.6. This contrasts with observations on the HPSt 1000/35-25/80 in Figure 4.7.

The experiments were performed with the unloaded device ($T(0) = T(L) = 0$), with the same setup presented in Section 3.4. The excitation was directly provided by the function generator with 2 MHz sampling rate. The measurements were performed at 120 kHz sampling rate.

As one can remark, the experimental result and the theoretical developments do not match after the first resonant point. This could be due to the assumption of bulk and

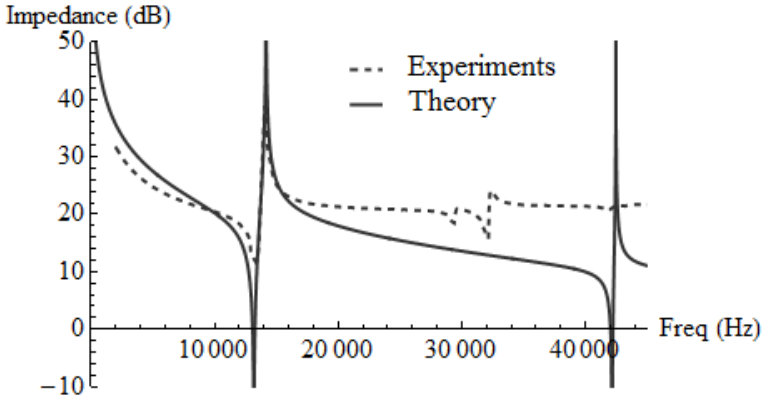

Figure 4.7: Electric impedance: Model vs Experiments

homogenous element which could be not valid.

Elsewhere, one can notice a second drawback of the approach as soon as one care about it is question of practice; it is always necessary to know in advance the frequency's value. Therefore, in addition to the two physical ports, this approach involves a third input: the frequency value. This constitutes a lack of autonomous of the model.

Lumped-mass approach allows to remedy this drawback [39, 41]. In literature, this approach is also called *Mason Lumped Circuit* [40]. The approach consists in supposing at the beginning that only the first resonant frequency is needed. This leads to one analogical element (stack) with respect to Mason principle. Then upon parameters distribution on two stacks we obtain the second resonant frequency and by the way the first anti-resonant frequency. Following the same methodology one can reproduce the third, the fourth... dynamics modes. The obtained models could therefore be called *resonance models* because they are more realistic around the resonant frequencies.

4.6 Lumped-mass approach

Many lumped-parameter system models exist that have provided satisfaction. For example the reader could refer to [33, 34, 35] where lumped-parameters approaches were applied to fluids systems.

Thereafter, these approaches have been extended to piezohydraulic systems [36, 37, 42]. One could also refer to other works [38, 39, 40, 41].

More generally, lumped-parameters modeling consists in developing electrical and mechanical components that are analogous to the concerned system under certain conditions.

Lumped parameters approaches consist of assumptions and approximations which minimize computation efforts while achieving good accuracy as long as the assumptions made are satisfied. This makes it possible to simulate the response of the system and quantify the importance and tradeoffs between several design parameters [42].

4.6.1 Device clamped at its low face

We consider a device clamped at one face, and we assume that only the first vibration mode is required. In this case, the lumped mass approach is illustrated in Figure 4.10.

Accordingly, the piezo-bar is split into two parts. The first one is massless and conserves piezoelectric properties. On the other hand the second part is inertial (mass m) but does not present any piezoelectric property. Therefore Equation 4.6 can be simplified as follows:

$$\begin{array}{rcl} S & = & s.T + d.E \\ D & = & d.T + \varepsilon.E \end{array} \quad \forall\, x \in \text{Part1} \tag{4.23a}$$

$$\sum F_{->m} \;=\; m.\ddot{u} \;\; \forall x \in \text{Part2} \tag{4.23b}$$

Hence, the physical variables S, D, T and E can be considered as constant in $Part1$ and upon integration on x one gets:

$$\begin{array}{rcl} u_L & = & \frac{F}{K_m} + d.V \\ q & = & d.F + C_e.V \end{array} \tag{4.24a}$$

$$F \;=\; F_L - m.\ddot{u}_L \tag{4.24b}$$

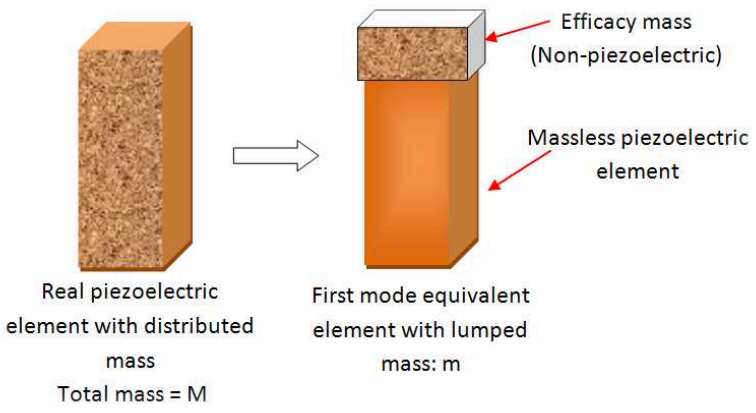

Figure 4.8: Lumped mass principle: case of clamped device

Or simply:

$$u_L = \frac{F_L - m.\ddot{u}_L}{K_m} + d.V \tag{4.25a}$$

$$q = d.(F_L - m.\ddot{u}_L) + C_e.V \tag{4.25b}$$

Let us note:

$$\omega_s^2 = \frac{K_m}{m} \tag{4.26}$$

ω_s is the natural frequency of the model.

$$\ddot{u}_L = -\omega^2 u_L$$

Then Equation 4.25 yields:

$$u_L = \frac{1}{1 - \frac{\omega^2}{\omega_s^2}} \left(\frac{F_L}{K_m} + d.V \right) \tag{4.27a}$$

$$q = \frac{1}{1 - \frac{\omega^2}{\omega_s^2}} \left(d.F_L + \left(1 - (1 - k^2) \frac{\omega^2}{\omega_s^2} \right) C_e.V \right) \tag{4.27b}$$

The mass m is called effective or efficacy mass. It is determined by assuming that the natural frequency of the model equals the first natural frequency of the clamped piezo-device.

4.6.2 General case: 3-ports model

More generally, the piezo-bar actuator operates between two structures (Figure 4.9). One distinguishes an electric port (Ep) and two mechanical ports (Mp_1 and Mp_2). Their variables are respectively (V, q), (F_1, u_1) and (F_2, u_2).

Figure 4.10 depicts the lumped mass approach in this case.

Equation 4.23 becomes:

$$\begin{array}{lcl} u_1 - u_2 & = & \frac{F_1 - m.\ddot{u}_1}{K_m} + d.V \\ q & = & d.(F_1 - m.\ddot{u}_1) + C_e.V \\ F_1 - F_2 & = & m(\ddot{u}_1 + \ddot{u}_2) \end{array} \tag{4.28}$$

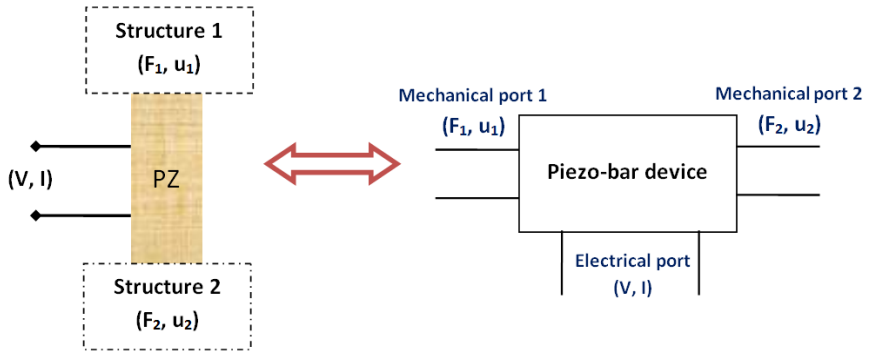

Figure 4.9: General configuration of a piezo-actuator

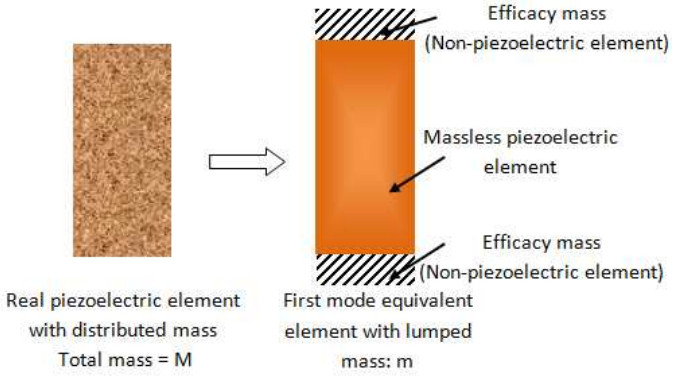

Figure 4.10: Lumped mass principle: general case

An analogical interpretation of this case could correspond to Figure 4.11.

In literature, authors are used to model the electromechanical energy conversion in a piezo-device by a virtual transformer [77, 41, 89, 59]. However, piezoelectric devices are versatile, they can be used as sensor, actuator, voltage transformer, vibrations dampers, etc. However, it is difficult to establish one model ensuring all those functions. In [41], the authors dealt with transformers whereas in [89], the authors dealt with damping function.They all chose to model these functions by a virtual transformer.

In our approach we adopt a virtual gyrator in order to highlight the actuating function of the device. Thereafter, instead of $\dot{u}_L$, I (velocity and current), we shall use u_L and q (displacement and charge).

Moreover we should notice that the inductances in Figure 4.11 correspond to mechanical masses. In common models in literature, these elements do not appear because either the authors work in static or they consider the mass as an element extern to the piezo-device. Here, we integrate the device inner moving mass in the model because we deal with the device dynamics independently of the external structure. This approach was introduced by Van Dyke (Figure 4.1) and recommended by the IEEE Standard 176-1987 on Piezoelectricity [43].

The mass m is determined by assuming that the natural frequency of the model equals the first natural frequency of the unloaded piezo-device ($F_1 = F_2 = 0$). One can verify that the natural frequency of the model in Figure 4.11 equals $\frac{2m}{Km}$.

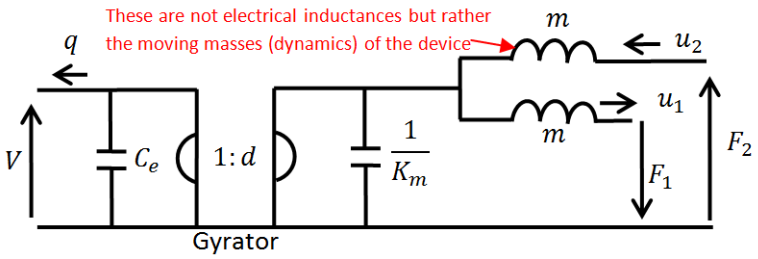

Figure 4.11: Proposal analogical model of a piezo-bar actuator

In addition, we showed in Chapter 3:

$$\omega_a^0 = \sqrt{\frac{\pi^2 K_m}{(1-k^2)M}}$$
$$\omega_r^0 \simeq \sqrt{\frac{\pi^2 K_m}{M}}$$

Accordingly:

$$\begin{aligned} \frac{\pi^2 K_m}{M} &= \frac{2K_m}{m} \\ m &= \frac{2M}{\pi^2} \end{aligned} \tag{4.29}$$

Then, we adopt energy exchange formalism, namely bond graph approach. Bond graph modeling allows to dissect an energetic system and thereby better understand its elementary functions. Bond graph modeling can be used both for linear and nonlinear phenomena. Constructed in 20-Sim 4.C program, Figure 4.12 shows the associated bond graph to system in Figure 4.11.

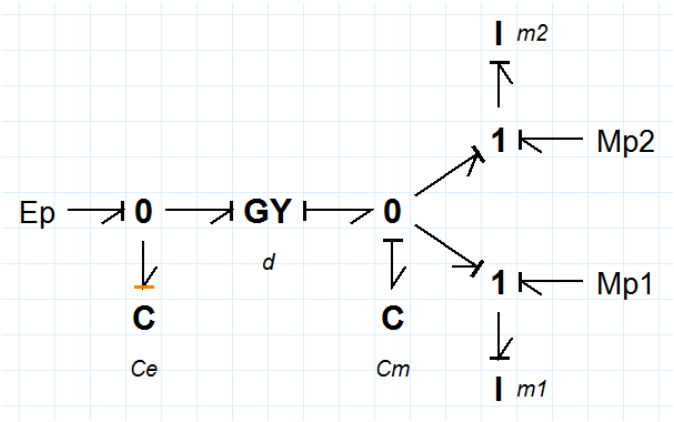

Figure 4.12: Proposal bond graph model of piezo-bar actuator: ideal case

Equations describing the elements of the proposal bond graph are different from ordinary bond graph equations. As a matter of fact, instead of generalized velocity we use generalized displacements because displacement variables make the model more robust for stabilizing runs [5]. Table 4.1 lists the differences between our proposal approach and ordinary bond graph. 20-Sim allows users to customize the bonds equations.

As discussed in [90] and well mentioned in the previous chapter on piezo-device characterization, a mechanical quality factor Q_M is associated to the piezo-device as well as a factor

Concerned Differences	Ordinary (Classical) bond graph	Proposal model particularities
Physical variables	Effort: p.e Flow: p.f	Effort: p.e Displacement: p.f
Effort Source Se	$p.e = effort$ $flow = p.f$	$p.e = effort$ $displacement = p.f$
Flux Source Sf	$p.f = flow$ $effort = p.e$	$p.f = displacement$ $effort = p.e$
Element C	$p.e = \frac{\int p.f}{c}$	$p.e = \frac{p.f}{c}$ remark here no integral
Element I	$p.f = \frac{\int p.e}{i}$	$p.f = \frac{\int\int p.e}{i}$ remark here double integral
Element R	$p.e = r * p.f$ or $p.f = \frac{p.e}{r}$	$p.e = r * \frac{dp.f}{dt}$ remark here one derivation or $p.f = \frac{\int p.e}{r}$ remark here one integral
Element GY-n	$p1.e = n * p2.f$ $p2.e = n * p1.f$	$p1.e = n * p2.f$ $p2.e = n * p1.f$
Element TF-n	$p1.e = n * p2.e$ $p2.f = n * p1.f$	$p1.e = n * p2.e$ $p2.f = n * p1.f$
One-Junction	$\sum direct(p.e) = 0$ equal(collect(p.f)) flux = first(p.f)	$\sum direct(p.e) = 0$ equal(collect(p.f)) flux = first(p.f)
Zero-Junction	$\sum direct(p.f) = 0$ equal(collect(p.e)) effort = first(p.e)	$\sum direct(p.f) = 0$ equal(collect(p.e)) effort = first(p.e)

Table 4.1: Particularities of the proposal bond graph

relative to electric losses angle $\eta = \tan(\delta)$ (generally determined at relative low frequencies). Therefore resistors (R_e, R_m) should be associated to each capacitor in Figure 4.12.

For ceramics capacitors, η hardly exceeds 0.03 at $50Hz$. One can set:

$$\begin{array}{rcl} R_m & = & \frac{\sqrt{m.Km}}{Q\sqrt{2}} \\ R_e & = & \frac{\eta}{2\pi f C_e} \quad < \quad \frac{10^{-4}}{C_e} \end{array} \tag{4.30}$$

In Chapter 3, we saw that:

$$Q_M = \frac{1}{2\pi \left(f_r^0\right) Z_r C_e^1} \left(\frac{\left(f_a^0\right)^2}{\left(f_a^0\right)^2 - \left(f_r^0\right)^2} \right)$$

where Z_r denotes the device impedance at resonance.

However in literature, it is also common to define Q_M as:

$$Q_M = \frac{\omega_r}{\omega_1 - \omega_2} \tag{4.31}$$

where f_1 and f_2 are frequencies for which:

$$\mid Z_{El}(\omega_1) \mid = \mid Z_{El}(\omega_2) \mid = \frac{\sqrt{2}}{2} \mid Z_{El}(\omega_r) \mid \tag{4.32}$$

The model with damping elements corresponds to Figure 4.13.

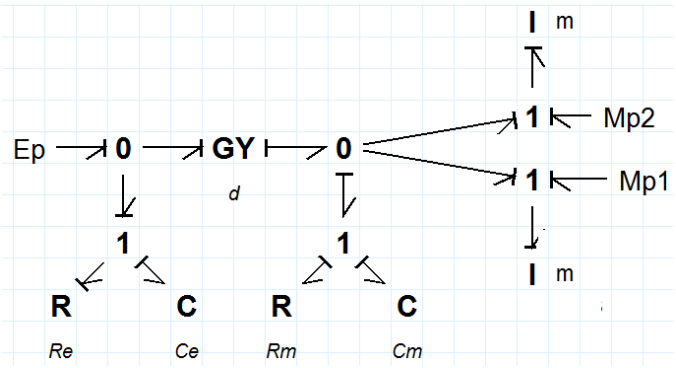

Figure 4.13: Damped model

The proposal model reveals an algebraic loop due to R_m non preferred causality. An algebraic loop in a model is a loop consisting of elements without memory like functions. To calculate the variables in this loop, the variable values themselves are needed. A good explanation is given in 20-Sim web-help [91]. 20-sim is able to solve many algebraic loops at equation level like the one we have in our model. Though, the occurrence of unbreakable loops can not always be prevented. The occurrence of algebraic loops may lead to an increase of simulation time, or even stop simulation when iteration fails. This time consuming can particularly be remarkable in Matlab-Simulink when is translated the model into block-diagram.

20-Sim suggests in [91], some solutions to this problem:

1. Algebraic Loops occur when the order of calculations is arbitrary. When an algebraic loop occurs in an equation model or in a set of equation models, you may change the order of calculation by rewriting the equations. The calculation order in bond graph models can be changed by introducing hand-defined causality.

2. Introduce parasitic energy storage elements (e.g. a small mass, a small capacitor etc.) to break an algebraic loop. These elements introduce however, large poles in the state equations, which might increase the simulation time considerably.

3. Delete elements in the algebraic loop which are not relevant for the model's simulation output (e.g. small dampers, very stiff springs etc.). Care should however be taken, since correct deletions are not always possible and require considerable modeling skill and intuition.

4. Combine dual elements. Sometimes elements of the same type can be combined by adding the parameter values (e.g. combining a mass m1 and a mass m2 to a mass m1 + m2). This will in most cases decrease the amount of algebraic loops.

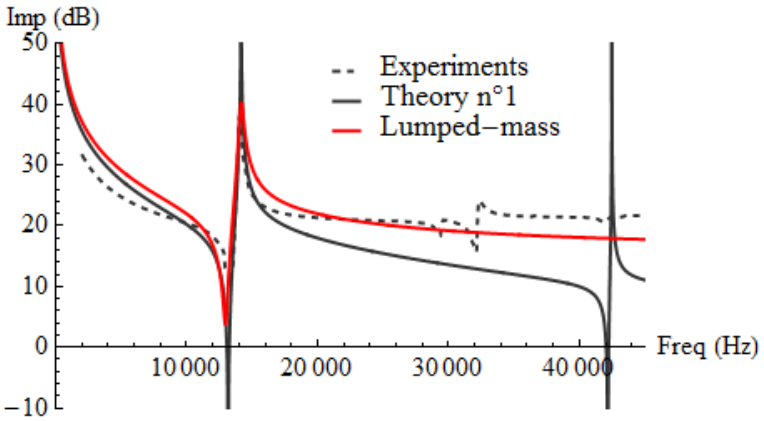

Figure 4.14: Current ($\dot{q}$) frequency response with respect to voltage

However in our case there is no serious problem in this algebraic loop. Comparison between experiments and the proposal lumped-mass model (with $R_e = 5.5\Omega$, $Q = 50$) is depicted in Figure 4.14.

As predicted above, only the first dynamics mode can be approximated if the lumped-mass approach is applied to one stack. The observed difference at low frequencies could be explained by incertitude in data acquisition.

In order to improve the approach and cover the second dynamics mode, we should add a second stack and distribute the parameters.

4.6.3 Distributed parameters approach

Piezo-bar devices have many close and non-regular resonance frequencies. However one-stack (one-layer) lumped mass approach allows to depict only the first resonance (Figure 4.14).

Moreover, continuous mass approach presented in the frame of Mason's model, does not depict so well the dynamics of all piezo-bar device contrary to what one could expect.

Researchers [41, 77] therefore adopt an approach that we named *Distributed parameters approach*. It rises from piezo-devices elaboration. Indeed, by construction a piezo-device is made of several stacks mechanically in series but electrically in parallel. So the piezo-bar is subdivided into n distributed elements as shown in the Figure 4.15.

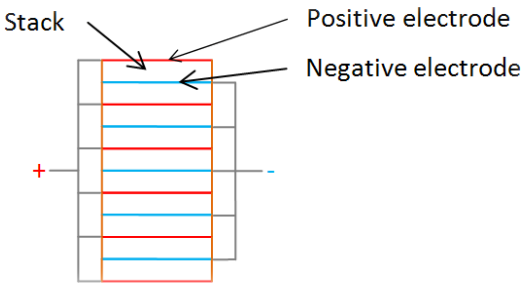

Figure 4.15: Multi-layers piezoelectric device

Following their methodologies, the authors systematically distributed the effective mass in

equal proportion on the n layers. However, in this way, the models would predict resonances at regular intervals contrary to experimental observations.

We assume elements $1, 2, 3, ..., n$ from the bottom to the top to be of the mass m_i. They are mechanically in series and electrically in parallel. Each element represents a module and the methodology used above applies again to each module with the following particularities: considering two neighbors modules i (lower) and $i+1$ (upper) we have:

Parameters	One stack modeling	Multi-layers approach Stack Ni
Stiffness	K	$K_i = n.K$
Capacitance	C	$C_i = \frac{C}{n}$
Piezoelectricity	d	$d_i = \frac{d}{n}$
Damping	R_e R_m	$R_{ie} = \frac{R_e}{n}$ $R_{im} = n.R_m$
Mass	m	m_i?
Voltage	V	$V_i = V_{i-1} = V$
Current	I	$I = \sum I_i = V$

Table 4.2: Distributed parameters approach

The mass distribution shall be determined later.

4.6.3.1 Case of two resonances modeling

Without lost of generality, we deal with the case $n = 2$. The multi-layers piezoelectric device is now considered as made of two stacks (Figure 4.16).

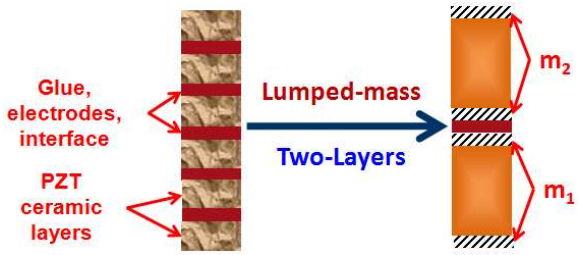

Figure 4.16: Mason modeling when one face is fixed

By applying the lumped mass approach, in terms of bond graph we obtain Figure 4.17

CGlue represents the glue used to assemble the two stacks. Since the stacks are supposed to be fitted to each others, the glue is considered as an infinitely rigid spring: $K_{Glue} \simeq \infty$. In practice, we set $K_{Glue} = 20GN.m^{-1}$

In signal formalism the model corresponds to Figure 4.18.

The determination of the mass of each module depends on resonance analysis. Let us set m_1 the mass of stack 1 (lower stack) and m_2 that of the stack 2 (upper stack). We assume $\omega_{r1} = 2\pi f_{r1}$ and $\omega_{r2} = 2\pi f_{r2}$ respectively the first and second resonant frequencies in Hz. One can verify that the resonant frequencies are solutions of Equation 4.33.

$$\left(4K_m - \omega^2 (m_1 + m_2)\right)\left(-\omega^2 m_1 m_2 + 2K_m (m_1 + m_2)\right) = 0 \tag{4.33}$$

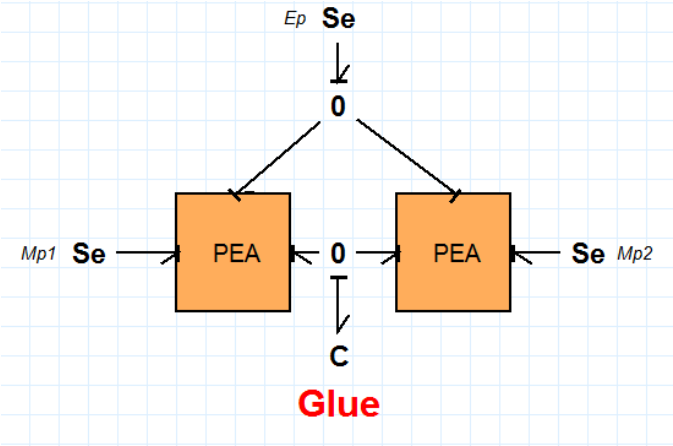

Figure 4.17: 2-stacks modeling approach

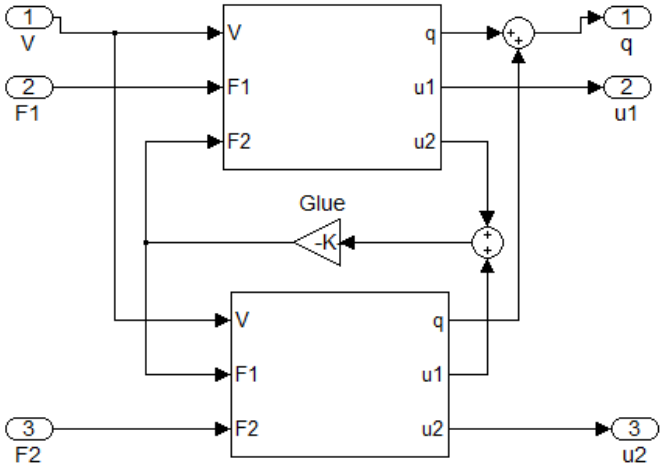

Figure 4.18: 2-stacks modeling approach

We already know:

$$\omega_{r1} \simeq \sqrt{\frac{\pi^2 K_m}{M}}$$

Therefore:

$$m_1 = \frac{2M\left(f_{r2} + \sqrt{-2f_{r1}^2 + f_{r2}^2}\right)}{\pi^2 f_{r2}} \tag{4.34a}$$

$$m_2 = \frac{2M\left(f_{r2} - \sqrt{-2f_{r1}^2 + f_{r2}^2}\right)}{\pi^2 f_{r2}} \tag{4.34b}$$

f_{r1} and f_{r2} can be experimentally determined. In our case, from the HPSt 1000/35-25/80 characterization we have:

$$\begin{aligned} f_{r1} &= 12180Hz \\ f_{r2} &= 32000Hz \end{aligned}$$

Comparison between experiments and 2-stacks approach is depicted in Figure 4.19. The result is satisfying. Our approach allows to remedy to the limitations of continuous mass approach.

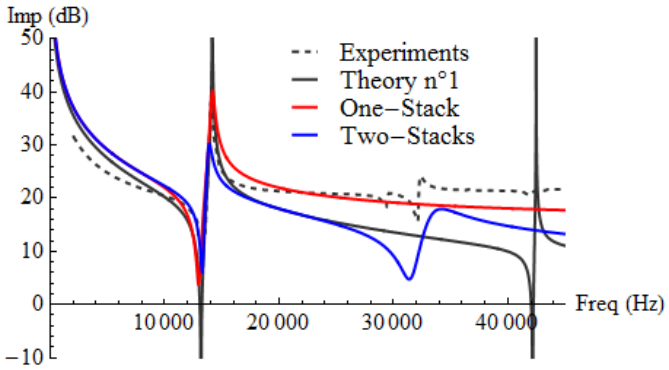

Figure 4.19: Current ($\dot{q}$) frequency response with respect to voltage

However, we observe errors in the magnitude prediction. This could be due to our assumption considering the interfaces between the layers, as simple and linear stiffness. Actually, these interfaces are not simple glues and the manufacturers do not provide more information about that. One could dwell on this aspect in future work.

One could follow the same methodology with three (3) or more stacks. However the high is the number of stacks modeling, the difficulty will be the determination of the corresponding masses $m(i)$. Moreover, as in FEA models, the increasing of the elements number does not guarantee the convergence of the solution or more accurate result. One therefore has to find the best tradeoff.

4.7 Piezo-device's dynamic enhancement

Industrial piezo-devices are made of brittle ceramics. They tolerate extension lesser than compression. It is therefore recommended to pre-load (P) the device by means of elastic discs (or sometimes springs) of stiffness k_p and a system of vis-screw before using it so that the device is initially compressed. Moreover, an additional mass (M_a) can be used.

Correct value of pre-load grants a longer lifetime for piezo-actuator. Experimental studies had been performed both by materials scientists [92] and piezo-device manufacturers [62, 71]. The authors of [92] reported that literature showed different values for the optimum pre-load ranging from 20% to 50% of the maximum force that the device can generate. However manufacturers usually recommends values around 10% of the maximum force [62, 71].

The pre-loading elements integration in the model depends on the physical configuration. For example let us consider the assembly in Figure 4.20 realized for experiments.

Table 4.3 provides the parts list of the setup in Figure 4.20.

Accordingly, the lower face of the piezo-device is clamped to the item 3. This corresponds to a flux source combined with an infinite stiffness $K_{Assembly}$. In practice we set $K_{Assembly} = 20GN.m^{-1}$. The item 2 is the main pre-loading element of stiffness K_p. The elements 1 and 4 should be regarded as additional mass M_a.

Its equivalent in bond graph is given in Figure 4.21.

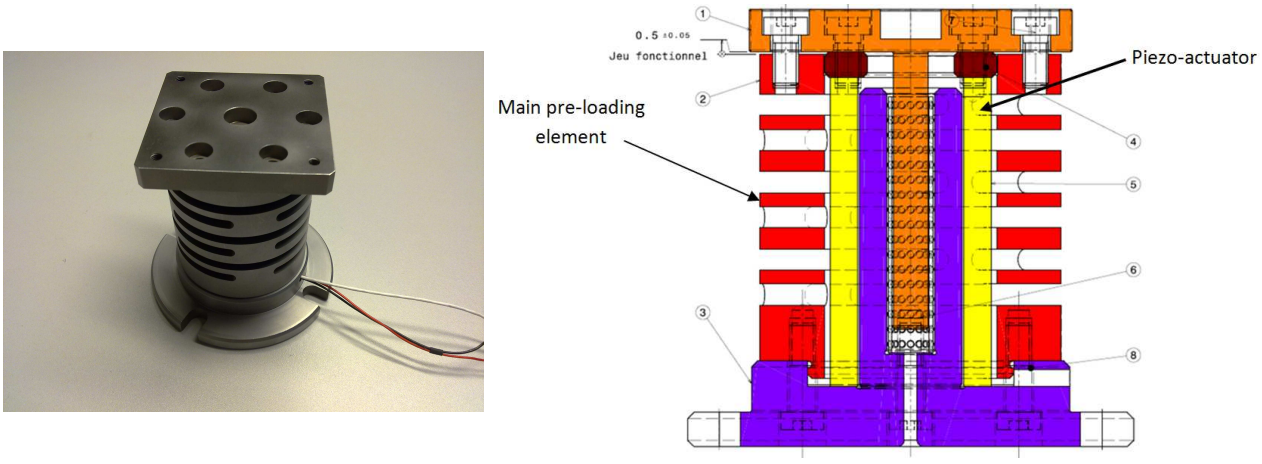

Figure 4.20: Test bed

Parts	Names	Role	Quantities
n ° 1	Contact piece	Receives an eventual workpiece	1
n ° 2	Compressive piece	Pre-loads the piezo-device	1
n ° 3	Fixation piece	To be clamped on a table	1
n ° 4	Wedge	Allows an assembly-set	1
n ° 5	Piezo-bar actuator		1
n ° 6	Linear ball bearing	Lows friction movements	1
n ° 7	Screws	For tightening	6
n ° 8	Screws	For tightening	6

Table 4.3: Parts list of the mechanism in Figure 4.20

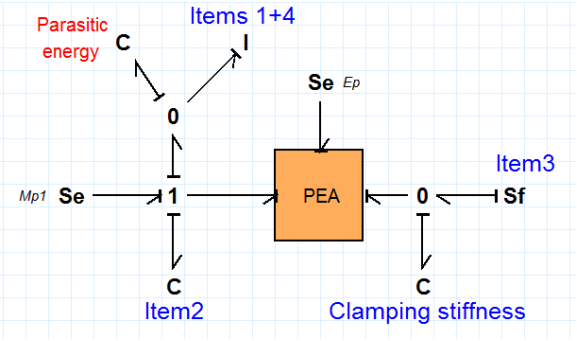

Figure 4.21: Equivalent bond graph of the setup

One can notice the introduction of a parasitic an energy storage element $KParasitic$ (the small capacitor i.e. a high stiffness) in accordance with [91]. It aims to break algebraic loop appearance due to the additional mass. The pre-load value P is introduced in $Mp1$.

We have: $K_p = 7.6N.\mu m^{-1}$, $P \simeq 3000N$, $M_a = 0.480Kg$. We take $KParasitic = 10GN.m^{-1}$.

In block-diagram modeling approach one would obtain Figure 4.22.

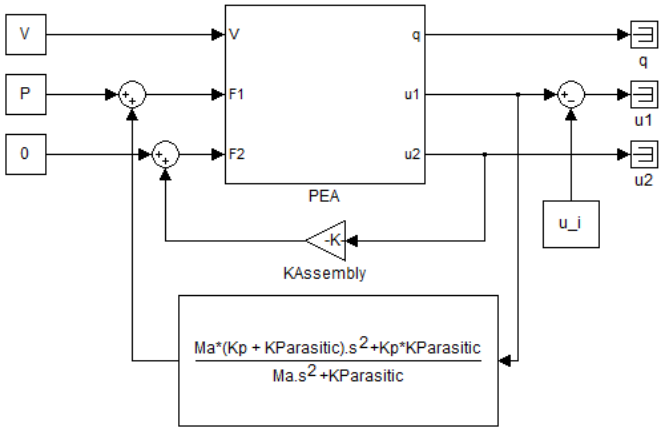

Figure 4.22: Equivalent block-diagrams of the setup

Both models in Figures 4.21 and 4.22 allow to analyze the dynamic of the whole system. For this purpose, one could depict the step response of the system. In order to obtain good results, one should be careful about numerical method. In Figure 4.23 we present simulation using Backward Euler Integration method [93, 94].

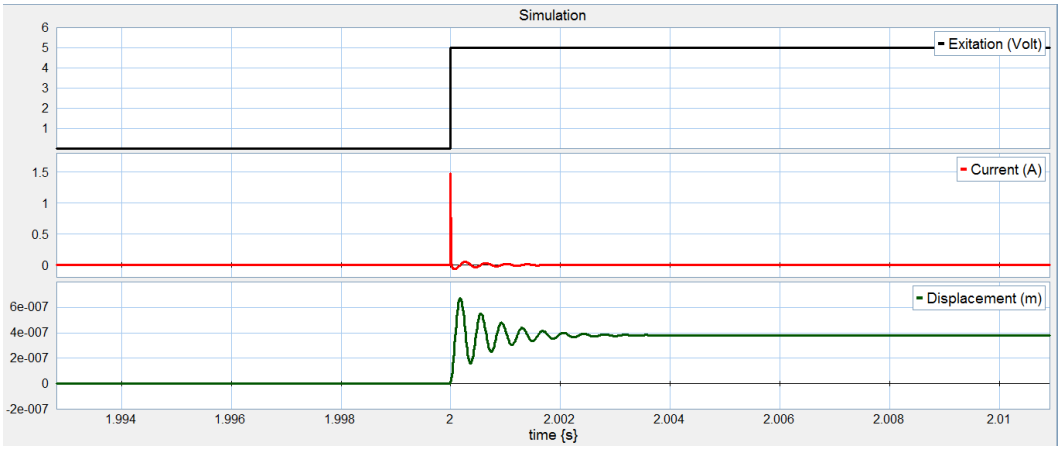

Figure 4.23: One-stack model simulation with Backward Euler

According to the simulation, the whole system natural frequency is about $2642Hz$. For $5V$, the steady value of the displacement is $0.4\mu m$. They predict an overshoot of the current to be about $1A$.

Figure 6.19 is realized for measurements. FFT analysis of the experimental data shows that the system frequency resonance is about $2500Hz$. This is quite similar to simulation prediction.

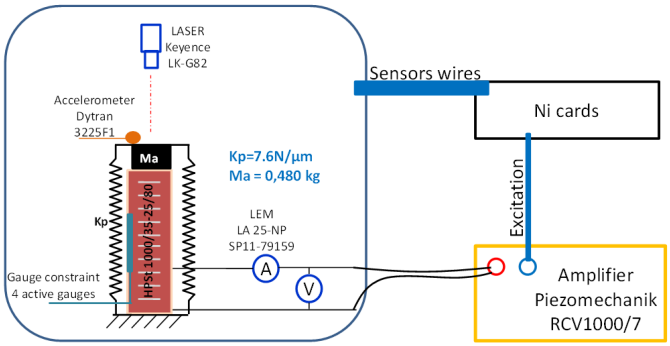

Figure 4.24: Instrumentation for experimental measurements

4.7.1 Influence of prestress on the structure dynamics

In this Section, we study the influence of pre-load value on the structure dynamics. The physical system is the same as in Figure 4.20. The pre-load is changed by varying to the assembly set between item2 and item1. The electrical setup is equivalent to Figure 3.5. Therefrom, we depict in Figure 4.25 the variation of the piezo-device impedance with respect to pre-load value. Accordingly, the pre-load value has not any impact on the resonance occurrence. Its unique influence concerns the resonance accuracy which increases when the pre-load increases.

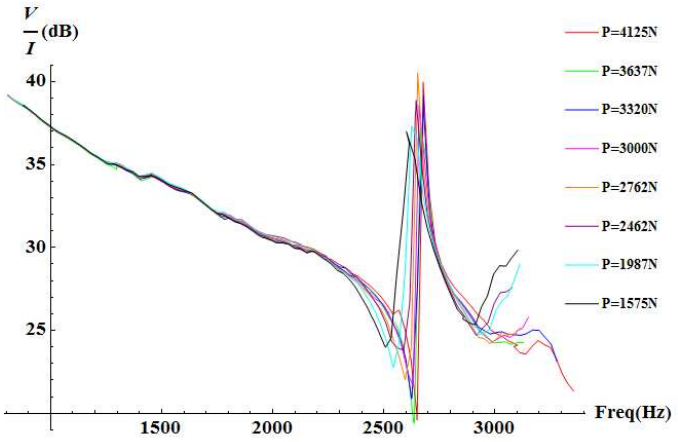

Figure 4.25: Analysis of pre-load influence

4.8 Conclusion

This chapter mostly based on piezo-materials constitutive laws given by IEEE Standard [43]. We highlighted that developments basing only on these equations do not well depict the device dynamics contrary to what one could expect. Improving approaches were then suggested and tested. Elsewhere we saw that it is also necessary to choose the best simulation method. However we did not dwell on nonlinear effects. Using the nonlinear domain could allow the generation of important strains and forces [95] while being responsible of nonproportional losses, saturation, excessive heating, and thereby damage the device [74].

Chapter 5

Modeling nonlinearities in piezo-devices

5.1 Résumé du chapitre en Francais

Dans les chapitres précédents, nous nous sommes limités aux équations linéaires données par le standard IEEE [43]. Ce qui nous a permis d'établir des modèles valables autour d'un point de fonctionnement.

Dans le présent chapitre, nous prenons en compte les non-linéarités au nombre de trois selon [96]: les non-linéarités dans le gain, le phénomène de fluage (dû à un alignement graduel des dipôles), et l'hystérésis.

Ces non-linéarités sont analysées et expliquées en détail par les spécialistes de matériaux. Mais ces descriptions sont le plus souvent difficiles à utiliser.

Dans la section 5.2.1, nous nous intéressons à la caractéristique tension-déplacement. En régime statique, le courant électrique ne présente que peu d'intérêt. Pour une meilleure analyse, les autres parties du système sont sollicitées dans leurs domaines linéaires. Les paramètres de l'élément piézoélectrique sont ceux déterminés au chapitre 3. la Figure 5.2 donne le profil d'excitation. Le montage expérimental est celui décrit en Figure 6.19. Nous nous intéressons ici au front montant de la tension.

Les résultats expérimentaux révèlent de faibles non-linéarités expliquables par une variation du coefficient piézoélectrique d. Pour celà on pourrait utiliser le développement de Taylor d'ordres supérieurs [97, 74]. Mais l'introduction de l'Equation 5.11 dans les logiciels de simulation utilisés fait apparaître des perturbations numériques.

Nous nous sommes orientés donc vers d'autres lois d'évolution. En particulier, nous proposons l'utilisation d'une loi de comportement sigmoïdal. C'est un classique dans la modélisation de certains phénomènes naturels. Pour cela, nous appliquons l'équation de Verhulst-Pearl à l'actionneur piézoélectrique.

Analytiquement, il suffirait de connaître le déplacement maximal, la pente à l'origine et le point d'inflexion pour déterminer les paramètres requis. Mais on ne dispose pas toujours de mesures balayant entièrement la plage de tension.

Nous procédons alors par optimisation numérique. Ce qui nous donne les paramètres dans la Table 5.1.

Le modèle est validé par les Figures 5.4 et 5.5. Toutefois certains spécialistes trouvent cette approche trop rigide. Le lecteur intéressé peut consulter[98] à cet effet.

Richards [99] introduit alors un paramètre b de relaxation de forme. Mais son approche peut rapidement devenir instable à cause de la fonction puissance.

Colin P.D. Birch dans [100] suggère alors une alternative (Equation 5.22). Par contre, cette dernière équation n'est plus analytiquement intégrable. Il faut passer par des méthodes numériques parfois coûteuses et nécessitant de lourds solveurs, ce dont ne disposent pas les logiciels de simulation classiques.

Nous retenons par la suite le premier modèle (Equation 5.16). Il reste applicable en dynamique moyennant une détermination de α, β, γ et λ. Pour ce faire, nous relevons les réponses indicielles du système pour différentes valeurs de l'échelon de $10-20\%$ de la plage de tension applicable.

Ensuite dans la section 5.3, nous traitons de l'hystérésis, un phénomène fréquent dans de nombreux domaines. La réponse du système n'est plus déterminée par l'unique entrée, mais aussi par l'évolution histoirique de cette dernière.

On distingue l'hystérésis statique liée à un phénomène de mémoire, et l'hystérésis dynamique qui est plutôt due à un déphasage entre l'entrée et la sortie.

Nous optons pour le modèle de Preisach pour la modélisation de l'hystérésis statique [101, 102, 103, 104].

Il consiste en l'Equation 5.23 où $\hat{\gamma}(\alpha,\beta,V(t))$ est l'opérateur élémentaire de Preisach et $\mu(\alpha,\beta)$ la fonction de distribution. α et β décrivent le triangle de Preisach (Figure 5.8).

Par symmétrie dans la boucle principale, on peut poser:

$$\mu(\alpha,\beta)=\mu(-\beta,-\alpha)$$

Ainsi on a:

$$\mu(\alpha,\beta)=\varphi(-\beta)\varphi(\alpha)$$

Nous adoptons ensuite la fonction de distribution de Lorentz.

$$\varphi(x)=\frac{ae^{-bx}}{\left(1+ce^{-bx}\right)^2}$$

Sur le front montant, on a:

$$u(V)=u_R(V)=\int_{-V_s}^{V(t)}\left(\int_{-V_s}^{\alpha}\mu(\alpha,\beta)\hat{\gamma}(\alpha,\beta,V(t))d\beta\right)d\alpha \tag{5.1}$$

Et sur le front descendant, on a:

$$u(V)=u_D(V)=\int_{V(t)}^{V_s}\left(\int_{V(t)}^{\alpha}\mu(\alpha,\beta)\hat{\gamma}(\alpha,\beta,V(t))d\beta\right)d\alpha \tag{5.2}$$

Par intégration sur le front montant:

$$\begin{aligned} u_R(V) &= u_s+\frac{a^2}{b^2(c^2-1)^2\left(c+e^{bV}\right)\left(c+e^{bV_s}\right)}.\Bigg[\left(c^2-1\right)\left(e^{b(V+V_s)}-1\right) \\ &+ \left(c+e^{bV}\right)\left(c+e^{bV_s}\right).\mathrm{Log}\left(\frac{\left(c+e^{bV}\right)\left(1+ce^{-bV_s}\right)}{\left(1+ce^{bV}\right)\left(c+e^{-bV_s}\right)}\right)\Bigg] \end{aligned} \tag{5.3}$$

Et sur le front descendant:

$$\begin{aligned} u_D(V) &= u_s+\frac{a^2}{b^2(c^2-1)^2\left(1+c.e^{bV}\right)\left(c+e^{bV_s}\right)}.\Bigg[\left(c^2-1\right)\left(e^{bV}-e^{bV_s}\right) \\ &+ \left(1+ce^{bV}\right)\left(c+e^{bV_s}\right).\mathrm{Log}\left(\frac{\left(c+e^{bV}\right)\left(1+ce^{bV_s}\right)}{\left(1+ce^{bV}\right)\left(c+e^{bV_s}\right)}\right)\Bigg] \end{aligned} \tag{5.4}$$

Ensuite grâce à une programmation adéquate, nous reproduisons les boucles principale et mineures (Figure 5.9).

Contrairement à l'hystérésis statique, l'hystérésis dynamique est liée à la fréquence d'excitation.

Afin de tenir compte de la dépendance fréquencielle, un modèle dynamique de Preisach a été introduit [105, 106, 107, 108]. $\xi\left(\frac{dV}{dt}\right)$ dépend de la vitesse d'excitation. Mais il est pratiquement difficile de trouver les bons paramètres de Preisach.

Nous optons alors pour une analogie entre les matériaux viscoélastiques et les piézoélectriques [96]. Les modèles les plus usuels sont ceux de Maxwell et Kelvin Voigt (Figure 5.13).

A l'instar de plusieurs auteurs, nous appliquerons le principe de Voigt au gyrateur, grâce à l'équivalence $K \Longleftrightarrow \frac{1}{C} \Longleftrightarrow \frac{1}{d}$. Mais notre approche se distingue quelque peu des leurs qui consistent essentiellement a un agencement des diverses sous-unités.

En effet, nous avions déjà abordé la non-linéarité du gain dans la Section 5.2.

En ce qui concerne la viscoélasticité, on pose:

$$\dot{u} = \left(\frac{V}{R_p}\right)^p \tag{5.5}$$

Pour la détermination de R_p et de p nous nous basons sur l'aire de la boucle d'hystérésis. De nombreuses études montrent que les pertes d'énergie sont plus importantes aux fréquences moyennes. Elles le sont moins en basses fréquences et absente en hautes fréquences.

Une série d'expériences de 1 à 400 Hz nous a permis de calculer les énergies dissipées en fonction de la fréquence pour ensuite déterminer R_p et p. Nous trouvons $R_p = 10300\Omega$ and $p = 1.043$.

afin d'améliorer le modèle, nous avons ensuite construit un modèle hybride composé d'un étage Preisach suivi d'un étage de Voigt.

Cette combinaison Preisach-Voigt nous a permis de mieux modéliser le phénomène d'hystérésis. Toutefois certaines imperfections persistent encore en basses fréquences. Par contre, elles ne sont plus significatives à partir d'une certaine fréquence.

In the previous chapters, we assumed the linearity of piezoelectric materials according to [43]. This allows to establish simplified but efficient models in restricted functioning domain. However, for years, scientists and specialists communities have well mentioned that piezoelectric materials and devices could present high nonlinearities because of their anisotropy and depending on their micro constitution.

One distinguishes three non-linear effects in a piezo-device [96]: the first one is the non-linear gain which is physically explained by the voltage/force dependency of the material parameters. This effect could be responsible of saturation phenomena.

The second effect is the creep (non linear or not) which is the gradual expansion of the material subject to a step input voltage. This is physically explained by the gradual alignment of the dipoles of the material. However, convergence is achieved over a much lager period of time than the time constant of any practical control system [96]. Therefore we shall not dwell on this aspect in our works.

The third non-linear effect concerns the hysteresis more complex than simple losses phenomena.

As mentioned in [96], all these non-linearities in piezoelectric materials are well analyzed but mostly in the framework of the fundamental physics of crystals and thermodynamics and these descriptions are extremely difficult to handle. Moreover the phenomena differ from static to dynamic.

Contrary to Chapter 3 where we used resonance methods to characterize the piezo-devices, we shall use direct methods in order to investigate the device behaviour in regards to nonlinearities.

5.2 Gain nonlinearities

5.2.1 Static case

We integrate the piezo-bar into a system. Then we apply a known voltage and record the corresponding output. In fact, in statics, the electrical current or charge does not present any interest. Therefore, the unique output is the displacement u.

The equivalent system is depicted in Figure 5.1. A driving voltage V is applied to the actuator. In response it produces a displacement u to which the loading system resists (F).

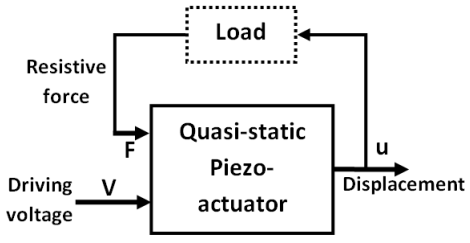

Figure 5.1: Static experimental setup

In order to not hedge the modeling task, the loading system must be well known. It is the same system as shown in Figure 4.20. In static, it is equivalent to a linear spring of stiffness $K_{Load} = 7.6N\mu m^{-1}$. Therefore, a starting approach could consist of linear equations [109, 70]. In this case we have:

$$u = \frac{F}{K_m} + d.V \tag{5.6}$$

where $K_m = 165.165 N\mu m^{-1}$ is the device's short circuited electrode stiffness and $d = 0.066\mu m.V^{-1}$ denote respectively the piezo-actuator short-circuited stiffness and its piezoelectric constant. These parameters were those experimentally determined for the HPSt 1000/35-25/80 in previous chapters.

Assuming F the resistive force, we have: $F = -K_{Load}.u$.

$$u(V) = \frac{-K_{Load}.u}{K_m} + d.V \tag{5.7}$$

Then:

$$u(V) = \frac{d.K_m}{K_m + K_{Load}}.V \tag{5.8}$$

The applied voltage profile is depicted in Figure 5.2

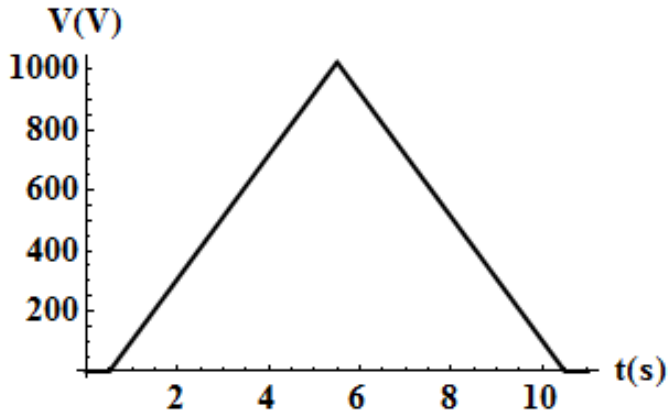

Figure 5.2: Static excitation profile

The experimental setup is the same as in Figure 6.19. We consider the displacement measured with the Keyence optic device(see Annexes). Details concerning these equipments are given in Annexes C.

In order to study the nonlinearity of gain, we shall focus on the rising part of the voltage. Let us plot the relation $V - u$ (Figure 5.3).

Small nonlinearities are observed. The experiments match with the model prediction only for low voltages ($< 150V$). As mentioned by many studies [110, 97], the observed nonlinearities express the dependency of the piezo-device parameters on the applied voltage:

$$d \neq Constant$$

In order to take into account these nonlinearities, an approach could consist of combination of Taylor developments and thermodynamic laws [97, 74]. Following this approach the constitutive laws given by [43] are modified:

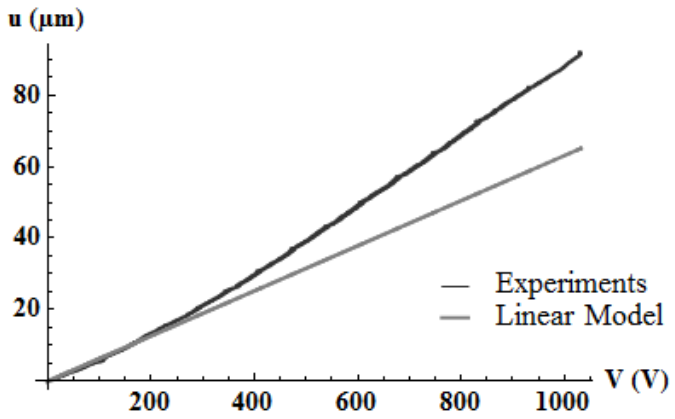

Figure 5.3: Linear model compared to experiments

$$S = \left(s + \frac{\alpha}{2}.T\right).T + \left(d + \frac{\beta}{2}.E + \gamma.T\right).E \tag{5.9a}$$

$$D = \left(d + \beta.E + \frac{\gamma}{2}.T\right).T + \left(\varepsilon + \frac{\delta}{2}.E\right).E \tag{5.9b}$$

where α and γ are called elastostriction coefficients and δ and β electrostriction coefficients. Since in static we do not care about the electric current.

$$S = \left(s + \frac{\alpha}{2}.T\right).T + \left(d + \frac{\beta}{2}.E + \gamma.T\right).E \tag{5.10}$$

In static we have $u = S.L$, $F = T.\sigma$, $V = E.L$. Therefore it comes

$$u = \left(\frac{s.L}{\sigma} + \frac{\alpha.L}{2\sigma^2}.F\right).F + \left(d + \frac{\beta}{2L}.V + \frac{\gamma}{\sigma}.F\right).V$$

One recognizes $K_m = \frac{\sigma}{s.L}$.
Let us note

$$\begin{aligned} \alpha^* &= \frac{\alpha.L}{2\sigma^2} \\ \beta^* &= \frac{\beta}{2L} \\ \gamma^* &= \frac{\gamma}{\sigma} \end{aligned}$$

Then we have:

$$u = \left(\frac{1}{K_m} + \alpha^*.F\right).F + \left(d + \beta^*.V + \gamma^*.F\right).V$$

Upon considering the whole system, since $F = -K_{Load}.u$ it comes:

$$u = -\left(\frac{1}{K_m} - \alpha^*.K_{Load}.u\right).K_{Load}.u + \left(d + \beta^*.V - \gamma^*.K_{Load}.u\right).V \tag{5.11}$$

Therefore there are three coefficients to be determined: α^*, β^* and γ^*. The classical method for this task is curve fitting with respect to experimental data. The objective function to be minimized is:

$$h(\alpha^*, \beta^*, \gamma^*) = \frac{\sum \left[u_i + \left(\frac{1}{K_m} - \alpha^*.K_{Load}.u_i \right) .K_{Load}.u_i - \left(d + \beta^*.V_i - \gamma^*.K_{Load}.u_i \right) .V_i \right]^2}{Ns} \tag{5.12}$$

where u_i, V_i are the measurement data. Ns denotes the samples number.

Since we have few parameters to estimate (3 parameters, it is not too high), simple methods could be used. Especially grid discretization method which consists in subdividing the continuous search area into discreet areas and then transforming the optimization problem into an easiest combinatorial problem. However, as shown in [111], this method provides satisfying solution only for the discreet points. In order to remedy this weakness, the number of grid has to be augmented and this leads to time consuming.

Nelder-Mead method can also be used [112]. Obviously, it is not the best methods in many mathematicians and computers scientists point of view [113, 114]. However Nelder-Mead simplex algorithm is extensively used in many fields for its rapid convergence [115]. Moreover, this method is utilized by many software like Mathematica [116]. Rightly, we use Mathematica optimization function *NMinimize* which is based on Nelder-Mead algorithm.

The minimum research has been yield without any constraint on the coefficients to be determined, no matter with the time this operation consumes. We use $Ns = 3042$ points for the operation.

The global minimum found by *NMinimize* is $h_{min} = 0.2689\mu m^2$ for: $\alpha^* = -0.0017$, $\beta^* = -0.0006$ and $\gamma^* = -0.0021$. The computing operation has been performed several times in order to be confident in the values. For these values, the displacement is no longer real but rather a complex number.

By analyzing the experimental curve and others in literature and piezo-device suppliers data sheets, one can remark that they tend towards an exponential form at low driving voltage. Then it becomes nearly linear after a threshold and then after another threshold it saturates.

This behaviour is similar to some vegetal species growth [100]. Some vegetation rate of growth increases as size increases from low values, reaches a maximum at a point of inflexion and then decreases towards zero at an upper asymptote, so that they look like the central part of a rotated S [117]. However, we do not find in literature, references applying this to piezoelectric devices.

The quantity $\frac{\partial u}{\partial V}$ is similar to the growth rate, the displacement u similar to the size and the voltage V similar to the time. Therefore one could set for any piezo-bar device:

$$\frac{du}{dV} = g(u).u \tag{5.13}$$

where $g(u)$ equals the relative growth rate which reduces as u increases.

Classically, logistic and improved logistic (Verhulst-Pearl, Gompertz-Richards, Colin) functions are used to handle this kind of problems [98].

5.2.1.1 Adaptation of Verhulst-Pearl equation

Verhulst-Pearl equation is a immediate improvement of basic growth equation. Applied to the piezo-device it would lead to Equation 5.14.

$$\frac{du}{dV} = \lambda.u\left(1 - \frac{u}{\alpha}\right) \tag{5.14}$$

where λ denotes the relative growth rate at very low displacement and α the maximum reachable displacement.

However, because piezo-device could present offset values, we introduce a third parameter γ as follows:

$$\frac{du}{dV} = \lambda.(u+\gamma)\left(1 - \frac{u+\gamma}{\alpha}\right) \tag{5.15}$$

The task then consists of the estimation of the parameters λ, α and γ.

Analytically, this seems easy. As a mater of fact, according to Equation 5.15, $\alpha - \gamma$ would be the maximum reachable displacement. λ would be the curve slope at very low voltage. Elsewhere, the curve would present an inflexion point for a displacement equal to $\alpha/2 - \gamma$ and at this point the slope would equal $\lambda.\alpha/4$.

In this way the problem would be so simple and would consist in reading from experimental figures the above listed geometrical points. However this is not so easy in practice.

An alternative solution therefore consists of curve fitting problem formulation. For this purpose, we integrate Equation 5.15 in order to obtain analytical function that will be used for curve fitting process. For an unloaded device we have:

$$u(V) = \frac{\alpha}{1 + \exp^{-\lambda(V-\beta)}} - \gamma \tag{5.16}$$

where β is the value of V for which the inflexion point is theoretically reached. We therefore have to estimate four parameters with respect to experimental data. That is, we have to minimize an objective function $h(\alpha, \beta, \gamma, \lambda)$ under large constraints. We judge that the constraints are large because the unique sure constraint on these parameters is the positiveness $(\alpha, \beta, \gamma, \lambda > 0)$.

In the case of loaded device we should take into account the force. It comes:

$$u(V) = \frac{-K_{Load}.u(V)}{K_m} + \frac{\alpha}{1 + \exp^{-\lambda(V-\beta)}} - \gamma$$

Then:

$$u(V) = \frac{K_m}{K_m + K_{Load}}\left(\frac{\alpha}{1 + \exp^{-\lambda(V-\beta)}} - \gamma\right) \tag{5.17}$$

Assuming (V_i, u_i) the experimental data, the objective function to minimize yields:

$$h(\alpha, \beta, \gamma, \lambda) = \frac{\sum_i \left(u_i - \frac{K_m}{K_m + K_{Load}}\left(\frac{\alpha}{1+\exp^{-\lambda(V_i-\beta)}} - \gamma\right)\right)^2}{Ns} \tag{5.18}$$

The minimum research is performed with the 3042 points used above. The global minimum found by *NMinimize* is $h_{min} = 0.1081\mu m^2$ for:

α	β	γ	λ
$193.943\mu m$	$704.908V$	$34.1\mu m$	$0.0022V^{-1}$

Table 5.1: Parameter estimated

The computing operation has been performed several times.
Experiments are compared to the adapted Verhulst-Pearl model in Figure 5.4.

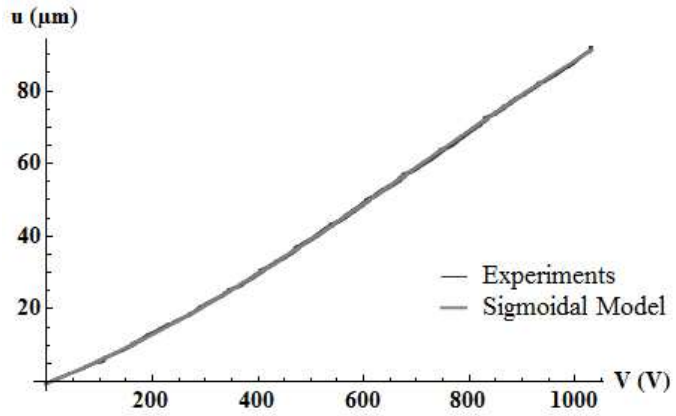

Figure 5.4: Experiments Vs adapted Verhulst-Pearl model

In order to check the robustness of the model, other experiments are performed and compared to the models prediction in Figure 5.5:

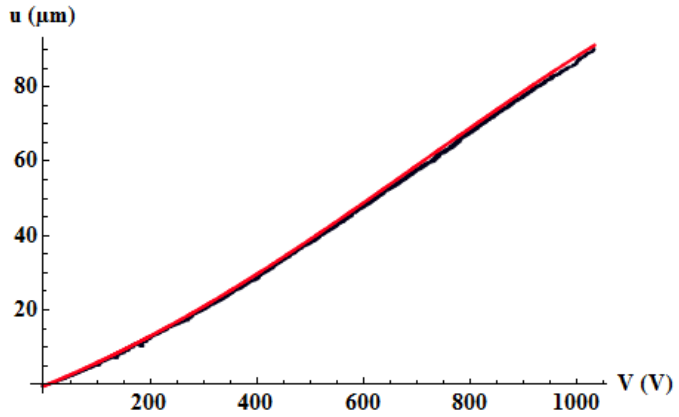

Figure 5.5: Experiments (Black) Vs adapted Verhulst-Pearl model (Red)

Although this approach is satisfying, some limitations of Verhulst-Pearl growth equation are well-known [98]. It is known to be extremely rigid in that way the curve upper shape is dependent on the lower shape. It obliges the inflexion point to be at $u_{max}/2$. This problem of rigidity has been treated by several scientists as reported in [98].

5.2.1.2 Other approaches

In order to make growth equation more flexible, Richards [99] suggested a modified equation consisting in:

$$\frac{du}{dV} = \lambda.u\left(1 - \left(\frac{u}{\alpha}\right)^b\right) \tag{5.19}$$

where b is called the shape constant. A sigmoid form is obtained for $\lambda, b > 0$. Under this condition, an integral of Equation 5.19 is:

$$u(V) = \alpha\left(1 + \exp^{c-\lambda.b.V}\right)^{-1/b} \tag{5.20}$$

We could then adapt Equation 5.20 to our need as follows

$$u(V) = \frac{\alpha}{(1 + \exp^{-\lambda(V-\beta)})^{\delta}} - \gamma \tag{5.21}$$

Hence instead of four (4) parameters, we have now to estimate five ones (5): $\alpha, \beta, \gamma, \lambda, \delta > 0$.

Although Richards equation remedies to Verhulst-Pearl function limitation, some mathematicians and informatics scientists are critical about it. They argue that this approach generates numerical troubles [100]. Especially in our case where we have 3042 points we have got these problems.

Colin P.D. Birch in [100] suggested and successfully validated an improved growth equation as follows:

$$\frac{du}{dV} = \frac{\lambda.u(\alpha - u)}{\alpha - u + \delta.u} \tag{5.22}$$

where δ is also a shape parameter.

Contrary to the above approach, Colin proposal equation can not be integrated in order to find an analytical expression of u. Therefore, the optimization process should concern $\frac{du}{dV}$ instead of u. Since the optimization involves finite differences to approximate function derivative values, robust parameters estimation requires a high number of samples. However experimental setup does not always allow it. Moreover, the impossibility to deduct an analytical expression of u could be a drawback. Especially in our situation, the piezo-device will be integrated into another more global and complex system. For the whole system design, we shall then have to introduce the piezo-device equation into other software like for example Matlab-Simulink which are not as powerful as Mathematica or Sigmaplot.

5.2.2 Dynamic case

The sigmoidal structure suggested above for static case (Equation 5.16), can also be used in dynamics. However the parameters α, β, γ and λ could vary. For this purpose, similarly to the authors in [96], a set of steps is applied to the system presented above and the normalized responses are depicted in Table 5.2. The inconvenient of this approach is that it requires measures recovering the solicitation interval ($0-1000V$ in our case). However, because of the brittleness of piezoelectric devices, one can not afford applying high step values. Therefore we limit the steps application to $10 - 20\%$ of the interval.

Using optimization methods we find α, β, γ and λ. The values are compared to the static case in Table 5.3.

Table 5.4 compares experimental results to the linear model (in Chapter 4) and sigmoidal model (Section 5.2.1).

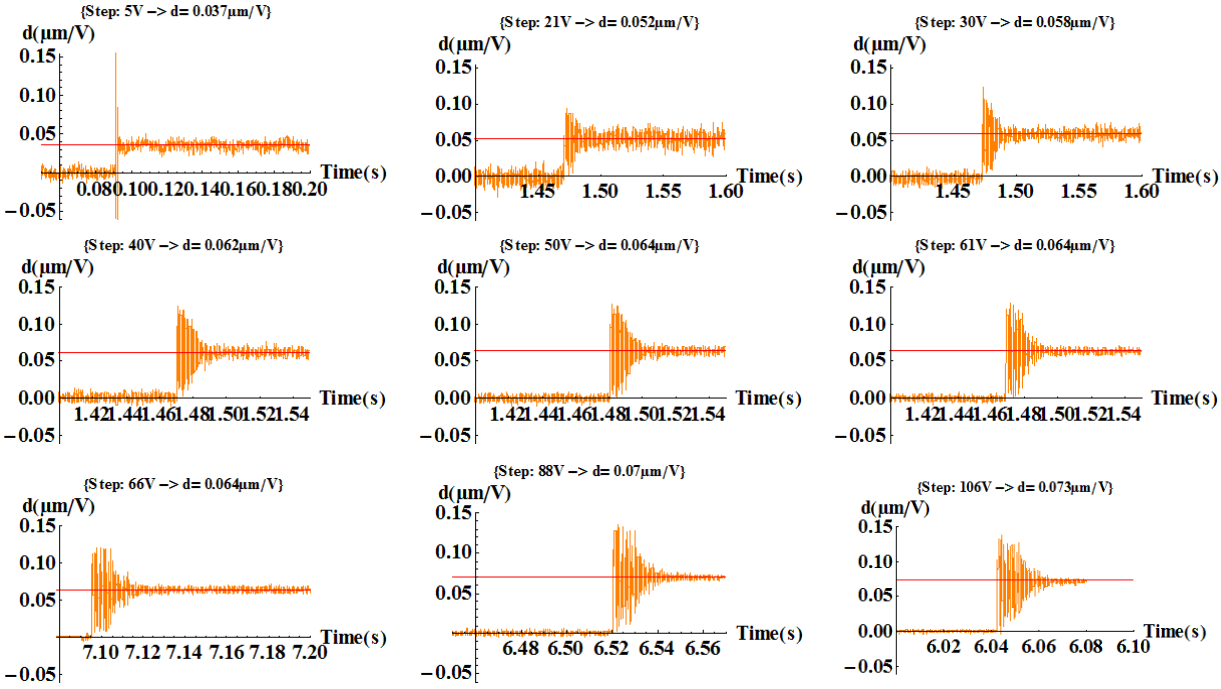

Table 5.2: Step responses normalized by input values

Modes	α	β	γ	λ
Static	$193.943\mu m$	$704.908V$	$34.1\mu m$	$0.0022V^{-1}$
Dynamic	$235.363\mu m$	$778.386V$	$36.207\mu m$	$0.0022V^{-1}$

Table 5.3: Sigmoid model $d(V) = \frac{\alpha}{1+\exp^{-\lambda(V-\beta)}} - \gamma$: Dynamic vs Static

Step value	Experimental d	Linear model d	Sigmoidal model d
5V	$0.037\mu m.V^{-1}$	$0.066\mu m.V^{-1}$	$0.020\mu m.V^{-1}$
21V	$0.052\mu m.V^{-1}$	$0.066\mu m.V^{-1}$	$0.054\mu m.V^{-1}$
30V	$0.058\mu m.V^{-1}$	$0.066\mu m.V^{-1}$	$0.058\mu m.V^{-1}$
40V	$0.062\mu m.V^{-1}$	$0.066\mu m.V^{-1}$	$0.061\mu m.V^{-1}$
50V	$0.064\mu m.V^{-1}$	$0.066\mu m.V^{-1}$	$0.062\mu m.V^{-1}$
66V	$0.064\mu m.V^{-1}$	$0.066\mu m.V^{-1}$	$0.064\mu m.V^{-1}$
88V	$0.070\mu m.V^{-1}$	$0.066\mu m.V^{-1}$	$0.066\mu m.V^{-1}$
106V	$0.073\mu m.V^{-1}$	$0.066\mu m.V^{-1}$	$0.067\mu m.V^{-1}$

Table 5.4: Experimental gains compared to models prediction

5.3 Hysteresis in piezoelectric devices

Hysteresis is common for various branches of science and technology. It is associated with many physical phenomena such as ferromagnetism, ferroelectricity, plasticity and superconduction [118]. Hysteresis is a very complex phenomenon and its modeling is still a challenge for scientists.

There is not a definite definition of the term *hysteresis* and only few works point out its physical origin in the case of piezo-materials [119]. However one could agree that hysteresis appears when the output is not uniquely determined by the input, but depends on the evolution or history of the input [118]. Some scientists distinguish in materials two kinds of hysteretic behaviour: static hysteresis and dynamic hysteresis [120, 121]. Static hysteresis is explained by the ability of the material to memorize information about its previous solicitation. Therefore, the larger is its memory, the wider will be the hysteresis loop. On the other hand, the dynamic hysteresis is mostly due to the incapability of the material to respond in phase with the solicitation.

However we experimentally observed a systematic combination of the two hysteresis parts in a piezoelectric device.

5.3.1 Static hysteresis

The same setup used for static nonlinear gain characterization is used again for static hysteresis study. The applied voltage profile is the same depicted in Figure 5.2.

The static hysteresis loop is depicted in Figure 5.6.

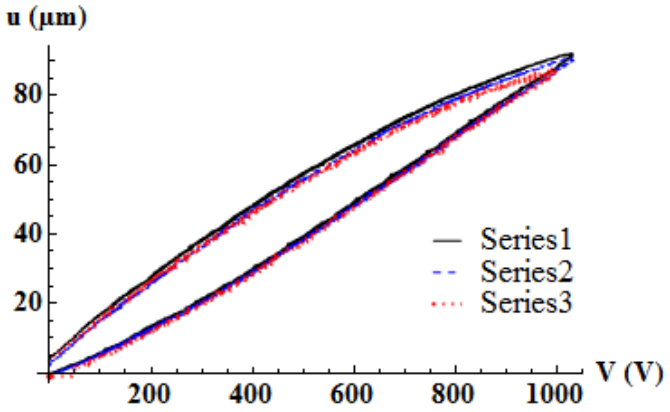

Figure 5.6: Static hysteresis in HPSt 1000/35-25/80

For such a hysteresis handling, Preisach modeling approach is the most common. Preisach model had been established by the physicist Preisach in 1935 [101]. This approach is well exposed by many authors [102, 103, 104].

In continuous domain, Preisach formula is set as follows:

$$u(V(t)) = \int\int_{\alpha \geq \beta} \mu(\alpha, \beta)\hat{\gamma}(\alpha, \beta, V(t))d\alpha d\beta \tag{5.23}$$

where $V(t)$ denotes the system input (here the voltage), $u(t)$ its output (the displacement), $\hat{\gamma}(\alpha, \beta, V(t))$ the elementary hysteresis operator (see Figure 5.7), $\mu(\alpha, \beta)$ the distribution function (Preisach function); it can be regarded as a material constant.

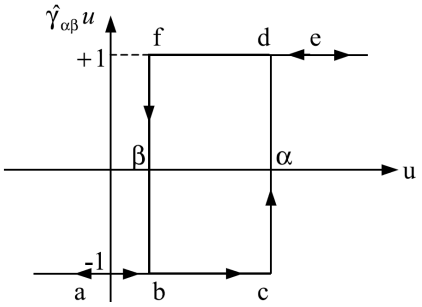

Figure 5.7: Elementary hysteresis function

The elementary hysteresis operator can be set as follows:

$$\hat{\gamma}(\alpha,\beta,V(t)) = \begin{cases} 1 & \text{if } V(t) \geq \alpha \\ -1 & \text{if } V(t) \leq \beta \\ \eta & \text{if } \beta < V(t) < \alpha \end{cases} \tag{5.24}$$

where $\eta = -1$ if the last time V was outside of the boundaries $\beta \leq V(t) \leq \alpha$, it was in the region of $V(t) \leq \beta$; and $\eta = 1$ if the last time V was outside of the boundaries $\beta \leq V(t) \leq \alpha$, it was in the region of $V(t) \geq \alpha$.

Due to saturation phenomena, there exists A so that $\alpha \leq A$ and $\beta \geq -A$. So α and β describe a domain called Preisach triangle with vertices $(-A,-A)$, $(-A,A)$ and (A,A) (Figure 5.8).

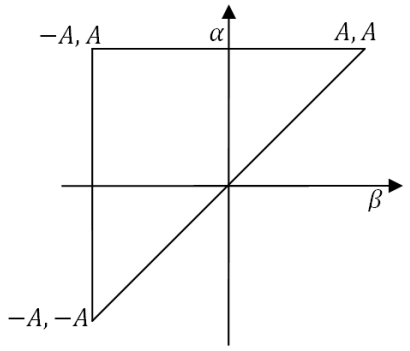

Figure 5.8: Preisach Triangle

Assuming the symmetry of the concentric hysteresis loops, one sets:

$$\mu(\alpha,\beta) = \mu(-\beta,-\alpha)$$

where $\alpha > \beta$.

Therefore one suggests to express the Preisach distribution as follows:

$$\mu(\alpha,\beta) = \varphi(-\beta)\varphi(\alpha) \tag{5.25}$$

In literature, one can meet different analytical expressions of Preisach distribution. Especially, the most common are Lorentz law, Gaussian law and T law [122].

Using Lorentz formulation [123], one sets:

$$\varphi(x) = \frac{ae^{-bx}}{(1+ce^{-bx})^2} \tag{5.26}$$

Along the increasing branch, it comes:

$$u(V) = u_R(V) = \int_{-V_s}^{V(t)} \left(\int_{-V_s}^{\alpha} \mu(\alpha,\beta)\hat{\gamma}(\alpha,\beta,V(t))d\beta \right) d\alpha \tag{5.27}$$

where (u_s, V_s) refers to the starting point from which the voltage starts to increase.

Since along this branch $V(t) \geq \alpha$, according to Equation 5.24, $\hat{\gamma}(\alpha,\beta,V(t)) = 1$. Therefore

$$u_R(V) = \int_{-V_s}^{V(t)} \left(\int_{-V_s}^{\alpha} \mu(\alpha,\beta)d\beta \right) d\alpha \tag{5.28}$$

Therefore the increasing rate yields:

$$\left.\frac{du}{dV}\right|_R = \frac{a^2 e^{bV}\left(e^{b(V+V_s)}-1\right)}{b\left(c+e^{bV}\right)^2\left(1+ce^{bV}\right)\left(c+e^{bV_s}\right)} \tag{5.29}$$

On the other hand, along a decreasing branch one has:

$$u(V) = u_D(V) = \int_{V(t)}^{V_s} \left(\int_{V(t)}^{\alpha} \mu(\alpha,\beta)\hat{\gamma}(\alpha,\beta,V(t))d\beta \right) d\alpha \tag{5.30}$$

where (u_s, V_s) refers to the starting point from which the voltage starts to decrease.

Since along this branch $V(t) \leq \beta$, according to Equation 5.24, $\hat{\gamma}(\alpha,\beta,V(t)) = -1$. Therefore

$$u_R(V) = \int_{V(t)}^{V_s} \left(\int_{V(t)}^{\alpha} -\mu(\alpha,\beta)d\beta \right) d\alpha \tag{5.31}$$

Therefore the decreasing rate yields:

$$\left.\frac{du}{dV}\right|_D = \frac{a^2 e^{bV}\left(e^{bV}-e^{bV_s}\right)}{b\left(c+e^{bV}\right)\left(1+ce^{bV}\right)^2\left(c+e^{bV_s}\right)} \tag{5.32}$$

So, the classical Preisach approach would consist in determining the three coefficients a, b and c. Different methods of Preisach model identification are reported in literature. One of them consists in calculating the coefficients only from the increasing branch of the major loop [104]. However, due to some experimental conditions, a part of this branch, especially the beginning one, can not be measured. Therefore, in our approach we used the second half of the increasing branch and the first half of the decreasing branch.

Upon integrating expression 5.29 it comes:

$$\begin{aligned} u_R(V) &= u_s + \frac{a^2}{b^2(c^2-1)^2\left(c+e^{bV}\right)\left(c+e^{bV_s}\right)} \cdot \Bigg[\left(c^2-1\right)\left(e^{b(V+V_s)}-1\right) \\ &+ \left(c+e^{bV}\right)\left(c+e^{bV_s}\right).\mathrm{Log}\left(\frac{\left(c+e^{bV}\right)\left(1+ce^{-bV_s}\right)}{\left(1+ce^{bV}\right)\left(c+e^{-bV_s}\right)} \right) \Bigg] \end{aligned} \tag{5.33}$$

and on the decreasing branch:

$$\begin{aligned} u_D(V) &= u_s + \frac{a^2}{b^2(c^2-1)^2\left(1+c.e^{bV}\right)\left(c+e^{bV_s}\right)}.\Big[\left(c^2-1\right)\left(e^{bV}-e^{bV_s}\right) \\ &+ \left(1+ce^{bV}\right)\left(c+e^{bV_s}\right).\mathrm{Log}\left(\frac{\left(c+e^{bV}\right)\left(1+ce^{bV_s}\right)}{\left(1+ce^{bV}\right)\left(c+e^{bV_s}\right)}\right)\Big] \end{aligned} \tag{5.34}$$

Using curve fitting program in Mathematica we obtain:

$$\begin{aligned} a &= 0.022 \\ b &= 0.0045 \\ c &= 2.149.10^{-6} \end{aligned}$$

By means of good codes algorithms, this approach allows to depict both major and minor hysteresis loops. In our case, we used 20-Sim and Matlab-Simulink codes. The model is simulated with 20-Sim and depicted in Figure 5.9.

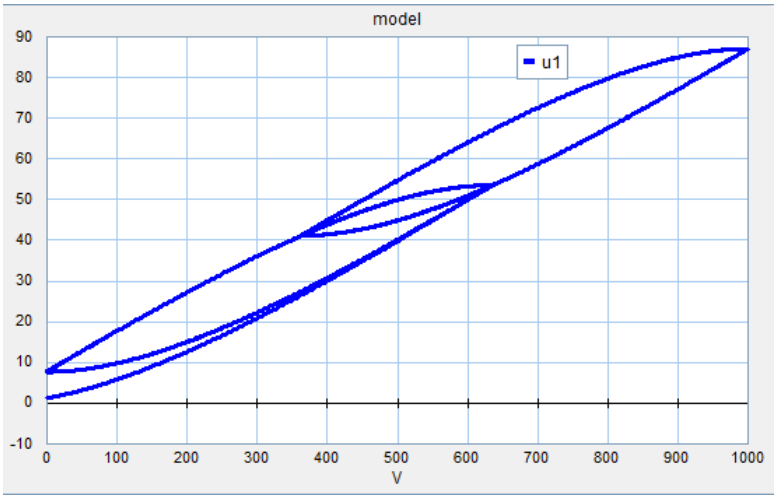

Figure 5.9: Static Preisach Model prediction

Comparison between experiments and the model is given in Figure 5.10.

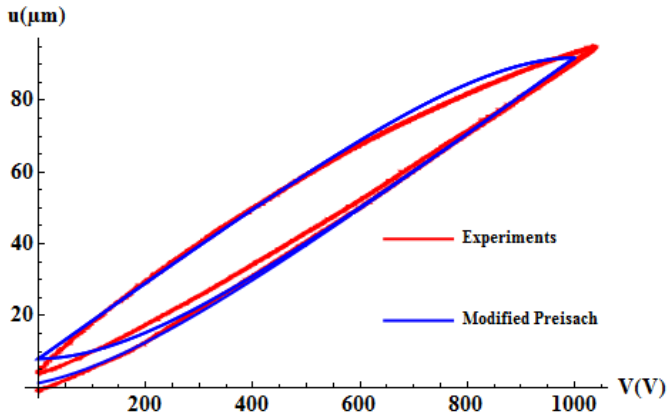

Figure 5.10: Experiments Vs Classical Preisach Approach (CPM)

The results are satisfying. However, one could improve it. Indeed, an alternative could consist of discrete Preisach approach (Equation 5.35):

$$u(V(t)) = \sum_{i}^{N} \mu_i(\alpha_i, \beta_i)\hat{\gamma}(\alpha_i, \beta_i, V(t)) \tag{5.35}$$

Therefore Preisach approach consists of many relay connected in parallel (Figure 5.11).

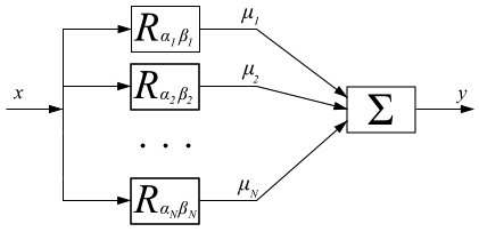

Figure 5.11: Discrete Classical Preisach Approach

Several computational program such as 20-Sim [6], Lab-Amesim [5] and Matlab-Simulink [124] integrate modules based on this approach.

Such an approach requires the determination of N triplets $(\alpha_i, \beta_i, \mu_i)$ i.e. $3.N$ parameters. One of its disadvantage is that it requires a huge amount of parameters and thereby a huge amount of data.

5.3.2 Dynamic hysteresis

Contrary to static hysteresis, dynamic hysteresis is due to the incapability of the material response to be in phase with the input and it is highly dependent on the driving voltage frequency as shown in Figure 5.12.

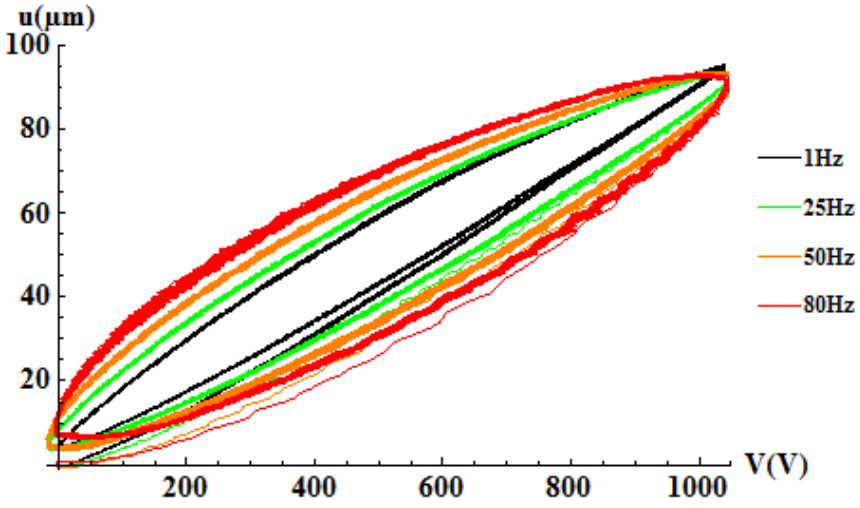

Figure 5.12: Dynamic hysteresis loops: sinusoidal input

5.3.2.1 Dynamic Preisach Approach

In dynamics, the Classical Preisach Approach fails to depict the hysteresis loops because they are rate-dependent. For example, many experiments as in Figure 5.12, show that the hysteresis loops tilt when the driving voltage frequency varies. Hence, dynamic Preisach models were proposed to deal with such problems [105, 106, 107, 108]. The authors introduced a dependence of μ-function on input variation rate $\frac{dV}{dt}$ [108].

$$u(V(t)) = \int\int_{\alpha\geq\beta} \mu\left(\alpha, \beta, \xi\left(\frac{dV}{dt}\right)\right) \hat{\gamma}(\alpha, \beta, V(t)) d\alpha d\beta \tag{5.36}$$

where the time variable t is independent of the corresponding α and β. $\xi\left(\frac{dV}{dt}\right)$ is a function of the input variation rate which describes the relationship between the input variation rate and the hysteresis loop. Its choice is based on experimental data. Details are given by the authors of the approach in [108].

The ξ function is chosen so that a power series development can be used and leads to:

$$u(V(t)) = \int\int_{\alpha\geq\beta} \mu_0(\alpha, \beta)\hat{\gamma}(\alpha, \beta, V(t)) d\alpha d\beta + \int\int_{\alpha\geq\beta} \xi\left(\frac{dV}{dt}\right) \mu_1(\alpha, \beta)\hat{\gamma}(\alpha, \beta, V(t)) d\alpha d\beta \tag{5.37}$$

Then:

$$u(V(t)) = \hat{u}(t) + \int\int_{\alpha\geq\beta} \xi\left(\frac{dV}{dt}\right) \mu_1(\alpha, \beta)\hat{\gamma}(\alpha, \beta, V(t)) d\alpha d\beta \tag{5.38}$$

where the term $\hat{u}(t)$ stands for the Classical Preisach Model.

The authors in [108] proposed a numerical implementation method and a process for the dynamic parameters identification.

Although this approach could be satisfying in certain situations, it is difficult to find a set of parameters that can match experimental data [96].

5.3.2.2 Analogy with viscoelastic materials

It had been observed and unanimously accepted that piezoelectric materials behaviour and viscoelastic/viscoplastic materials behaviour are similar [96]. There are many viscoelastic models [110, 97, 125, 95, 126].

The most common are Maxwell and Kelvin-Voigt's models (Figure 5.13). Nevertheless, the last one is more appropriate to solids, as piezo-bar devices, than Maxwell's model that it is appropriate to liquids. Maxwell unit is used to model creep effect in solids. The analogical model of the Kelvin-Voigt's viscoelastic solid is made with a spring (nonlinear or not) in parallel to a damper (nonlinear or not).

T.J.YEH and al. [127, 128] suggested to model hysteresis by adding step by step nonlinear Maxwell Voigt units to the electrical and mechanical ports until obtaining approximatively the real behavior of the device. This approach provides good between models and experiments. However, its drawback is the number of units which must be associated and thereby the number of corresponding parameters in order to cover wide range of frequencies.

H. Richter and al. [96] applied Maxwell-Voigt principle to the piezoelectric coefficient thanks to the equivalence $K \Longleftrightarrow \frac{1}{C} \Longleftrightarrow \frac{1}{d}$. The method consists of a series arrangement of n Voigt units and a non-linear dashpot (the damper of Maxwell solid).

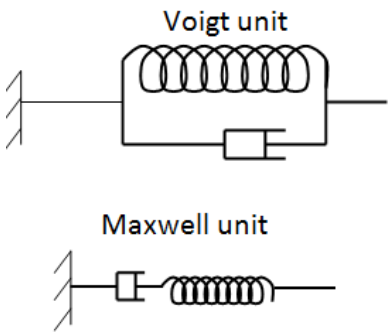

Figure 5.13: Maxwell and Voigt hysteresis units

5.3.2.3 Proposal approach

The spring of Voigt unit corresponds to the device gain (the gyrator in Figure 4.13). And the damper element stands for the piezoelectric losses different from mechanical and electrical losses respectively denoted R_m and R_e. We consider a nonlinear behaviour.

In previous sections, we experimentally showed that the piezoelectric coefficient d varies with the applied voltage. By analogy with natural growth law (Verhulst-Pearl), we established Equation 5.39.

$$d(V) = \frac{\alpha\lambda.exp^{-\lambda(V-\beta)}}{\left(1+exp^{-\lambda(V-\beta)}\right)^2} \tag{5.39}$$

where α, β and λ are a sigmoid parameters to determine with respect to experiments performed in static. For the HPSt 1000/35-25/80 piezo-device, we found $\alpha = 193.943\mu m$, $\beta = 704.908V$ and $\lambda = 0.0022V^{-1}$.

Concerning the piezoelectric losses, Voigt approach consists in setting:

$$\dot{u} = Sign(V).\left(\frac{\mid V \mid}{R_p}\right)^p \tag{5.40}$$

where R_p and p are coefficients to be determined with respect to experiments.

Consequently, the gyrator differential equation is:

$$\begin{array}{rcl} d(V) & = & \frac{\alpha\lambda.exp^{-\lambda(V-\beta)}}{\left(1+exp^{-\lambda(V-\beta)}\right)^2} \\ \dot{u} + \frac{u}{d.R_p} & = & Sign(V).\left(\frac{|V|}{R_p}\right)^p \end{array} \tag{5.41}$$

Taking into account the experimental setup in Figure 6.19, Equation 5.41 becomes:

$$\begin{array}{rcl} d(V) & = & \frac{K_m}{K_m+K_p}\frac{\alpha\lambda.exp^{-\lambda(V-\beta)}}{\left(1+exp^{-\lambda(V-\beta)}\right)^2} \\ \dot{u} + \frac{u}{d.R_p} & = & Sign(V).\left(\frac{|V|}{R_p}\right)^p \end{array} \tag{5.42}$$

In this equation, only R_p and p are unknown. For their estimation, we suggest to base on the hysteresis loop area (A_{hyst}) known to be proportional to the energy dissipations.

Series of experiments are performed on the HPSt 1000/35-25/80 with an input voltage as $V(t) = V_0\left(1 + \mathrm{Sin}(2\pi ft - \pi/2)\right)$, where $V_0 = 125$ Volts and f varies from $1Hz$ to $400Hz$. For each frequency the hysteresis loop area is computed and depicted in Figure 5.14.

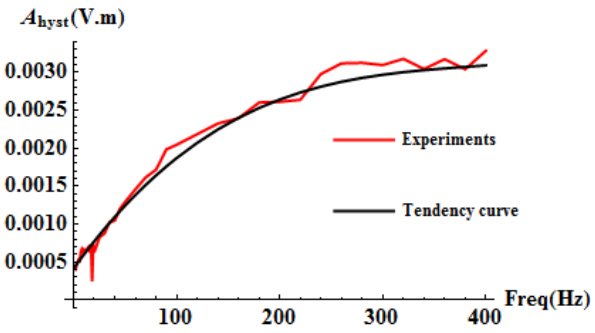

Figure 5.14: HPSt 1000/35-25/80: Hysteresis loop area

The modeling task therefore consists in finding p and R_p that provide the best approximation. Since $p \neq 1$, analytical solving is no longer possible. An efficient algorithm for numerical solving is therefore required.

For this purpose, we proceed in two steps.

Step 1: Set $p = 1$ and estimate a mean value of R_p

- Set d_m: mean value of d_{gyr} (in our case $d_m = 0.66.10^{-8} m.V^{-1}$
- Initialize $A = 0$
- A_{he}, n_A the table containing experiments frequencies ($A_{he}[n, 1]$) and their corresponding hysteresis loop area in International Units ($A_{he}[n, 2]$)
- For $\left[k = 1,\ k < n_A + 1,\ k++,\ A = A + \left(V_0 \frac{8\pi.d_m^2.R_p.A_{he}[k,1]}{1+4d_m^2.(A_{he}[k,1])^2\pi^2.R_p^2} - A_{he}[k,2]\right)^2\right]$
- Find R_{pm} minimizing A. In our case we used Mathematica function NMinimize [116] and found $R_{pm} = 11894.6\Omega$

Step 2: Determine p and R_p

- Set a table of n_{Rp} elements symmetrical about R_{pm}
- Set a table of n_p elements symmetrical about 1
- For each couple of (R_p, p), and each frequency, solve numerically the differential equation $\dot{u}[t] + \frac{u[t]}{d_m.R_p} = \left(\frac{V[t]}{R_p}\right)^p$. In our case we used the function NDSolve of Mathematica
- Evaluate the area of corresponding hysteresis
- Find the couple (R_p, p) which minimizes the difference between experimental loops' areas and theoretical ones. In our case, we got $R_p = 10300\Omega$ and $p = 1.043$.

Figure 5.15 depicts the energy losses predicted by the determined model.

However, at relative low frequencies, both the linear and proposal nonlinear Voigt-based models fail to predict the piezoelectric dissipations. By contrast, the experiments show (Figure 5.14) that at $1Hz$ there is a non-negligible hysteresis loop. This is a systematic

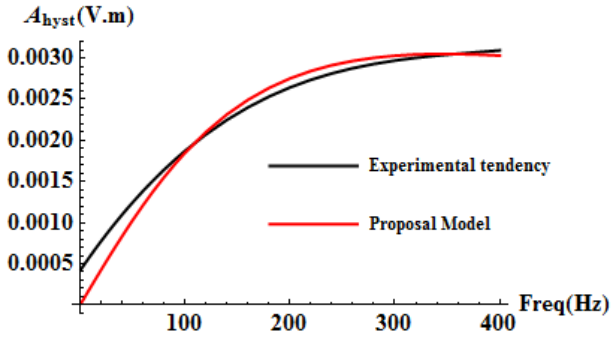

Figure 5.15: Proposal model ($R_p = 10300\Omega$, $p = 1.043$)

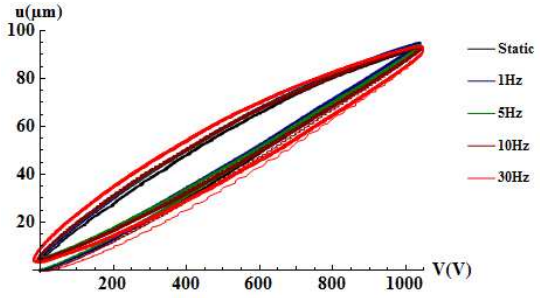

Figure 5.16: Piezo: HPSt 1000/35-25/80, hysteresis loop almost invariable under 25Hz

hysteresis at low frequencies. Moreover, we noticed (Figure 5.16) that this systematic hysteresis loop is almost invariable until a threshold frequency (about $25Hz$ in the case of HPSt 1000/35-25/80).

Since static hysteresis was well model by Preisach approach, we therefore suggest to combine it with Voigt approach in order to obtain a more efficient model.

5.3.3 Proposal mixed Preisach-Voigt approach

Se suggest an hybrid model. It consists of an addition of Preisach model (to account for invariable hysteresis loop) and Voigt model (to account for dynamic hysteresis loop).

Then, we obtain in Figure 5.17 the final proposal model.

In terms of bond graph formalism, the main change occurs in the gyrator as follows:

parameters real global a, b, c,Vs0, α, β, γ, λ, R_p, p;

variables real dp, d_{gyr}, oldin, oldout, speed, sp, sp2, V_s, us, uint, Vint;

equations

$p2.e = (1/dp) * p1.f$;

$dgyr = \frac{\alpha\lambda.exp^{(\lambda(\beta - p1.e))}}{\left(1+exp^{(\lambda(\beta-p1.e))}\right)^2}$;

$oldin = dly(p1.e, 0.0)$; $oldout = dly(uint, 0.0)$; $speed = p1.e - oldin$;

if $time == 0$ then

$Vs = Vs0; us = 0; sp = 0; sp2 = 0$

end;

if $speed >= 0$ then

if $sp == 1$ then

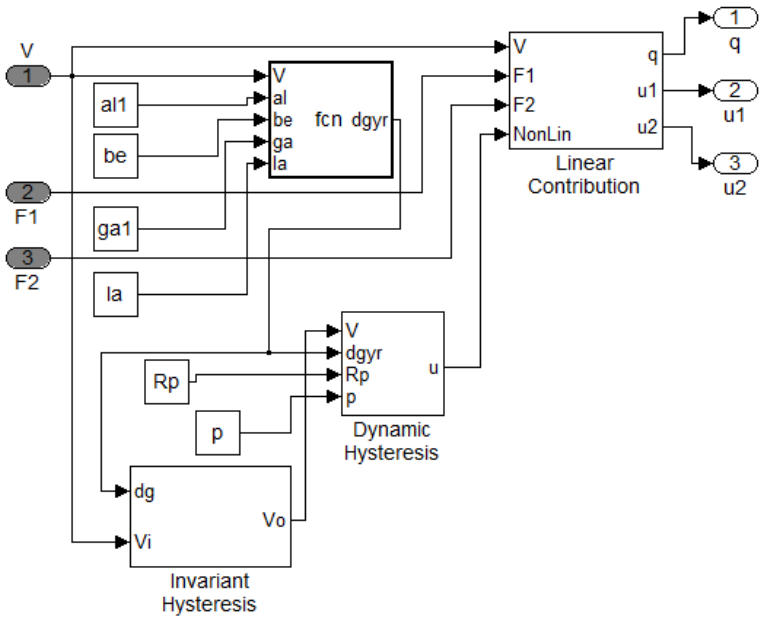

Figure 5.17: Complete model of a piezo-bar actuator

$Vs = oldin$; $us = oldout$; $sp = 0$;
end;

$$uint = us + \frac{a^2}{b^2(c^2-1)^2\left(c+e^{bp1.e}\right)\left(c+e^{bVs}\right)}.\Bigg[\left(c^2-1\right)\left(e^{b(p1.e+Vs)}-1\right)$$
$$+\left(c+e^{bp1.e}\right)\left(c+e^{bVs}\right).\mathrm{Log}\left(\frac{\left(c+e^{bp1.e}\right)\left(1+ce^{-bVs}\right)}{\left(1+ce^{bp1.e}\right)\left(c+e^{-bVs}\right)}\right)\Bigg];$$

$Vint = uint/dgyr$;
else
$sp = 1$;
if $sp2 == 0$ then
$Vs = oldin$; $us = oldout$; $sp2 = 1$;
end;

$$uint = u_s + \frac{a^2}{b^2(c^2-1)^2\left(1+c.e^{bp1.e}\right)\left(c+e^{bVs}\right)}.\Bigg[\left(c^2-1\right)\left(e^{bp1.e}-e^{bVs}\right)$$
$$+\left(1+ce^{bp1.e}\right)\left(c+e^{bVs}\right).\mathrm{Log}\left(\frac{\left(c+e^{bp1.e}\right)\left(1+ce^{bVs}\right)}{\left(1+ce^{bp1.e}\right)\left(c+e^{bVs}\right)}\right)\Bigg];$$

$Vint = uint/dgyr$;
end;

$$ddt(p2.f) + \frac{p2.f}{dgyr*R_p} = \left(\frac{Vint}{Rp}\right)^p;$$

The model is compared to experiments in Table 5.5.

The combination of Preisach approach and viscoelasticity approach (Voigt) shows good fitting with experiments. However, some imperfections are still noticed as one can remark in Table 5.5. These imperfections could be due to many factors: inaccuracies in our modeling approach, non-robustness of the models' parameters estimation process, inaccuracies in the signal acquisition procedure.

However, despite the approximations and simplifications made during the modeling pro-

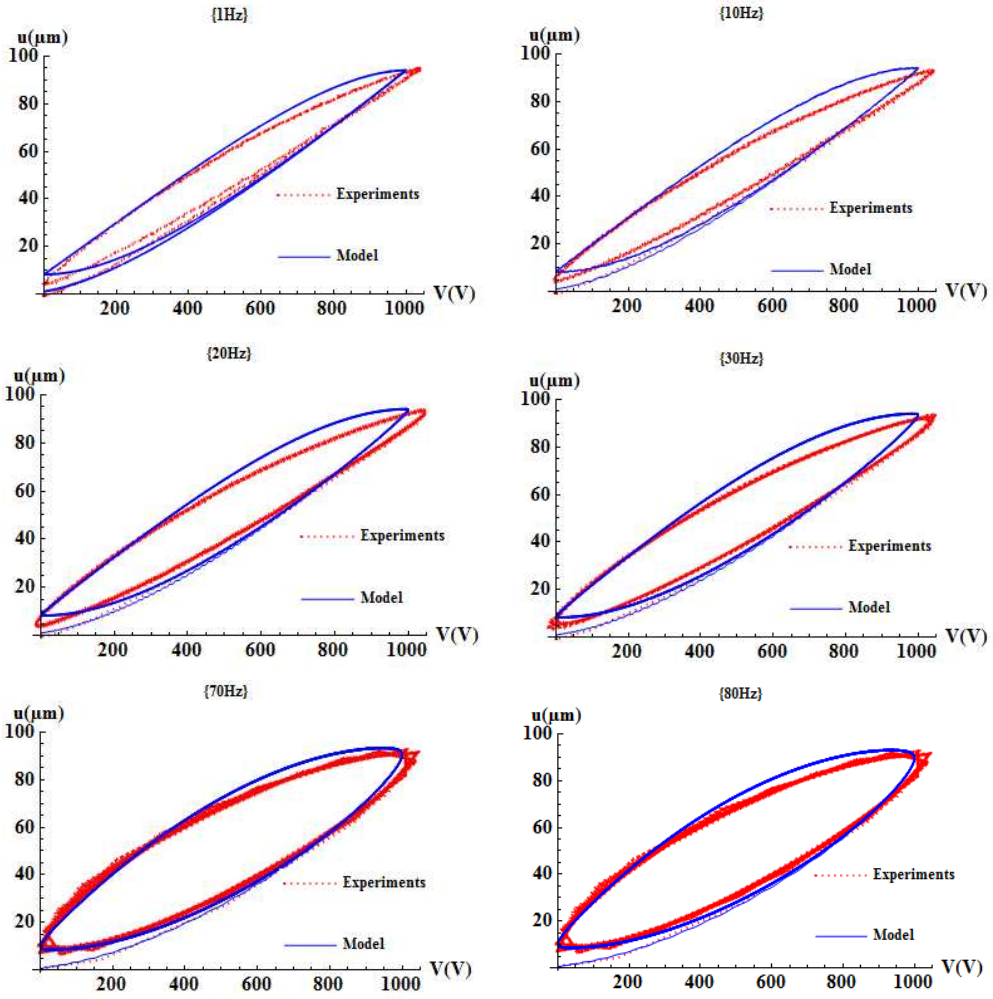

Table 5.5: Proposal nonlinear model compared to experiments

cess, we adopted a rigorous physics-based approach. The imperfections are more likely due to non-robustness of the models' parameters estimation process. Indeed, the optimization algorithm that we suggested and programmed for determining the parameters, are all based on least squares methods. However these methods are highly sensitive to estimation errors. Robust estimation methods are needed for better parameters determination.

Moreover, the model is expected to be extendible to high frequencies as shown in Figure 5.18. Simulations in Figure 5.18 are not supposed to demonstrate the validity of the model at high frequencies. They only allow predicting the piezoelectric actuator's behavior at high frequencies. The results are acceptable since they are coherent with general observations. Experiments are not performed beyond 400 Hz because of the limits of mechanical pre-loading elements in Figure 4.20.

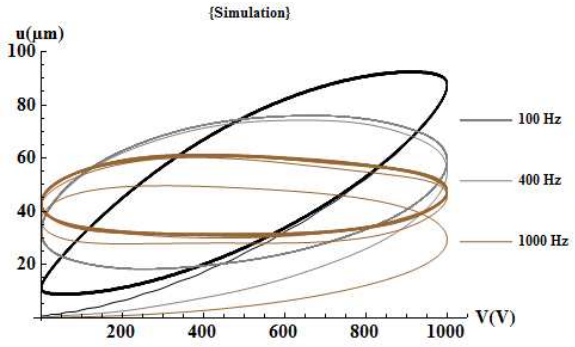

Figure 5.18: Model predictions at relative high frequencies

5.4 Conclusion

Piezoelectric device nonlinearities were analyzed and models to account for these aspects were proposed. To account for nonlinear gain, a sigmoidal model (Verhulst approach) had been proposed with good agreement between the model and experiments. However we showed that the corresponding parameters change according operating modes: static or dynamic. Then Preisach approaches were tested in order to model hysteresis in systems built with piezo-devices. We highlighted their limits in the case of piezoelectric materials. Then we combined them to Kelvin Voigt approach. For the established model's parameters estimation, we based on the energy lost within one cycle of solicitation. A clear and efficient algorithm was suggested for. We were rigorous in our methods but we kept in mind the necessity for the proposal models to be easy to integrate in simulation tools.

Chapter 6

Complex systems control

6.1 Résumé du chapitre en Francais

Comme le montre le tableau 6.1, les livrables de ce travail sont un ensemble de modèles paramètriques. Dans ce chapitre, nous montrerons comment ces modèles sont intégrables dans une structure et ce qu'on peut en tirer.

Dans la section 6.3, nous montrons l'utilisation qui pourrait être faite de la sortie de courant. En effet, il est parfois difficile de placer dans un montage des capteurs de déplacement ou d'effort à cause de l'encombrement.

Nous considérons un actionneur piézoélectrique dont on dispose des modèles. Cependant il est intégré dans une structure dont les autres parties sont difficiles à modéliser. Nous montrons dans cette section que lorsque le piézoélectrique est préchargé, en excitant l'actionneur avec une tension sinusoïdale à une fréquence arbitraire, la FFT du signal du courant (Figure 6.4) donne la fréquence du signal et la fréquence propre du système.

Par ailleurs, en fabrication par enlèvement de matière, la mesure et le contrôle de la force de résistance à la coupe permet d'améliorer les opérations. Les vibrations injectées par l'actionneur piézoélectrique doivent être réglées en fonction de cette résistance. Mais pour les mêmes raisons évoquées ci-haut, il nous est impossible d'implémenter un capteur d'effort. Ce que nous proposons c'est d'alors utiliser l'actionneur pour à la fois générer des vibrations mais aussi mesurer l'effort au même instant.

Mais avant nous présentons les techniques usuelles utilisant des éléments piézoélectriques pour la mesure de l'effort. Elles consistent en général à mesurer les variables indépendantes u et q pour en déduire F. C'est le principe utilisé par le fabricant de tables Kistler. En plus ils choisissent un élément infiniment rigide. Ce qui permet alors de négliger $u \simeq 0$.

Dans notre cas, u n'est pas négligeable car il s'agit d'un actionneur. Mais pour les raisons évoquées plus haut sa mesure est problématique.

Ce que nous proposons est l'utilisation des variables dépendantes V et I (courant électrique). Pour déterminer q nous intégrons I. Pour éviter les problèmes de condition initiale nous ne prenons que la composante variable de I.

Les parties critiques du modèle d'estimation de l'effort sont surlignées dans la Figure 7.4. Les limitations de cet estimateur sont qu'une petite erreur dans la mesure du courant entraine une divergence de l'estimée.

En outre, comme nous l'avions noté précédemment, la problématique en usinage vibratoire concerne la génération des vibrations avec les bonnes caractéristiques (phase, fréquence,

amplitude). Dans la section 6.5.1 nous proposons la commande par inversion de modèle, contrairement aux méthodes de contrôle par feedback [129, 130, 131, 132, 133, 134, 135, 136]. Les avantages d'une telle approche sont énumérés dans [137]. Mais contrairement aux auteurs de [137] qui ont utilisé le GIC (Graphe d'Information Causal), nous restons cohérents à notre démarche en utilisant les bond graph (Figure 6.15). La mesure du courant en temps réel est nécessaire. Le problème posé plus haut n'est plus car u et I sont indépendants.

Nous vérifions alors la stabilité de modèle inversé sans tenir compte du système de perçage. Une étude ultérieure traitera de ce cas. Pour ce faire, le modèle est ramené à un système à entrée/sortie unique dont la fonction de transfert correspond à l'Equation 6.10. S est l'opérateur de Laplace.

Afin de compenser les incertitudes des modèles et des mesures, nous devrons ultérieurement concevoir un correcteur.

Dans la section 6.6, plutôt que de générer les vibrations, nous voulons les inhiber. Pour ce faire l'énergie mécanique des vibrations est évacuée à travers une circuit électrique qui peut être résistif ou contenir des éléments capacitifs ou inductifs [138].

Dans ce cas, la résistance R_s prévaut sur les non-liéarités du piézoélectrique. La stabilité du système G est vérifiée par le critère de Routh-Hurwitz.

On montre que l'amortissement du système est proportionnel à $\frac{k^2}{1-k^2}$ [139, 14]. Il est alors possible de l'améliorer à l'aide d'une capacité négative. Les techniques de construction de capacité négative sont présentées dans [140].

Enfin dans la section 7.2.2, nous analysons la possibilité d'étendre notre approche aux actionneurs magnétostrictifs.

Le comportement des matériaux magnétostrictifs est semblable à celui des piézoélectriques. L'Equation 6.1 décrit en un point du matériau, la loi de comportement.

$$\begin{array}{rcl} S & = & \left[s^H\right].T + [d]^t.H \\ B & = & [d].T + \left[\mu^T\right].H \end{array} \tag{6.1}$$

où S est la déformation, T la contrainte, B l'induction magnétique et H le champ magnétique. s est le tenseur de flexibilité, μ le tenseur de perméabilité et d le tenseur piézomagnétique.

En 1-D cette équation se réduit aux relations 6.2 où on peut omettre les indices et exposants.

$$\begin{array}{rcl} S_3 & = & s_{33}^H.T_3 + d_{33}.H_3 \\ B_3 & = & d_{33}.T_3 + \mu_{33}^T.H_3 \end{array} \tag{6.2}$$

Une technique de génération du champ magnétique consiste à utiliser des bobines parcourues par un courant électrique. Notons ϕ_t le flux magnétique total. On obtient:

Toutefois, on utilise de plus en plus des moyens complexes de génération du champ. De ce fait, l'étude devra se faire au cas par cas.

Dans cette section nous nous intéresserons uniquement à la relation $u = f[H]$.

Bien que le domaine des actionneurs magnétostrictifs soit mûr [141, 142, 143, 144, 145, 146, 63, 147, 148], nous voulons montrer comment notre approche peut se transposer.

D'après les Equations 5.33 et 5.34 (Chapitre 5), si $H \geq 0$ on peut écrire:

$$\begin{array}{rcl} u & = & u_R(H) \text{ On the increasing branch} \\ u & = & u_D(H) \text{ On the decreasing branch} \end{array} \tag{6.3}$$

Et si $H \leq 0$, on remplace H par $-H$.

$$\begin{array}{rcl} u & = & u_D(-H) \text{ On the increasing branch} \\ u & = & u_R(-H) \text{ On the decreasing branch} \end{array} \tag{6.4}$$

Après intégration de ces modifications dans le modèle Bond Graph, nous obtenons la Figure 7.7.

Les paramètres a, b et c de la partie de Preisach dépendent de la précharge P.

Il faudra ultérieurement élaborer une méthode expérimentale de détermination des paramètres comme dans le cas des piézoélectriques.

The main objective of this thesis is to make it available for all, ready-to-use models. In this vein, the performed study and thereby the established models should be formalized by means of common tools and tutorials should be associated to the models. Elsewhere practical benefits of the proposal models should be demonstrated.

6.2 Models formalization

The outcome of this thesis is the construction of a library of models as follows (Table 6.1).

Operating modes	Models	Parameters
Static	Linear	K_m, C_e, d_{mean}
	Sigmoidal	K_m, C_e, α, β, λ, γ
	Hysteretic	K_m, C_e, d_{mean}, a, b, c
Dynamic	Linear 1,2 -stacks	K_m, C_e, d_{mean}, M, Q_m, η, f_{r2}^*
	Sigmoidal 1,2 -stacks	K_m, C_e, M, Q_m, η, f_{r2}, α, β, λ, γ
	Hysteretic 1,2 -stacks	K_m, C_e, M, Q_m, η, f_{r2}, α, β, λ, γ
		R_p, p, a, b, c

Table 6.1: Proposal formalized models both in bond graph and block-diagram

Following is the procedure for the models parametrization.

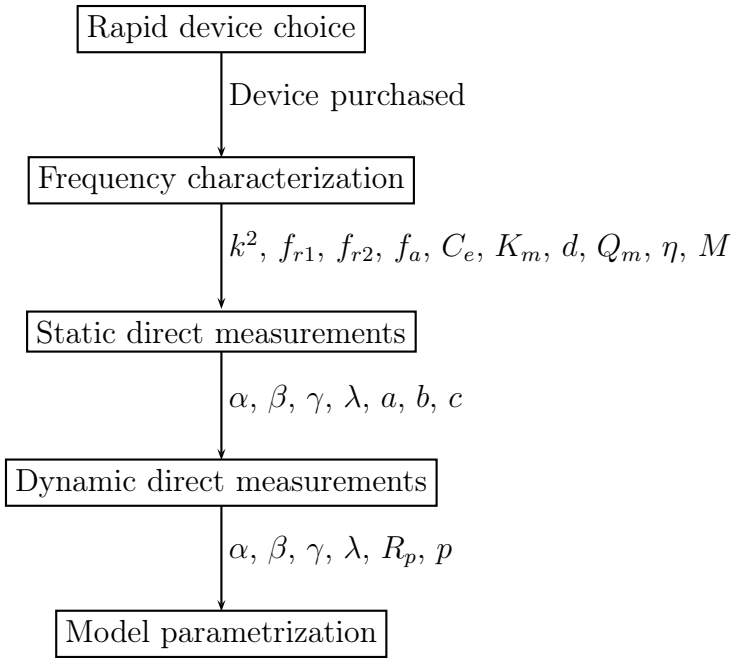

Figure 6.1: Formalized procedure for parameters determination

6.3 Using electric current output

Let us consider a complex structure in which a piezo-bar is integrated. We are interested in the structure behaviour in the longitudinal direction of the piezo-device. Nevertheless, the structure size does not ease installation of any sensor (displacement or effort sensors). Metallic constraint gauges are often mounted on piezo-devices. However, these gauges usually have a delay time in their response (Figure 6.2).

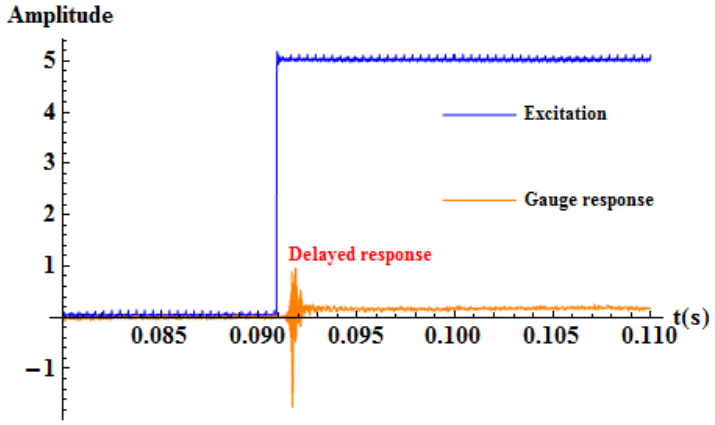

Figure 6.2: Contrary to piezo-sensors, metallic gauges introduce a delay in their response

Moreover, even though efficient models of piezo-actuators have been established, the other parts of the structure could take time to model. Therefore, electric current measurements could be precious for rapid information gathering about the structure

6.3.1 Dynamic information from electric current output

Let us consider a complex structure with a piezo-bar. The user has at its disposal models for the piezo-device but not for the other parts of the structure.He would like to check the first resonant frequency of the system. However, he meets obstacles that were enumerated above. In addition, step excitation could be harmful to the system.

We observe and verify that a single, simple and non-harmful experiment provides this information. The experiment consists of a sinusoidal voltage excitation. The frequency of the signal is arbitrary; for example $1Hz$ makes it. The amplitude too, is not so important. For example 2% is sufficient. However, it is important that the piezo-device be pre-loaded.

Then the electric current response is measured and its spectrum depicted. The FFT reveals the resonant frequency of the system. The induced electric current is the sum of two (2) waves: the frequency of the first one equals the first resonant frequency of the whole system and the second one corresponds to the driving voltage frequency. Such a behaviour is due to the initial pre-load applied to the piezo-device.

As an example, let us reconsider our thesis experimental setup.

Figure 6.4 demonstrates the above assessments.

However, in order to measure with good accuracy the resonant frequency, a better method consists of the method exposed in Chapter 3.

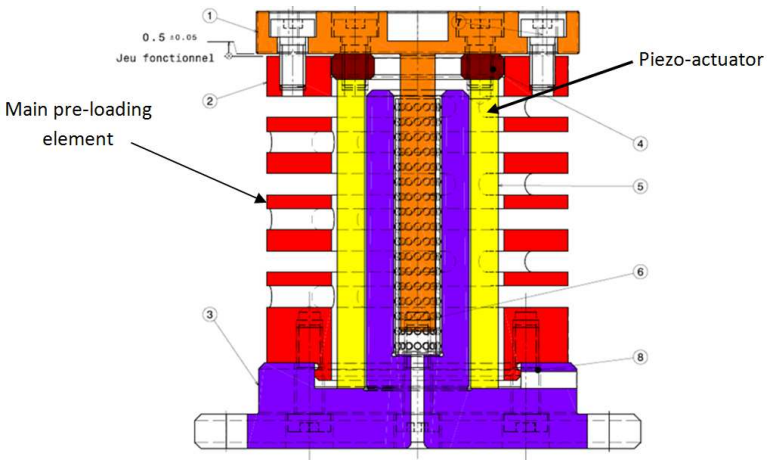

Figure 6.3: Experimental setup

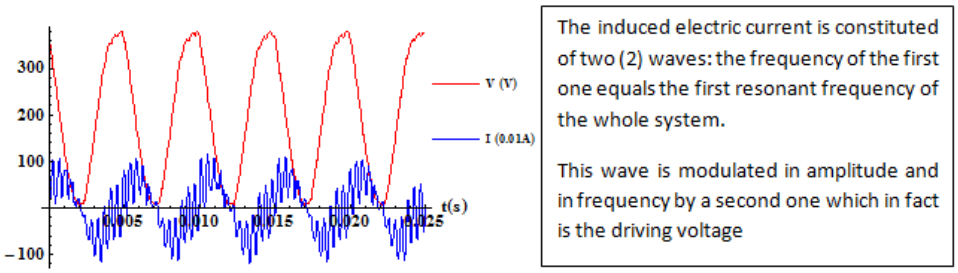

Figure 6.4: Dynamic information from electric current output

6.4 Using the model for vibration drilling

Let us consider the drilling setup in Figure 6.5.

The corresponding model is represented in Figure 6.6.

A part from the piezoelectric actuator nonlinearities, the system's complexity is also due to the vibration drilling kinematics but also to the law of the cutting resistive force (Cutting Stiffness).

6.4.1 How complex is the system?

Four elements are coupled in the system shown in Figure 6.6: the piezoelectric actuator with its pre-loading parts, the excitation source, the workpiece and drilling machine and tools (drilling laws).

6.4.1.1 Piezoelectric actuator with its pre-loading parts

We use the HPSt 1000/35-25/80. For simulation and comparison, we use the static, the linear dynamic, and the final proposal models. The parameters of each type of model were enumerated in Section 6.2. The pre-loading parts were presented in Chapter 4.

Figure 6.5: Vibrational drilling setup up

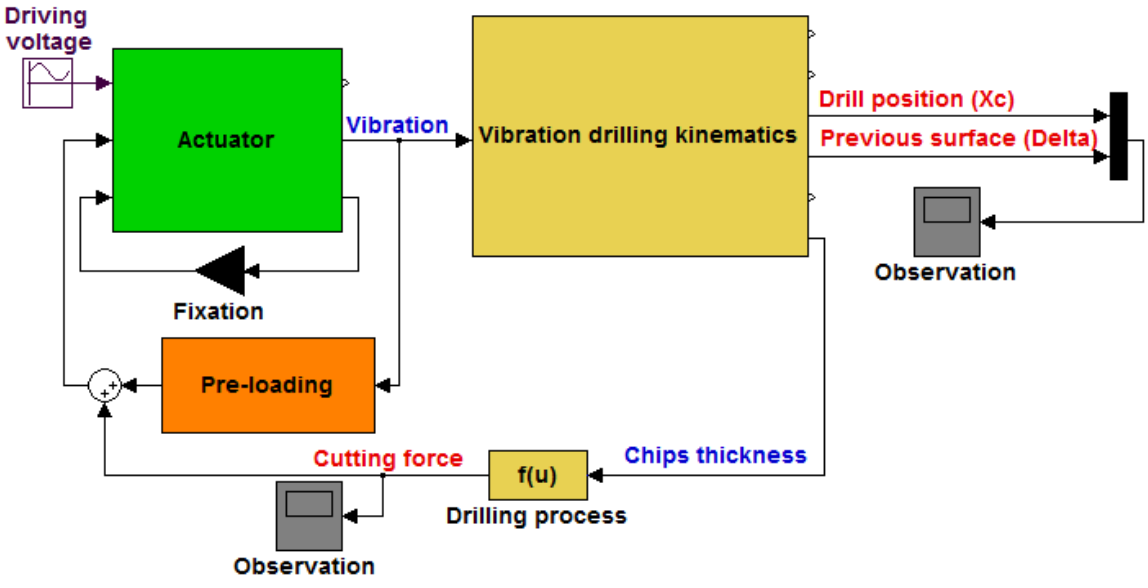

Figure 6.6: Vibrational drilling model

6.4.1.2 Excitation source

The input voltage is firstly design on computer. Then via National Instruments Cards an analogical form is transmitted to an amplifier RCV 1000/7. The output of the amplifier then constitutes the input voltage for the piezo-device.

However, assuming that the excitation equipments are used in their linear range, only two parameters are really important in the global system: the excitation magnitude V_{cc} and its frequency. Let us denote it $freq_{oscillation}$.

Moreover, the simulation are run with the maximal magnitude $V_{cc} = 1000V$.

6.4.1.3 The workpiece

The influence of the workpiece on the system is about the resistive force that it opposes to the drilling operation. One defines the cutting stiffness $K_{cutting}$ which depends on the workpiece constitutive materials, the profile of the hole to be drilled (drill's diameter and geometry) but also the drilling kinematics (see bellows).

It is commonly accepted that $F_{cutting} = K_{cutting}.h^{w}_{cutting}$, where w is a coefficient from 0.8 to 1 [3].

We saw that the piezoelectric subsystem has its own stiffness $K_{Piezo-syst}$ which depends on electrical conditions.

It has been established the existence of a critical stiffness K_{cr} of the piezo-system, for which the vibration drilling process becomes unstable:

$$K_{cr} = \frac{K_{cutting}}{2\xi(1+\xi)} \tag{6.5}$$

where ξ refers to the damping factor of the piezoelectric subsystem.

6.4.1.4 Vibration drilling laws

Cutting and especially drilling were studied by G. Moraru in his thesis [3]. Accordingly, vibration drilling kinematics corresponds to Figure 6.7.

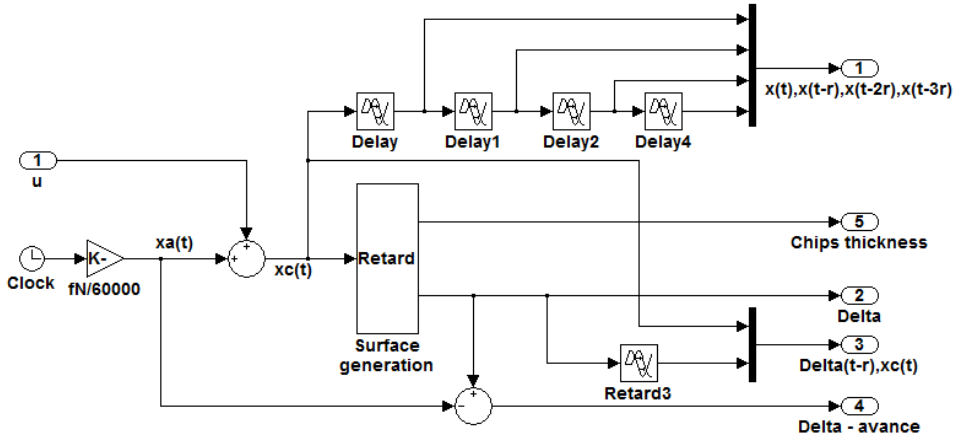

Figure 6.7: Vibration drilling kinematics [3]

$u(t)$ influences the generated surface is illustrated in Figure 6.8. Δ denotes the cutting surface variable. $X_a(t)$ (x in Figure 6.7) denotes the drilling toolŠs progress. $X_c(t)$ denotes the cutting movement and $u(t)$ the piezo-actuators' vibrations. N is the drill revolution rate (rev/min) and f its progress per revolution. We denotes h_{chips} the chips thickness.

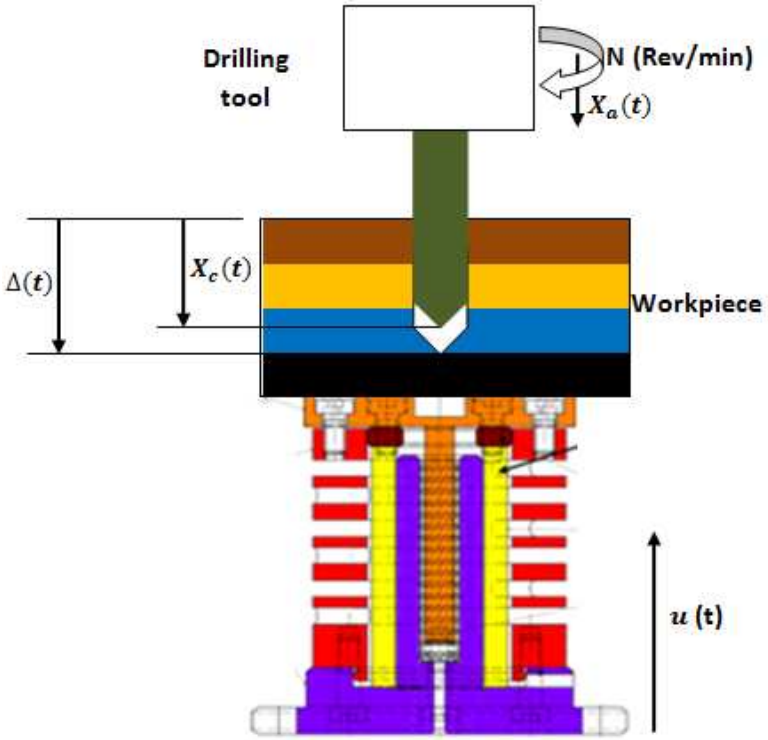

Figure 6.8: Cutting surface generation

The drilling laws are then given in Equation 6.6.

$$\begin{cases} X_a(t) & = & \frac{f.N}{60000}.t \\ X_c(t) & = & X_a(t) - u(t) \\ \Delta(t \leq 0) & = & 0 \\ \Delta(t > 0) & = & max\left[\Delta(t-r), X_c(t)\right] \\ h_{chips} & = & \Delta(t) - \Delta(t-r) \\ F_{cutting} & = & K_{cutting}.h_{cutting}^{w} \end{cases} \tag{6.6}$$

r denotes a delay of 1 period.

The drill bit intervenes through its diameter and especially through its number of edges z. One defines the cutting frequency as follows:

$$freq_{cut} = z.\frac{N}{60} \tag{6.7}$$

Then one defines the following ratio:

$$\eta_{freq} = \frac{freq_{oscillation}}{freq_{cut}} \tag{6.8}$$

We shall see in the following section, how this ration is used.

6.4.2 Chips shattering

h_{chips} depends on the injected piezo-vibration. Therefore, there is a need for controlling the vibration amplitude. This justifies the importance of modeling the hysteresis.

h_{chips} depends on the toolŠs progress i.e. there is a need for controlling the progress. $F_{cutting}$ depends on h_{chips} and the workpiece material. It is therefore necessary to be able to detect the material changing.

From the model, four (4) outputs provide useful information about the cutting operation: $F_{cutting}$, $X_c(t)$, $\Delta(t-r)$ and h_{chips}. Since they depend on the piezo-actuator's oscillation, the hysteresis phenomena could lead to important loss of amplitude. This could affect the process efficiency. The availability of a complete model allows to simulate and make the necessary decisions.

If $F_{cutting} = 0$ ($\Longleftrightarrow \Delta(t-r) > X_c(t)$) then the drill does not cut the workpiece. Otherwise, the condition for chips shattering, is that $\Delta(t-r) \leq X_c(t)$ and the two curves $X_c(t)$ and $\Delta(t-r)$ overlap each other as shown in Figure 6.9. In this Figure the drilling conditions correspond to n ° 2 in Table 6.2.

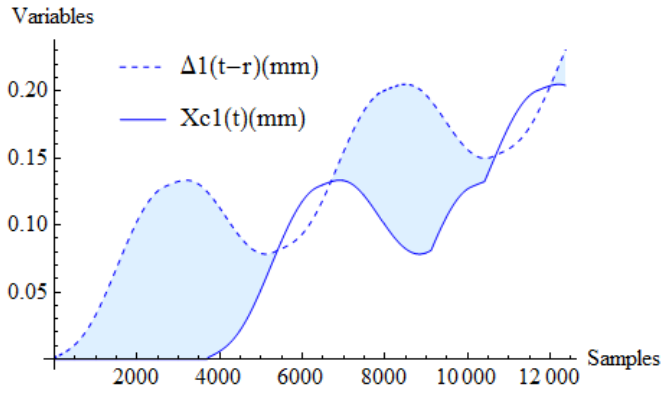

Figure 6.9: Vibration drilling: nonlinear piezo-model

It has been proved that a necessary condition for chips shattering is:

$$\eta_{freq} =\notin \mathbb{Z} \tag{6.9}$$

The blue colored regions in Figure 6.9 correspond to the chips. On the other hand, for the white colored regions, the workpiece is not cut. The existence of such regions mean that shocks will occur during the cutting process. This is harmful for the finish surface and also for the tool lifetime. The best drilling settings are those allowing to avoid such area but rather to obtain tangent lines. A better analysis is made possible by the cutting force observation.

In Figure 6.10 we suggest to vary η_{freq} and keep the other settings as in condition n ° 1.

Simulation show that a good value can be $\eta_{freq} = 0.714$. For $\eta_{freq} = 0.7$, the chips are shattered but shocks are observed. For $\eta_{freq} = 0.73$, the chips are no longer shattered. This settings search is made possible thanks to the availability of models.

Now we shall compare different models. For this purpose, let us consider the following conditions

In the sequel, variables followed by 1 (Example X_c1, $\Delta 1$) refer to the nonlinear model.

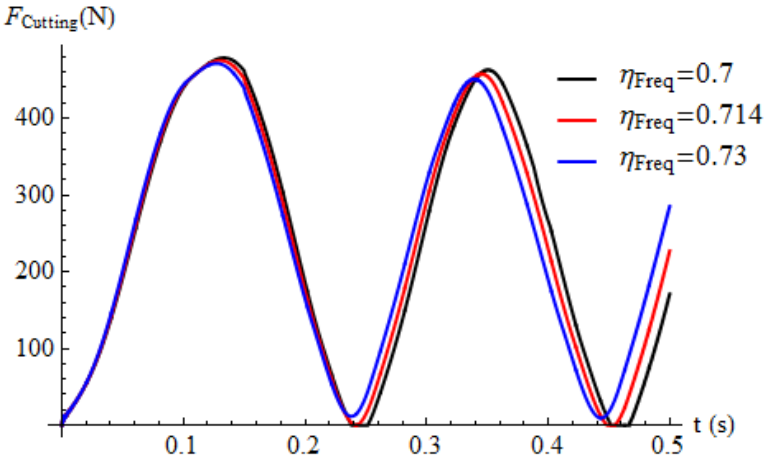

Figure 6.10: Best settings search

Conditions	feed rate (mm/rev)	z	N (rev/min)	η_{freq}	$K_{cutting}$	w
n ° 1	0.145	2	200	0.7	$1.3 * 10^6$	0.9
n ° 2	0.1	2	200	0.7	$1.3 * 10^6$	0.9
n ° 3	0.1	2	1500	0.7	$1.3 * 10^6$	0.9
n ° 4	0.1	2	1500	0.7	$1.3 * 10^7$	0.9

Table 6.2: Drilling simulation conditions

Using condition n ° in Figure 6.11, the linear model predicts continuous cutting ($F_{cutting}$ never equals 0). Consequently there the chips would not be shattered. By contrast, the nonlinear model predicts discontinuous cutting since $F_{cutting}$ sometimes falls to 0. This comparison shows how inaccurate models could lead to inappropriate decision.

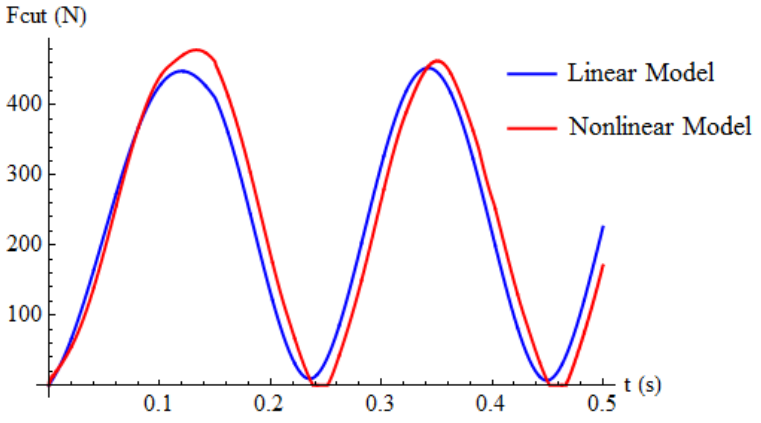

Figure 6.11: Cutting force predictions

Moreover, in Figure 6.12 (where simulation conditions correspond to n ° 3), apart from the phase shift between the two models, one can also observe differences in the chips forms.

For the same conditions, we now compare in Figure 6.13, our proposal model with the static model as proposed by LabAmesim [5]. Variables followed by 0 (Example X_c0, $\Delta 0$) refer to the static model. The static model predicts smooth chips contrary to the proposal

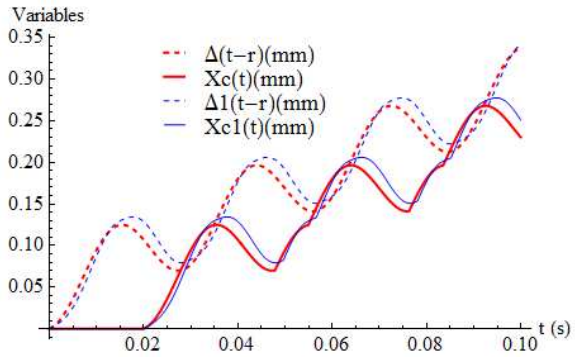

Figure 6.12: Linear Vs Proposal models

model.

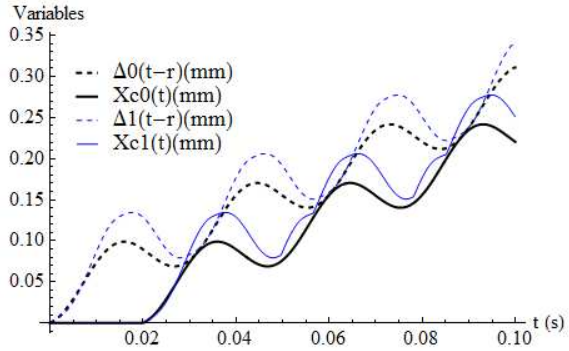

Figure 6.13: Static Vs Proposal models

Then in Figure 6.14, we increase the cutting stiffness by changing the workpiece material (simulation conditions n ° 4). In this case the static model predicts non-shattering of the chips contrary to our proposal model. Moreover, the static model does not reveal resonant excitation (contrary to our proposal model) which could be due to critical stiffness (Equation 6.5).

All these could influence the drilling process. However such an analysis would not be possible with a linear model or static model.

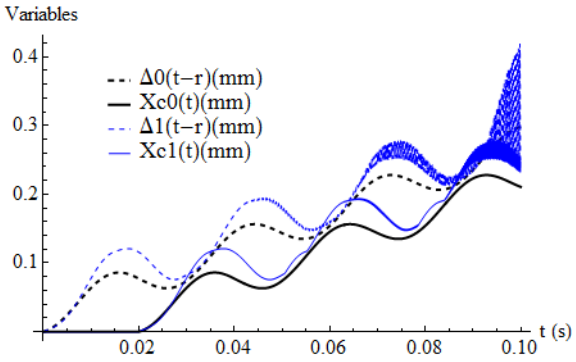

Figure 6.14: Static Vs Proposal models

6.5 Control loop synthesis

6.5.1 Model inversion

One of the stakes in vibrational drilling is about generating the right piezo-vibrations (in terms of frequency, amplitude and phase). For this purpose the user should construct the right command. Methods for complex systems's control are therefore required.

There are numerous methods for complex systems control [137]. More commonly, the system's outputs are measured or estimated in order to track the referee command via a synthesized feedback. In this category one could enumerate adaptive control [129, 130], state feedback control [131, 132], sliding model control [133, 134] etc. All provide satisfaction despite different sources of perturbations. These methods are classified as global control methods. On the other hand, other techniques (named local techniques) consist of interconnected subparts associated with the different parts of the system. This category includes nested control loops [135], backstepping control [136] and inverse model control [137].

Regarding the approaches we adopted during modeling tasks, inverse model control is more preferred than the others. Indeed, inverse model control offers an organized methodology using a decomposition of the systems' organs functionality with respect to exchange energy. It consists in synthesizing the input according to the desired output profile. Therefrom, the task is to determine the physical reverse function of the system (piezo). For this purpose, different formalisms could be used, for example GIC (Graphe Informationnel Causal) [137].

However, in order to remain consistent in our approach, the established bond graph models can be easily reversed as shown in Figure 6.15. The unique difficulty concerns the nonlinear equations of the gyrator which could introduce algebraic variables.

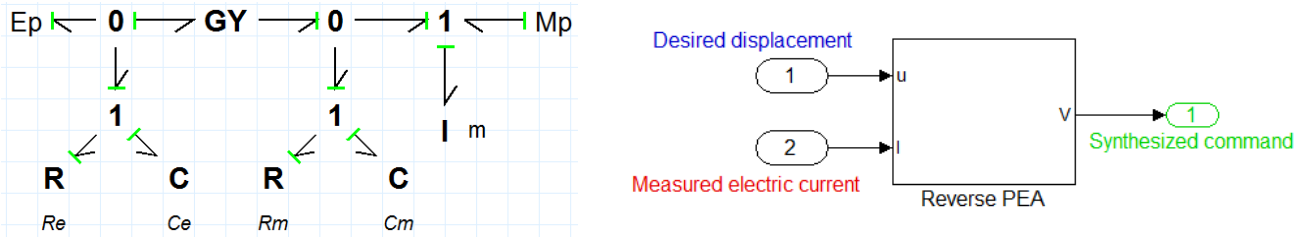

Figure 6.15: Piezo-bar actuator reverse control

Thereafter, the result can be translated into block-diagrams as shown in Figure 6.16.

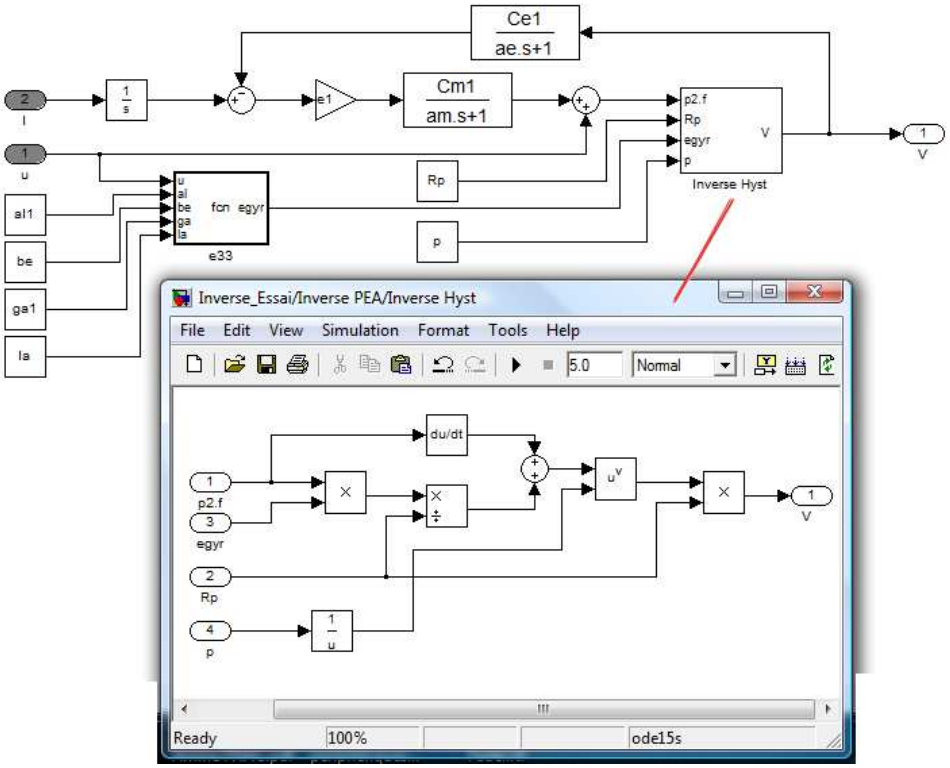

Figure 6.16: Block-diagram translation of the reverse model $e_{gyr} = \frac{\alpha}{\lambda.(u+\gamma)^2.\left(\frac{\alpha}{u+\gamma}-1\right)}$

6.5.1.1 Stability analysis

In this section, we shall study the proposal command loop in Figure 6.17. We consider a piezo-bar device clamped on one of its faces. In this section, we shall perform the study with unloaded device ($F_1 = 0$). However, further research should include the loading system. Models for drilling systems were proposed in [3].

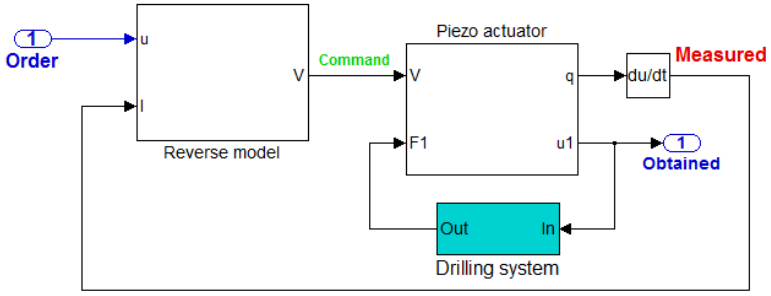

Figure 6.17: Proposal command loop

The most sensitive part of the proposal command architecture concerns the electric current loop. Generally, control loops' stability is studied with linearized models.

Assuming the exactness of the models and a good accuracy of the current sensor the command loop in Figure 6.17 would correspond to a SISO (single Input Single Output) system.

Therefrom, its transfer function can be determined. One could verified:

$$\frac{u_{obtained}}{u_{order}} = H[S] = \frac{K_m + R_m S}{1 + K_m + R_m S + mS^2} \tag{6.10}$$

where S stands for Laplace's operator.

$(1 + K_m) > 0$, $R_m > 0$ and $m > 0$. Therefore, according to Routh-Hurwitz criterion, the command loop is stable.

However, in order to balance the eventual modeling errors and the current sensor imprecision, compensator could be designed in further works.

6.5.1.2 Other alternative

In addition to the desired displacement, the suggested reverse model requires the electric current measuring in real time. The main difficulty with this concerns the lack in measuring the electric current with good precision. We experimentally verified that the reverse model is sensitive to inaccuracies of the electric current sensor.

Therefore, we suggest an alternative configuration in which the effect of electric current is replaced by noises source as shown in Figure 6.18.

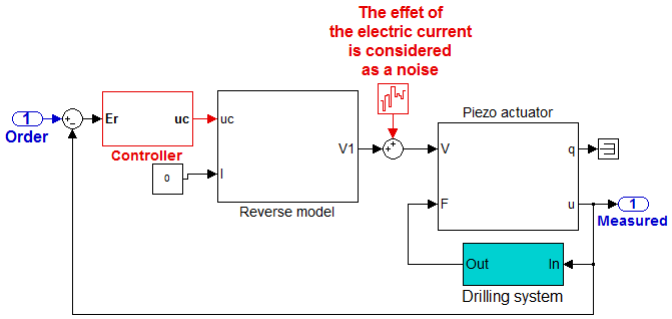

Figure 6.18: New command architecture

This requires the elaboration of a nonlinear systems controller. This will be dealt in future works.

6.5.1.3 Limits of the approach

Physics-based approach is an interesting approach as long as one needs to understand the nature of the system and modify or improve its physical behaviour. However, this could lead to models for which it could be difficult to estimate the appropriate parameters. Moreover, the corresponding reverse model could become unstable in certain conditions. This justifies the use of identification tools in order to construct another model for control loops elaboration.

6.5.2 Using robust identification tools

In multi-physical devices modeling, the common approaches consist of analogical representation of the physical phenomena as well as we did so in previous chapters. We obtained good agreements between the models and the experiments. For a given voltage profile, the proposal models were able to predict the output displacement.

However, could lead to models for which it could be difficult to estimate the appropriate parameters. Moreover, the corresponding reverse model could become unstable in certain conditions.

All these justify the use of identification tools. For this purpose, we shall excite the system by a Pseudo Random Binary Sequence (PRBS) with small amplitude ($\pm 10V$). This choice is motivated by two arguments.

The first and trivial one concerns the fullness (in term of excitation frequencies) of such a signal in comparison with steps and sinusoidal signals.

The second reason is related to the operating condition of the concerned system. We are dealing with piezo-systems applied to vibrational drilling. As a matter of fact, during the drilling process, the system is subjected to some random impacts. A PRBS allows therefore to reproduce such this environment.

6.5.2.1 Least squares estimator limits

Model identification and model validation still remain a delicate task [149]. In particular the system identification should deliver not only a relevant nominal model but also a reliable estimate of the uncertainty. Usually, the model's parameters estimation is based on least squares methods. The drawback in these techniques comes from their high statistical sensibility to large estimator errors named outliers. Two methods are generally used. The first one consists in simply deleting (filtering) the influencing outliers before the fitting process. This is often an efficient approach when expert knowledge assists this task, ensuring that the removed information are not relevant. However, because of its complexity, it could be difficult to proceed for physical analysis of the systems. Moreover, sometimes, data delation could lead to losing crucial information, since they often provide valuable information about the system's dynamic [150]. The second method therefore consists in treating these outliers, in order to capture relevant information about the system behavior they may contain. It is up to the user to interpret then the identified model and conclude on the origin of the system's behaviour. Since the underlying error estimation distribution presents a heavy tail [151] by the influence of these outliers, alternative solutions are brought. The LSAD (Least Sum Absolute Deviation) techniques leading to LP (Linear Programming) minimization problems with or without contraints proposes a family of robustly convergent algorithm's based on a smoothed LSAD criterion which seems to be more efficient than the classical least squares criterion in the case of a noise with Laplacian distribution. Another method uses a mixed $L_1 - L_2$ norm based on the parameterized objective function according the Huber's M-estimate [152]. A simple physical insight on the main noise characteristics provides an idea on the convenient scaling factor which automatically determines the balance between L_1 and L_2 contributions of the estimation procedure.

Hence, we use a mixed $L_1 - L_2$ criterion, parameterized with a scaling factor, fighting against outliers.

6.5.2.2 The $L_2 - L_1$ estimation criterion

In the general way, we denote in the sequel $x_t(\theta) = x(t, \theta)$ and $x_t = x(t)$, for a parameterized time varying signal. Let us consider a discrete-time SISO system with input signal u_t and output signal y_t described as follows

$$y_t = G\left(q^{-1}\right) u_t + H\left(q^{-1}\right) e_t \tag{6.11}$$

See [153] for more details. Here, $G(q^{-1})$ and $H(q^{-1})$ are the transfer functions of the system, respectively from u to y and e to y . The backward shift operator q^{-1} is defined by: $u_{t-1} = q^{-1}u_t$. $\{e_t\}$ is a sequence of random variables identical independent distributed (iid) with mean zero and variances λ , with a probability density function (pdf), f_e. Consider the general parameterized pseudo-linear models set $\mathrm{M}(\theta)$, with the parameter vector $\theta = [\theta_1....\theta_n]^T \in I\!R^n$ and

$$\hat{y}_t(\theta) = \varphi_t^T(\theta)\,\theta \qquad t = 1, 2, ... \tag{6.12}$$

represents the prediction model output on the base of a data set $\{u_1, y_1, ..., u_N, y_N, ...\}$. Here $\varphi_t^T(\theta)$, $t = 1, 2, ...$ denote the $t - th$ observation vector and

$$\varepsilon_t(\theta) = y_t - \varphi_t^T(\theta)\,\theta \tag{6.13}$$

the prediction error. Therefore, the prediction error estimation problem is the following optimization problem

$$\hat{\theta}_N = \arg\min_{\theta} \frac{1}{N} \sum_{t=1}^{N} \rho_\eta\left(\varepsilon_t(\theta)\right) \tag{6.14}$$

with respect to the data set $Z^N = \{u_1, y_1, ..., u_N, y_N\}$, where $\hat{\theta}_N$ is the estimator of θ and ρ_η a continuous nonnegative scalar function, i.e. the Huber's function, with η a fixed value of the scaling factor [149]. More precisely, the ρ_η norm is

$$\rho_\eta(\varepsilon) = \begin{cases} \frac{1}{2}\varepsilon^2 & \text{if } |\varepsilon| \le \eta \\ \eta\,|\varepsilon| - \frac{1}{2}\eta^2 & \text{if } |\varepsilon| > \eta \end{cases} \tag{6.15}$$

Here, ρ_η is chosen to render the estimation more robust than the classical L_2 estimate with respect to the outliers supposed to be present in the data set. The least informative distribution [152] is defined by the following probability density function

$$f_\varepsilon = \begin{cases} \frac{1}{\sqrt{2\pi}} e^{\frac{-\varepsilon^2}{2}} & \text{if } |\varepsilon| \le \eta \\ \frac{1}{\sqrt{2\pi}} e^{-\eta|\varepsilon| + \frac{\eta^2}{2}} & \text{if } |\varepsilon| > \eta \end{cases} \tag{6.16}$$

Moreover (6.14) may be represented by the condition

$$\frac{1}{N} \sum_{t=1}^{N} \Psi_t^H\left(\hat{\theta}_N\right) = 0 \tag{6.17}$$

where $\Psi_t^H(\theta) = \frac{\partial}{\partial\theta}\rho_\eta\left(\varepsilon_t(\theta)\right)$ is the gradient of the norm with respect to θ, called the Huber's M-estimate function.

Let us introduce the concept of active/inactive index sets [154], namely the subsets of integer, given a parameter θ, defined by

$$\nu(\theta) = \{t : |\varepsilon_t(\theta)| \leq \eta\} \quad \text{and} \quad \bar{\nu}(\theta) = \{t : |\varepsilon_t(\theta)| > \eta\}$$

These two active/inactive index sets define respectively the L_2 - contribution and L_1 - contribution of the residuals. Moreover, let us define the sign function of the prediction error

$$s_t(\theta) = \begin{cases} -1 & \text{if } \varepsilon_t(\theta) < -\eta \\ 0 & \text{if } |\varepsilon_t(\theta)| \leq \eta \\ +1 & \text{if } \varepsilon_t(\theta) > \eta \end{cases}$$

Practically, from the data set Z^N, the robust estimation criterion to be minimized can be writen as follows

$$W_N(\theta) = \frac{1}{N}\sum_{t=1}^{N} \frac{\varepsilon_{\nu,t}^2(\theta)}{2} + \frac{1}{N}\sum_{t=1}^{N} (\eta s_{\bar{\nu},t}(\theta)\varepsilon_{\bar{\nu},t}(\theta) - \frac{\eta^2 s_{\bar{\nu},t}^2(\theta)}{2}) \tag{6.18}$$

, where in the general way, we denote

$$f_{\nu,t} = \begin{cases} f_t & \text{if } t \in \nu(\theta) \\ 0 & \text{otherwise} \end{cases} \tag{6.19}$$

and

$$f_{\bar{\nu},t} = \begin{cases} f_t & \text{if } t \in \bar{\nu}(\theta) \\ 0 & \text{otherwise} \end{cases} \tag{6.20}$$

6.5.2.3 Choice of scaling factor

The scaling factor η is classically chosen to be in the *noise interval*, i.e. $1.5\sigma \leq \eta \leq 2\sigma$ ([154] and others) where σ is the standard deviation of the prediction errors $\varepsilon_t(\theta)$ during the classical L_2 estimation procedure. This value is computed from the emperical variance defined by

$$\sigma^2 \approx \hat{\lambda}_N = \frac{1}{N}\sum_{t=1}^{N} \varepsilon_t^2(\hat{\theta}_N) \tag{6.21}$$

Therefore, we denote outliers namely the measurements that typically exceed two times the standard deviation, and, above all, with an unpredictable underlying distribution. We believe it is pertinent to consider that the bigger and more numerous the outliers are, the more disrupted the real distribution of the estimation errors is deviating therefore from the gaussian distribution. Consequently it seems to be reasonable to investigate smaller values of η, namely $0.05\sigma \leq \eta \leq 2\sigma$. The main convergence properties of the estimator have been detailed in [155].

6.5.2.4 L_1-contribution function for the validation

We focus to present a validation tool, named L_1-contribution function which jointly the estimation criterion, lead to determine the convenient models. This validation tool is defined by

$$L_1C\left(\theta\right) = \frac{N_{\bar{\nu}}\left(\theta\right)}{N} = \frac{1}{N}\sum_{t\in\bar{\nu}(\theta)}\left|s_t(\theta)\right| \tag{6.22}$$

, where $N_{\bar{\nu}}\left(\theta\right)$ characterizes the behaviour of the ratio between the prediction errors treated in the L_1 framework in the inactive index set $N_{\bar{\nu}}\left(\theta\right)$.

In [155], we used the approximation of the *sign* function [156] to write the gradient and the Hessian of the estimation criterion. Here, from (6.22), in the same vein, we use the following approximation by

$$s_t\left(\theta\right) = \frac{1 - e^{-2K\varepsilon_t(\theta)}}{1 + e^{-2K\varepsilon_t(\theta)}}$$

, with K a real sufficiently large.

Remark: the outliers in the data set emphasize the large level of the estimation errors, therefore, the term $e^{-2K\varepsilon_t(\theta)}$ is zero and has no effect on the variation of the value of $|s_t(\theta)|$, since this value is always one. However, the quantity of the prediction errors greater than the scaling factor becoming more important, the *cardinal* of the inactive index set increases. Therefore, the effect of outliers is present in the L_1-contribution function. The term $e^{-2K\varepsilon_t(\theta)}$ is not zero only when these values are small.

Concretely, the L_1-contribution function becomes

$$L_1C\left(\theta\right) = \frac{1}{N}\sum_{t\in\bar{\nu}(\theta)}\left|\frac{1 - e^{-2K\varepsilon_t(\theta)}}{1 + e^{-2K\varepsilon_t(\theta)}}\right| \tag{6.23}$$

In the validation phase, this function presents a lot of minimas leading the user to choose the convenient models.

6.5.2.5 Experiments

Figure 6.19 is realized for measurements. K_p denotes the stiffness of Element 2 in Fig.4.20. M_a is the mass of Elements 1 and 4. The prestress is set to 3000 N. The gauge constraints are used for measuring the displacement of Element 1.

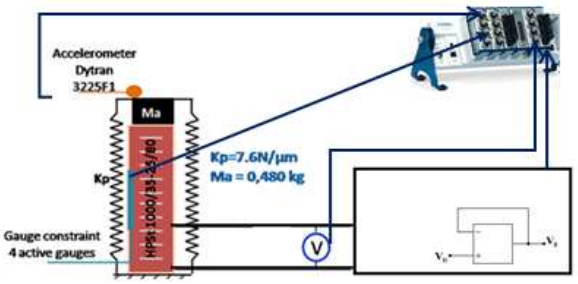

Figure 6.19: Instrumentation for experimental measurements

Details on the measuring instruments are available in the Annexes.

Figure 6.20 shows the excitation input signal. This signal is a pseudo random binary sequence (PRBS) with a length $L = 2^{10}-1$ and level $\pm 10V$ sufficiently exciting and persisting [157]. The sampling period is $T_S = 100\mu s$. For the identification process we use 5000 samples. In Figure 6.21, the response to this excitation presents a lot of large values, sometimes larger

than -10 and 10. These large samples certainly implie the prediction errors in the least squares estimation, as we shall see in the the sequel.

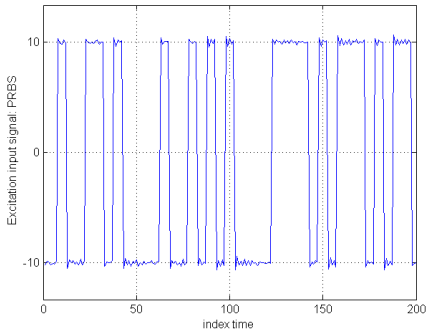

Figure 6.20: Excitation input signal: PRBS

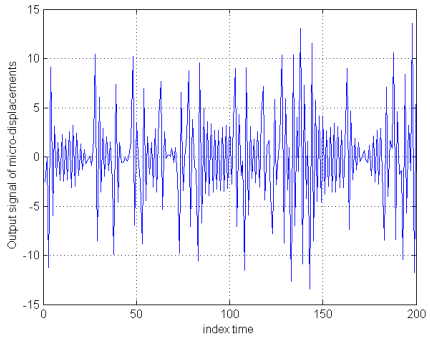

Figure 6.21: Output signal of Piezoelectric.

The distribution of the prediction errors of a estimated model in the classical least squares, is strongly disturbed and (see Figure 6.22). This non-trivial distribution is zero between -2 and $+2$ and presents two distributions around -3 and $+3$. These results show firstly, the necessity to use a parameterized robust estimation criterion with a scaling factor and secondly, to choose this parameter and reinforce the robustness of the least squares estimation.

6.5.3 Robust Estimation/Validation phases

Since the piezoelectric ceramic system is not a linear experimental device, the adopted models are the classical Output Error (OE) pseudo-linear models as already explained, given by

$$\mathrm{M}\left(\theta\right) : y_t = q^{-d}\frac{B(q^{-1})}{F(q^{-1})}u_t + e_t$$

, where d is the pure plant time delay and $F(q^{-1})$ is a monic polynomial. In our case $d = 1$ meaning the time delay of the sample and hold in the discritization. The parameter vector is

$$\theta = \left[b_1....b_{n_B} f_1....f_{n_F}\right]^T$$

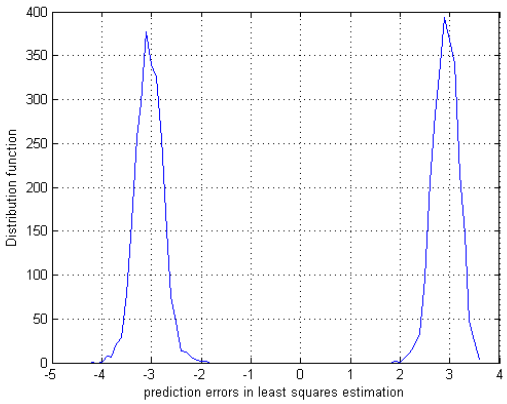

Figure 6.22: Case of L_2 estimation

The observations vector in this model is given by

$$\varphi_t^T(\theta) = [u_{t-1}...u_{t-n_B} - \hat{y}_{t-1}(\theta) ... - \hat{y}_{t-n_F}(\theta)]$$

The range of scaling factor is $0.05\sigma \leq \eta \leq 2\sigma$ where the empirical variance $\hat{\lambda}_N = \sigma^2$ is classically computed from the least-squares estimation (see (6.21)). The estimation criterion to be minimized is given by (6.18) with $N = 5000$. The variations of n_B and n_F are respectively $7 \leq n_B \leq 14$ and $4 \leq n_F \leq 15$.

The L_1-contribution function, we experimented different values of K. We choosed $K = 15$ since great values do not improve significantly the approximation. Fig.6.23 and Fig.6.24 show respectively the estimation criterion and the L_1-contribution function w.r.t. n_F. In a first step, an estimation campaign has led to derive the first convenient models $n_B = 9$. In Fig.6.23 the chosen minimum value of n_F leading to this first convenient model is 12 with the scaling factor $\eta = 0.0625\sigma = 0.2255$. The frequency response of this model is given in Fig.6.25 compared to the spectral estimation of the piezoelectric. The model presents a good $fit = 82.5\%$ in the frequency range $[0; 500Hz]$ used for the control. We recall that the fit is defined by $fit = 100\left(1 - \frac{\|\hat{y}-y\|}{\|y-\bar{y}\|}\right)$ where $\hat{y}$, y, $\bar{y}$ are respectively the vector of prediction model output, the vector of system output and the mean of output data.

The L_1-contribution function yields 97.48%, confirming the importance of outliers in the distribution of the prediction errors. The second model is given by the L_1-contribution function at $n_B = 12$. In Figure 6.24, this model is obtain at $n_F = 12$ with a scaling factor $\eta = 0.0875\sigma = 0.2619$. The L_1-contribution is 96.06% and the $fit = 87.2\%$ in the frequency range $[0; 500Hz]$. Its frequency response is shown in Figure 6.26. For these models, the dimension of the parameter vector is respectively $n = n_B + n_F = 21$ and $n = 24$.

In order to provide *a reference case*, Figure 6.27 shows the identified model and their spectral estimate obtained by a classical least squares estimation. The great sensitivity w.r.t. large estimation errors is clearly illustrated.

6.5.3.1 Remarks

Contrary to physics-based approach, identification approach provide a black-box in which one cannot differentiate each element of the system. The obtained model do not correspond

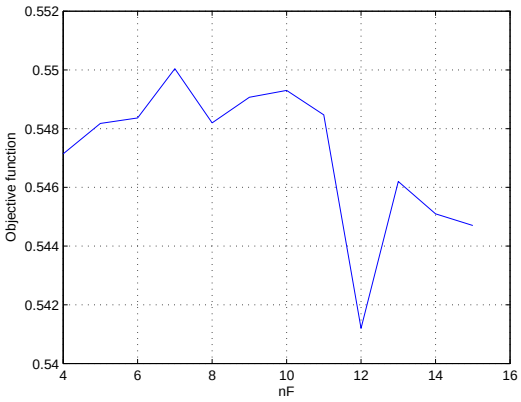

Figure 6.23: $L_2 - L_1$ estimation criterion w.r.t n_F at $n_B = 9$ when $\eta = 0.0625\sigma$.

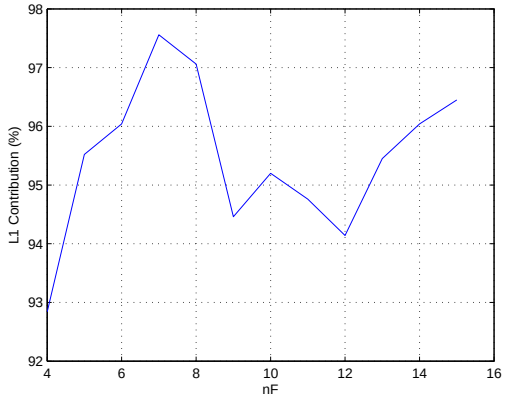

Figure 6.24: L_1-contribution function w.r.t n_F at $n_B = 12$ when $\eta = 0.0875\sigma$.

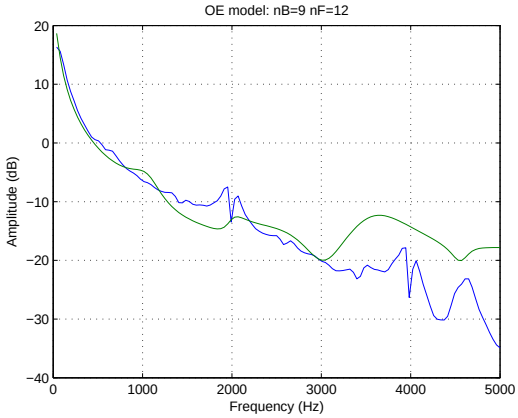

Figure 6.25: $n_F = 12$, $n_B = 9$ and $\eta = 0.0625\sigma = 0.2255$

to the unique piezo-device. It is the model of the whole system (piezo-actuator + mechanism + constraint gauge).

Therefore, this approach should be used at the end of the design process, after the system assembly.

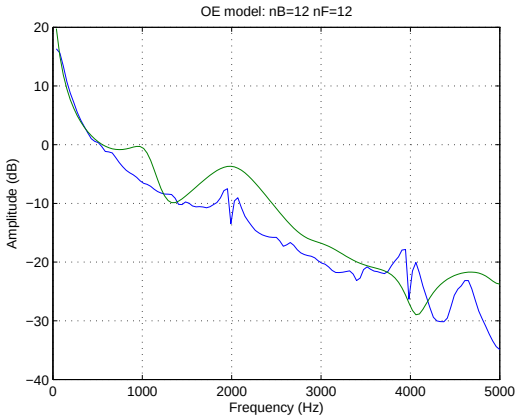

Figure 6.26: $n_F = 12$, $n_B = 12$ and $\eta = 0.0875\sigma = 0.2619$

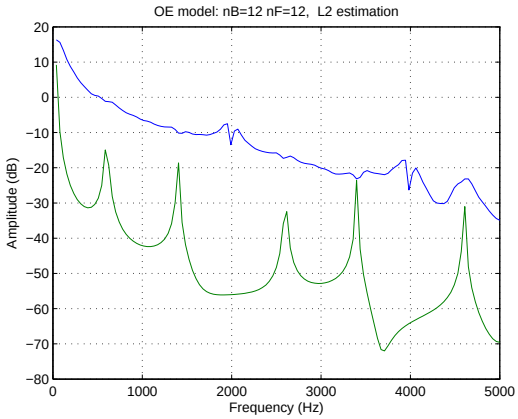

Figure 6.27: $n_F = 12$ and $n_B = 12$

6.6 Using the models for vibration damping

The versatility of piezo-devices makes it possible their usage for different applications. In this section, instead of using the piezo-device for vibration generation, the objective is to inhibit these vibrations. For this purpose, common technique consists in draining the vibration energy through an electric load Z_s shunted to the piezo-device electrical port [89]. There is no longer a voltage source but rather a flow source. Let us consider resistor R_s shunted to the electric port.

We assume that the piezo-device is clamped on its mechanical port Mp_2. Then, the unique considered mechanical port is Mp_1. Figure 6.28 is the damping function scheme.

In this configuration, the energy absorbing capability of R_s prevails the intrinsic non-linearities, hysteresis and losses of the piezo-device. Therefore, one could sort the transfer function of the open-loop system as follows.

$$\frac{u_1[S]}{F_1[S]} = G[S] = m\frac{C_e.R_s\left(1-k^2\right)S+1}{K_m\left(C_e.R_sS+1\right)+ms^2\left(C_e.R_s\left(1-k^2\right)S+1\right)} \tag{6.24}$$

Since $1 > 1-k^2 > 0$, and all the other coefficients are also positive, one could verify that according to Routh-Hurwitz the system G is stable.

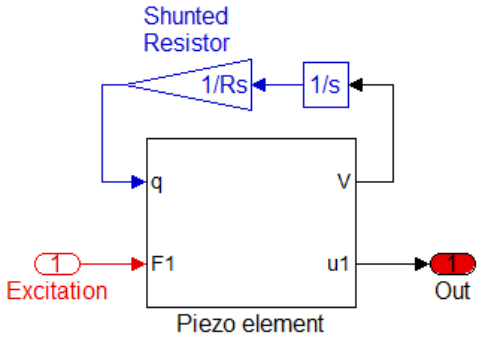

Figure 6.28: Piezo-bar usage for vibration damping

As in [14] let us set $\omega_1 = \sqrt{\frac{K_m}{m}}$ the first resonant frequency of the piezo-device, and $Q_R = C_e.R_s$. It comes

$$G[S] = \frac{Q_R\left(1-k^2\right)S+1}{\omega_1^2\left(Q_R S+1\right)+s^2\left(Q_R\left(1-k^2\right)S+1\right)} \tag{6.25}$$

It had been shown in [139, 14], that the maximum achievable damping is proportional to $\frac{k^2}{1-k^2}$ which increases when the electromechanical coefficient is augmented. Therefore, one places a negative capacitance C_1 in parallel to the piezoelectric transducer [158, 159] (Figure 6.29).

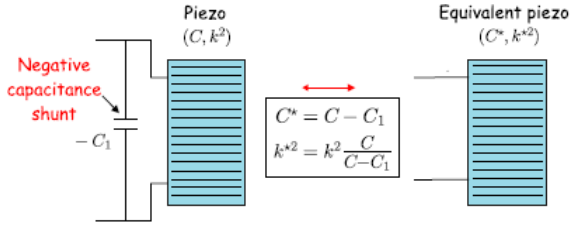

Figure 6.29: Negative capacitance for electromechanical coupling coefficient enhancement [14]

The synthesis of a negative capacitance consists of an active circuit that could become unstable [140, 14].

Moreover, Hagood and Von Flotow [160] showed that a suitable choice of and inductance in series with the resistor R_s could significantly yield the damping effect of the piezo-device [138].

6.7 Conclusion

We showed the outcome of our proposal models. Therefore, examples of our challenging applications were given. However, our objective in this chapter was to expose how the proposal models could be integrated in mechatronic systems. Moreover, we saw that the clear adopted approach can be transposed to other smart actuators modeling. As an example we dealt with magnetostrictive bar device.

Chapter 7

General conclusion and perspectives

7.1 Synthesis

Electroactive actuators offer many advantages. They can be robust and reliable but provided a good control.

In this thesis, we expected a clear methodology and user friend models of piezoelectric actuators. This work has been widely motivated.

For this purpose, we reviewed existing approaches and different commercial packages such as ANSYS, Lab AMESim and 20-Sim. Finite Elements Analysis offered by ANSYS was found not suitable. The high level of detail which is proposed does not correspond to ***upstream design***. The tools offered by Lab AMESim and 20-Sim were found interesting but very simplistic because they do not take into account non-linearities.

To achieve our goal, it was first necessary to re-formalize existing linear models in static and in dynamic. For this purpose we adopted lumped-parameters approach in reference to several concluding research.

We analyze the constitutive equations of piezoelectricity with respect to operating conditions. This allows us to deduce a first analog model. This is then translated into bond graph. The bond graph modeling offers several advantages. It is a trend in industries but it also provides a better view of the physical behaviour in engineers's language. The obtained models are translated in block-diagrams. As a matter of fact, the control part of the system involves signals rather than energy and it is not necessarily subject to physical principles.

The established models in this step differ from those proposed by AMESim or 20-Sim. Indeed we better integrate the dynamic nature of the actuator independently of the other parts of the structure. In fact we proposed two types of models. The first one only takes into account the first resonance mode while the second one takes into account two resonances.

Thereafter, in chapter 5, we suggested models taking into account nonlinearities and hysteresis. The Preisach approach was adopted for static hysteresis. Then we adapted Voigt approach in order to account for dynamic hysteresis. The two approaches were then merged in order to have a complete model.

The proposal models have been confronted with experimental results. We have been satisfied. However we are convinced that improvements can be made later.

7.2 Perspectives

7.2.1 Electric current output for load estimation

We consider the following drilling context in Figure 6.5. One of the greatest difficulties in regulating metal cutting processes is that these processes are inherently nonlinear and vary significantly under normal operating conditions [161]. Elsewhere, one showed that force control is an effective means of improving the quality and productivity of machining operations. This becomes problematic in the case of sandwich samples. To detect change in the sample material, one way could consist of drilling force estimation. It would be interesting to use simultaneously the single piezo-device both to generate the micro-vibration and sense the resistive force.

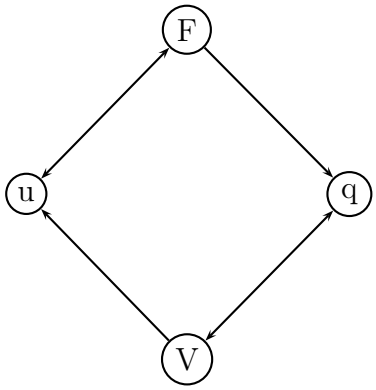

Figure 7.1: Piezoelectricity principle

According to Figure 7.1 (the arrows directions are important), there are two couples of independent variables: (V, F) and (u, q). The indication of one couple allows to deduct the second one and vice-versa. Hence, since F and V are independent, in order to estimate F, the normal way is to measure the u and q.

Instrumentation industries use this principle; for example Kistler Inc [162]. However, in generally, the sensor is made of piezo-material with high rigidity (compared to other piezo-materials). So the piezo hardly deforms ($u = 0$) and thereby, the branch $F \Longleftrightarrow u$ can be neglected. F would therefore be simply proportional to the electric charge.

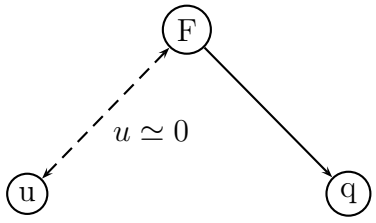

Figure 7.2: Standard use of piezo-device for force sensing: infinitely rigid device

In the case of piezo-actuators, the rigidity is not as so high (their are supposed to generate vibrations). Therefore the branch $F \Longleftrightarrow u$ is no longer negligible. Consequently, u is needed. However, for the reasons we enumerated at the beginning of this section, it could be difficult to install a displacement sensor. Moreover, electric charges sensors are not common.

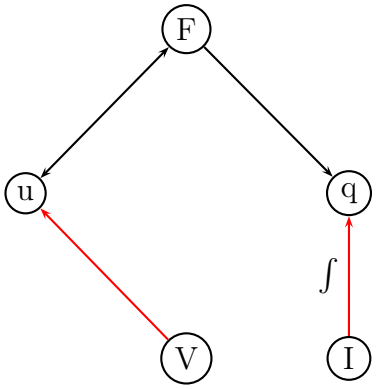

Figure 7.3: Challenging piezo-force sensing: actuator and sensor at the same time

So, we studied the feasibility to use a current sensor (instead of charge sensor) and a voltage sensor (instead of displacement sensor). V and I are dependent variables.

Branches $V \Longrightarrow u$ and $I \Longrightarrow q$ are both critical. The first one is the main place of piezo-device nonlinearities; whence efficient models are required. The second one rises numerical questions because it is about integration without feedback. This imposes to have a perfect alternative current. Otherwise, any offset in the current leads to diverging integration. In order to limit numerical problems, the leak of current in the piezo-device should be as lower as possible and the current sensor as perfect as possible.

Theoretically, the task will consist in inverting the models (Figure 7.4) suggested in previous chapters.

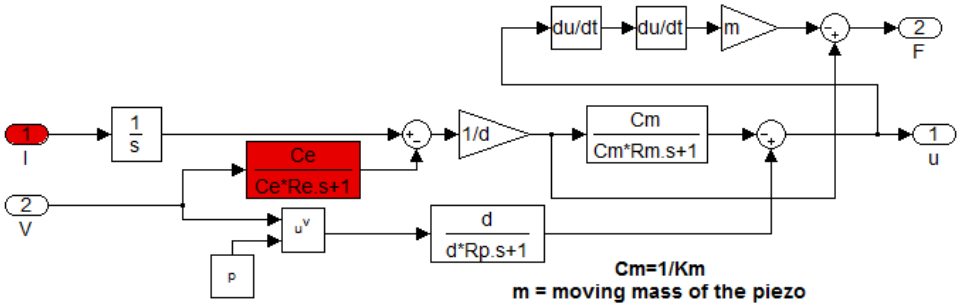

Figure 7.4: Nonlinear estimator of u and F

The highlighted blocks in Figure 7.4 are the critical elements of the estimator. Indeed, small errors in I or imperfection in the electric port model would introduce unacceptable errors in the force and the displacement estimation.

In the case that the model is correct, an incertitude of $d = 0.0000001$ coulombs implies an error of $1N$. Therefore, in order to obtain a precision of $1N$ in the force estimation, the current sensor should have a precision of $2\pi.f.d$. Where f denotes the excitation frequency.

Conversely, if the current sensor's precision is δ (in amperes), then the proposal force estimator would be efficient for frequencies higher than $\frac{\delta}{2\pi.d}$.

Consequently load estimation using current measurement requires high precision difficult to obtain with standard current sensors. Therefore, further works should analyze the cost benefit of this solution.

7.2.2 Adaptability of our approach to magnetostrictive devices

As already introduced in Chapter 2, magnetostrictive effect is a reversible exchange of energy form mechanical form to magnetic form. Magnetostrictive materials get deformed under magnetic field. Conversely an applied force on them, modifies the magnetic properties of their close area. Assuming a set point inside the material, the widely accepted local behavioral law in the case of pre-loaded bar-device is Equation 7.5.

$$\begin{array}{rcl} S_3 & = & s_{33}^H.T_3 + d_{33}.H_3 \\ B_3 & = & d_{33}.T_3 + \mu_{33}^T.H_3 \end{array} \tag{7.1}$$

where S stands for the strain, T the constraint, B the magnetic induction and H the magnetic field. s is the flexibility tensor, μ the permeability tensor, d the piezomagnetic tensor.

If there is no risk of ambiguity, the superscripts and subscripts could be hidden.

Under careful considerations, the approach adopted for piezoelectric actuators modeling could be applied to magnetostrictive case. For example, let us consider a magneto-bar actuator clamped at one of its faces. Using lumped mass approach, similarly to Chapter 4, a linear dynamics of magnetostrictive device could be set as follows:

$$\begin{array}{rcl} u & = & \frac{F - m.\ddot{u}}{K^H} + d.L.H \\ \phi_L & = & d.(F - m.\ddot{u}) + \mu.\sigma.H \end{array} \tag{7.2}$$

where K^H denotes the device stiffness at constant magnetic field, L is the device's length, m its efficacy mass. σ stands for the bar section. ϕ_L corresponds to the magnetic flux per unit of length.

There are many techniques for the magnetic field generation. In the case of an electric generation, for example by means of coils (Figure 7.5), if one notes ϕ_t the total magnetic flux, the electric potential yields:

$$V = \frac{d\phi_t}{dt} \tag{7.3}$$

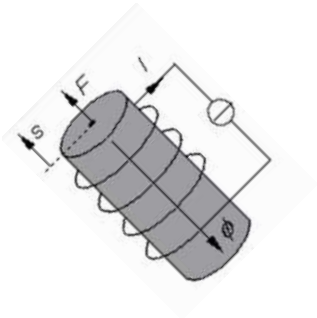

Figure 7.5: Fair case of magnetic field generation

This is a fair situation. In general case, systems for magnetic field generation are very complex. Therefore, they are studied on a case by case basis. However, from magnetostrictive actuators users' point of view, the most important is the relationship between the displacement and the magnetic field: $u = f[H]$. This relation is affected by the mechanical stress.

Contrary to piezoelectric materials, one observes more complex nonlinearities in magnetostrictive materials. As shown in Figure 2.12, commercial magnetostrictive alloys show ferromagnetic or ferrimagnetic behaviour which is affected by mechanical prestress [145]. Their micro magneto-domains are oriented in a way that the strain is always positive whatever is the sign of the magnetic field.

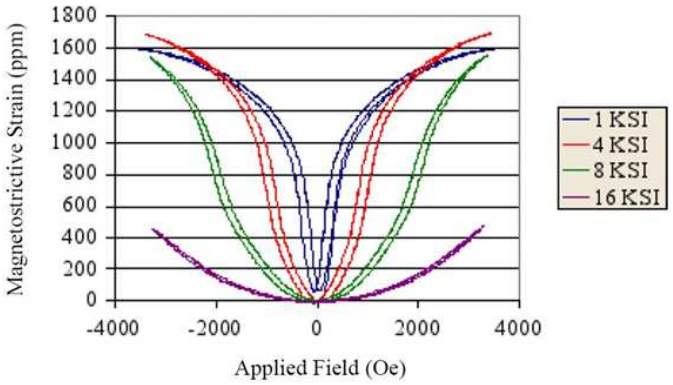

Figure 7.6: Strain vs magnetic field [15]

The knowledge branch of magnetostrictive materials has well evolved and one finds many recent publications in literature [141, 142, 143, 144, 145, 146, 63, 147, 148].

However, our modeling approach could be adapted to the case of magnetostrictive devices.

Indeed, for $H \geq 0$ the right hand parts of the curves in Figure 7.6 are a lot similar to piezo-devices. In order to obtain the left hand parts, only the Preisach contribution should be modified.

According to Equation 5.33 and 5.34 (Chapter 5) if $H \geq 0$ we could set:

$$\begin{array}{rcl} u & = & u_R(H) \text{ On the increasing branch} \\ u & = & u_D(H) \text{ On the decreasing branch} \end{array} \tag{7.4}$$

On the other hand, if $H \leq 0$ Equation 7.4 applies to the absolute value of H i.e. $-H$. It comes:

$$\begin{array}{rcl} u & = & u_D(-H) \text{ On the increasing branch} \\ u & = & u_R(-H) \text{ On the decreasing branch} \end{array} \tag{7.5}$$

One should notice that according to Figure 7.6 when $H < 0$ the increasing branch becomes the decreasing branch and vice versa.

After integrating these modifications in bond graph model we were able to depict magnetostrictive behaviour as shown in Figure 7.7.

The parameters a, b and c of the Preisach part strongly vary with the prestress value P. Regarding the simulation results, the proposal model is satisfying. Thereafter, further works should elaborate a method for experimental determination of the model parameters basing on the proposal architecture.

Another task will consist in determining the relationship between the magnetic field and the electric current. As we noticed it above, this task should be performed on a case by case basis.

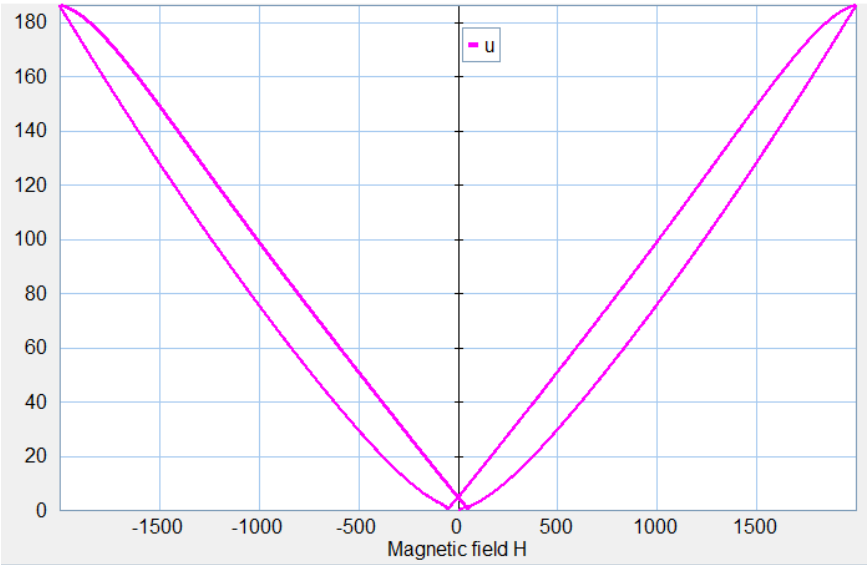

Figure 7.7: Piezo-model adapted for magnetostrictive actuator: random parameters

7.2.3 Other perspectives

In chapter 6 we showed the outcome of our proposal models. We presented some challenging applications. We showed how the proposal models could be integrated into mechatronic systems.

We showed the easiness to inverse the proposal models in order to elaborate control and command loops. However, we especially highlighted the difficulties associated with these reverse model in practice.

Indeed, the proposal estimators associated to the reverse models should be made robust. We saw that they were sensitive to inaccuracies of the electric current sensor. Moreover, further research should deal with rectifiers elaboration.

Furthermore, we saw that a piezoelectric material could heat up and lose its properties [163]. Our proposal hysteresis model could later be used to estimate in real time the temperature of the actuator in order to make good decision.

Moreover, other approaches for nonlinearities modeling such as dry friction and Rayleigh laws can be investigated.

7.3 Conclusion en langue française

Les actionneurs électro-actifs ont de nombreux atouts et ils peuvent être robustes et fiables mais à la condition d'une bonne maîtrise.

De cette thèse, nous attendions une méthodologie claire et des modèles prêts-à-utiliser d'actionneurs piézoélectriques. Nos motivations ont été explicitées dans l'introduction générale.

Pour ce faire nous avons procédé à une revue des approches existantes dans la litérature ainsi que les solutions offertes par certains logiciels tels que ANSYS, Lab AMESim et 20-Sim. Nous avons écarté les analyses éléments finis utilisées dans ANSYS parce qu'elles se situent à niveau de détails très élevé ne correspondant pas à la ***conception amont***. Les outils proposés par Lab AMESim et 20-Sim ont été trouvés intéressants mais très simplistes car ils ne prennent pas en compte les non-linéarités.

Il nous a été d'abord nécessaire de reformaliser les modèles linéaires existants, en statique et en dynamique. Pour ce faire nous avons adopté l'approche des paramètres concentrés à l'instar de beaucoup d'autres travaux.

Nous commençons par l'analyse des équations constitutives de la piézoélectricité associées aux conditions de fonctionnement de l'actionneur. Ce qui nous permet d'en déduire un premier modèle analogique. Ce dernier est ensuite traduit en bond graph. La modélisation bond graph nous offre plusieurs avantages. Non seulement l'utilisation du bond graph est une tendance industrielle, mais aussi elle nous donne une vue éclatée de la physique du matériau mais avec des paramètres dans un langage ingénieur et elle nous renseigne mieux sur l'influence de chacun de ces paramètres sur la réponse de l'actionneur. Les modèles bond graph obtenus peuvent être directement utilisés dans la conception pour en faire des simulations mais on doit aussi en déduire les modèles blocs-diagramme. Car, s'il est plus adéquat de modéliser un système mécatronique en termes de liens énergétiques entre les différents organes ou éléments, la partie contrôle du système met en jeu des signaux plutôt que de l'énergie et elle n'est pas nécessairement soumise aux principes physiques.

En plus de cet effort de formalisation, ces premiers modèles que nous avons établis se distinguent de ceux proposés par AMESim ou 20-Sim. En effet, nous avons mieux pris en compte la dynamique propre à l'actionneur. Nous avons proposé deux types de modèles. L'un rend uniquement compte du premier mode de résonance alors que le second rend compte de deux modes de résonance.

Ensuite, dans le chapitre 5, nous avons proposé des modèles prenant en compte les non-linéarités. L'approche de Preisach pour la modélisation de l'hystérésis statique et l'approche de Voigt dans le cas dynamique. Ces deux approches ont ensuite été fusionnées dans le but d'avoir un model plus complet.

Tous les modèles proposés ont été confrontés aux résultats expérimentaux. Nous en avons été satisfaits mais nous estimons que des améliorations peuvent être apportées ultérieurement.

Dans le chapitre 6 nous avons montré la valeur ajoutée de notre travail en présentant nos cas d'applications. Nous avons aussi montré comment les modèles proposés s'articulent avec les autres éléments d'un système plus complexe.

Nous avons montré qu'il est simple d'inverser nos modèles en vue d'élaborer la commande de l'actionneur piézoélectrique ou de s'en servir comme capteur de force en même temps qu'il assure son rôle d'actionnement.

Cependant, nous avons surtout mis en évidence les difficultés liées à ces inversions dans

la pratique. Ce qui ouvre la voie à des travaux ultérieurs.

En effet les estimateurs proposés par l'inversion des modèles doivent être robustufiés. Nous avons vu qu'ils étaient sensibles aux imprécisions du capteur de courant. De même, nous devrons ultérieurement concevoir des correcteurs associés à ces modèles inversés.

Par ailleurs, nous avions vu qu'un matériau piézoélectrique pouvait chauffer jusqu'à perdre ses propriétés. Les modèles d'hystérésis proposés pourront ultérieurement être mis à profit pour estimer en temps réel la température de l'actionneur.

Appendix A

Piezoelectric materials tensors in crystallographic systems

A.1 Hexagonal system

Flexibility coefficients	Dielectric coefficients
$[s^E] = \begin{bmatrix} s_{11}^E & s_{12}^E & s_{13}^E & 0 & 0 & 0 \\ s_{12}^E & s_{11}^E & s_{13}^E & 0 & 0 & 0 \\ s_{13}^E & s_{13}^E & s_{33}^E & 0 & 0 & 0 \\ 0 & 0 & 0 & s_{44}^E & 0 & 0 \\ 0 & 0 & 0 & 0 & s_{44}^E & 0 \\ 0 & 0 & 0 & 0 & 0 & s_{66}^E \end{bmatrix}$	$[\varepsilon^T] = \begin{bmatrix} \varepsilon_{11}^T & 0 & 0 \\ 0 & \varepsilon_{11}^T & 0 \\ 0 & 0 & \varepsilon_{33}^T \end{bmatrix}$

Hexagonal 6 leads to the same equation as Hexagonal $6mm$.

On the other hand, piezo-materials crystalizing in hexagonal $\overline{6}$, $\overline{6}2m$ and 622 do not present any interest for bar operating mode. The coupling character of piezoelectric device had disappeared.

Classes	Piezoelectric coefficients	Reduced equations for bar operating mode
$6mm$	$[d] = \begin{bmatrix} 0 & 0 & 0 & 0 & d_{15} & 0 \\ 0 & 0 & 0 & d_{15} & 0 & 0 \\ d_{31} & d_{31} & d_{33} & 0 & 0 & 0 \end{bmatrix}$	$\begin{cases} S_1 = d_{31}E_3 + s_{13}^E T_3 \\ S_2 = d_{31}E_3 + s_{13}^E T_3 \\ S_3 = d_{33}E_3 + s_{33}^E T_3 \\ D_3 = \varepsilon_{33}^T E_3 + d_{33} T_3 \end{cases}$
6	$[d] = \begin{bmatrix} 0 & 0 & 0 & d_{14} & d_{24} & 0 \\ 0 & 0 & 0 & d_{24} & -d_{14} & 0 \\ d_{31} & d_{31} & d_{33} & 0 & 0 & 0 \end{bmatrix}$	$\begin{cases} S_1 = d_{31}E_3 + s_{13}^E T_3 \\ S_2 = d_{31}E_3 + s_{13}^E T_3 \\ S_3 = d_{33}E_3 + s_{33}^E T_3 \\ D_3 = \varepsilon_{33}^T E_3 + d_{33} T_3 \end{cases}$
$\overline{6}$	$[d] = \begin{bmatrix} d_{11} & -d_{11} & 0 & 0 & 0 & -d_{22} \\ -d_{22} & d_{22} & 0 & 0 & 0 & -d_{11} \\ 0 & 0 & 0 & 0 & 0 & 0 \end{bmatrix}$	$\begin{cases} S_1 = s_{13}^E T_3 \\ S_2 = s_{13}^E T_3 \\ S_3 = s_{33}^E T_3 \\ D_3 = \varepsilon_{33}^T E_3 \end{cases}$
$\overline{6}2m$	$[d] = \begin{bmatrix} d_{11} & -d_{11} & 0 & 0 & 0 & 0 \\ 0 & 0 & 0 & 0 & 0 & -d_{11} \\ 0 & 0 & 0 & 0 & 0 & 0 \end{bmatrix}$	$\begin{cases} S_1 = s_{13}^E T_3 \\ S_2 = s_{13}^E T_3 \\ S_3 = s_{33}^E T_3 \\ D_3 = \varepsilon_{33}^T E_3 \end{cases}$
622	$[d] = \begin{bmatrix} 0 & 0 & 0 & d_{14} & 0 & 0 \\ 0 & 0 & 0 & 0 & -d_{14} & 0 \\ 0 & 0 & 0 & 0 & 0 & 0 \end{bmatrix}$	$\begin{cases} S_1 = s_{13}^E T_3 \\ S_2 = s_{13}^E T_3 \\ S_3 = s_{33}^E T_3 \\ D_3 = \varepsilon_{33}^T E_3 \end{cases}$

A.2 Monoclinic system

Flexibility coefficients	Dielectric coefficients
$\left[s^E\right] = \begin{bmatrix} s_{11}^E & s_{12}^E & s_{13}^E & 0 & 0 & s_{16}^E \\ s_{12}^E & s_{22}^E & s_{23}^E & 0 & 0 & s_{26}^E \\ s_{13}^E & s_{23}^E & s_{33}^E & 0 & 0 & s_{36}^E \\ 0 & 0 & 0 & s_{44}^E & s_{45}^E & 0 \\ 0 & 0 & 0 & s_{45}^E & s_{55}^E & 0 \\ s_{16}^E & s_{26}^E & s_{36}^E & 0 & 0 & s_{66}^E \end{bmatrix}$	$\left[\varepsilon^T\right] = \begin{bmatrix} \varepsilon_{11}^T & \varepsilon_{12}^T & 0 \\ \varepsilon_{12}^T & \varepsilon_{22}^T & 0 \\ 0 & 0 & \varepsilon_{33}^T \end{bmatrix}$

Classes	Piezoelectric coefficients	Reduced equations for bar operating mode
2	$[d] = \begin{bmatrix} 0 & 0 & 0 & d_{14} & d_{15} & 0 \\ 0 & 0 & 0 & d_{24} & d_{25} & 0 \\ d_{31} & d_{32} & d_{33} & 0 & 0 & d_{36} \end{bmatrix}$	$\begin{cases} S_1 = d_{31}E_3 + s_{13}^E T_3 \\ S_2 = d_{31}E_3 + s_{13}^E T_3 \\ S_3 = d_{33}E_3 + s_{33}^E T_3 \\ D_3 = \varepsilon_{33}^T E_3 + d_{33}T_3 \end{cases}$
m	$[d] = \begin{bmatrix} d_{11} & d_{12} & d_{13} & 0 & 0 & d_{16} \\ d_{21} & d_{22} & d_{23} & 0 & 0 & d_{26} \\ 0 & 0 & 0 & d_{34} & d_{35} & 0 \end{bmatrix}$	$\begin{cases} S_1 = s_{13}^E T_3 \\ S_2 = s_{13}^E T_3 \\ S_3 = s_{33}^E T_3 \\ D_3 = \varepsilon_{33}^T E_3 \end{cases}$

A.3 Orthorhombic system

Flexibility coefficients	Dielectric coefficients
$\left[s^E\right] = \begin{bmatrix} s_{11}^E & s_{12}^E & s_{13}^E & 0 & 0 & 0 \\ s_{12}^E & s_{22}^E & s_{23}^E & 0 & 0 & 0 \\ s_{13}^E & s_{23}^E & s_{33}^E & 0 & 0 & 0 \\ 0 & 0 & 0 & s_{44}^E & 0 & 0 \\ 0 & 0 & 0 & 0 & s_{55}^E & 0 \\ 0 & 0 & 0 & 0 & 0 & s_{66}^E \end{bmatrix}$	$\left[\varepsilon^T\right] = \begin{bmatrix} \varepsilon_{11}^T & 0 & 0 \\ 0 & \varepsilon_{11}^T & 0 \\ 0 & 0 & \varepsilon_{33}^T \end{bmatrix}$

Classes	Piezoelectric coefficients	Reduced equations for bar operating mode
222	$[d] = \begin{bmatrix} 0 & 0 & 0 & d_{14} & 0 & 0 \\ 0 & 0 & 0 & 0 & d_{25} & 0 \\ 0 & 0 & 0 & 0 & 0 & d_{36} \end{bmatrix}$	$\begin{cases} S_1 = s_{13}^E T_3 \\ S_2 = s_{13}^E T_3 \\ S_3 = s_{33}^E T_3 \\ D_3 = \varepsilon_{33}^T E_3 \end{cases}$
$2mm$	$[d] = \begin{bmatrix} 0 & 0 & 0 & 0 & d_{15} & 0 \\ 0 & 0 & 0 & d_{24} & 0 & 0 \\ d_{31} & d_{32} & d_{33} & 0 & 0 & 0 \end{bmatrix}$	$\begin{cases} S_1 = d_{31}E_3 + s_{13}^E T_3 \\ S_2 = d_{31}E_3 + s_{13}^E T_3 \\ S_3 = d_{33}E_3 + s_{33}^E T_3 \\ D_3 = \varepsilon_{33}^T E_3 + d_{33}T_3 \end{cases}$

A.4 Cubic system

Piezo-materials crystalizing in cubic system do not present any interest for bar operating mode.

Flexibility coefficients	Dielectric coefficients
$\left[s^E\right] = \begin{bmatrix} s_{11}^E & s_{12}^E & s_{12}^E & 0 & 0 & 0 \\ s_{12}^E & s_{11}^E & s_{12}^E & 0 & 0 & 0 \\ s_{12}^E & s_{12}^E & s_{33}^E & 0 & 0 & 0 \\ 0 & 0 & 0 & s_{44}^E & 0 & 0 \\ 0 & 0 & 0 & 0 & s_{44}^E & 0 \\ 0 & 0 & 0 & 0 & 0 & s_{44}^E \end{bmatrix}$	$\left[\varepsilon^T\right] = \begin{bmatrix} \varepsilon_{11}^T & 0 & 0 \\ 0 & \varepsilon_{11}^T & 0 \\ 0 & 0 & \varepsilon_{11}^T \end{bmatrix}$

Classes	Piezoelectric coefficients	Reduced equations for bar operating mode
23	$[d] = \begin{bmatrix} 0 & 0 & 0 & d_{14} & 0 & 0 \\ 0 & 0 & 0 & 0 & d_{14} & 0 \\ 0 & 0 & 0 & 0 & 0 & d_{14} \end{bmatrix}$	$\begin{cases} S_1 = s_{13}^E T_3 \\ S_2 = s_{13}^E T_3 \\ S_3 = s_{33}^E T_3 \\ D_3 = \varepsilon_{33}^T E_3 \end{cases}$

A.5 Other crystallographic systems

We consciously choose to not recall Trigonal, Tetragonal and Triclinic systems. Readers could refer to [59].

Appendix B

Piezo-bar characterization procedures

In this annexe we describe the procedure for piezo-bar device characterization. As we noticed it in the report, the results obtained by this procedure can provide a estimation of the device parameters.

B.1 The piezo-device

The theory used to determine the parameters supposes a bar form device. Therefore, the piezo-device must be at least five (05) times more longer than its lateral dimensions. The section can be rectangular or circular.

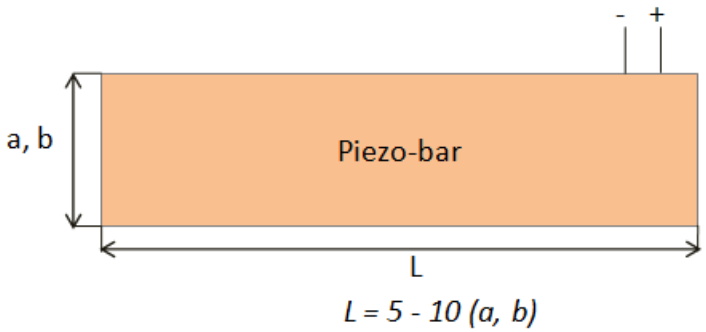

Figure B.1: Bar assumption condition

B.2 Resonance characterization

B.2.1 Experiments equipment

- A precision shunt. Its resistance must be as lower as possible in order to not affect the piezo-device impedance, and as higher as possible in order to limit the electric current consumption (0.1Ω to 100Ω).

- A multi-meter with high frequency excitation signal, more than ten kilo hertz ($> 10KHz$) if possible.

- A functions generator with an option for automatic frequency sweep.
- A scope.
- A channels turntable. This can be easily design by the user.
- A signal acquisition system, for example National Instruments devices.
- Some cables, coaxial cables are advised.

However, one could use impedance analyzers.

B.2.2 Experimental setup

Realize the equivalent setup in Figure B.2. Before connecting the piezo-device to the func-

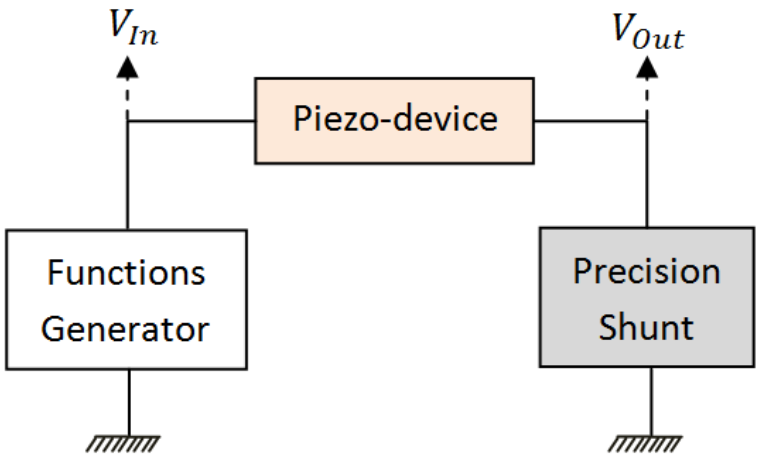

Figure B.2: Electrical circuit for resonant frequencies measurements

tions generator, it is strongly advised to set the generator and check the settings on the scope.

So:

- Set the generator to sinusoidal signal.
- Choose an amplitude ($3V$ enough).
- Set frequency sweeping mode (from some Hz to some tens KHz).
- Connect the generator output channel to the scope and check that you obtain the expected signal before you pass to the following step.
- If the scope confirms you the correct signal profile, then connect the generator output channel to the positive electrode of the piezo-device. Connect the piezo negative electrode to one of the shunt terminal. Connect the last terminal of the shunt to the circuit zero node.Then you obtain two channels V_{In} and V_{Out} as illustrated in figure B.2.

- Connect V_{In} and V_{Out} to the signals acquisition system.
- Perform some series of measurements (3 series for example) and store the measurements in files for subsequent processing. Do not forget to store the frequencies.

B.2.3 Data processing

The piezo-bar impedance is given by:

$$Z_{El} = \frac{(V_{In} - V_{Out}) * R_{Shunt}}{V_{Out}} \tag{B.1}$$

- Depict the impedance graph
- Read the first resonance f_{r1}, the first anti-resonance f_a, the second resonance f_{r2}
- Read the impedance Z_r at first resonance
- Measure the capacitance C_e^0 at $2f_a$
- Measure the electrical losses angle δ at $50Hz$
- Measure the device mass M and deduct its density ρ
- Calculate:

$$\begin{aligned}
k^2 &= \frac{\pi}{2}.\frac{f_{r1}}{f_a}.\cot\left(\frac{\pi}{2}.\frac{f_{r1}}{f_a}\right) \\
\varepsilon_{33}^T &= \frac{C_e^0.L}{(1-k^2).\sigma} \\
s_{33}^E &= \frac{1}{\rho(1-k^2)\left(2f_a^0.L\right)^2} \\
d_{33} &= \sqrt{k^2.s_{33}^E.\varepsilon_{33}^T} \\
Q_m &= \frac{1}{2\pi\left(f_{r1}\right)Z_r C_e^0}\left(\frac{\left(f_a\right)^2}{\left(f_a\right)^2-\left(f_{r1}\right)^2}\right) \\
\eta &= tan(\delta) \\
C_e &= \frac{\varepsilon_{33}^T.\sigma}{L} \\
K_m^E &= \frac{\sigma}{s_{33}^E.L}
\end{aligned}$$

where σ stands for the device section area and L for its length.

Appendix C

Instrumentation and Measuring

C.1 Equipment

1 accelerometer, ref DYTRAN 3225F1

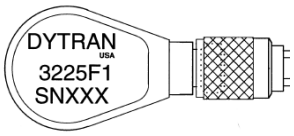

Sensitivity: 10 mV/G
Range F.S. for ±5 volts out: ±500g
Frequency response, ±10%: 1.6 to 10,000 Hz
Resonant frequency: 40 kHz
Linearity: 2% F.S max

1 laser displacement sensor, ref LK-G82

Resolution: $0.2\mu m$
Measuring range: $80 \pm 15mm$
Mounting mode: diffused reflection
Linearity: ±0.05% of F.S (F.S = $\pm 15mm$)
Sampling period: $20/50/100/200/500/1000\mu s$
Sensitivity: multiple

1 Function Generator, ref PM 5132

Waveforms: Sine, Square, Pulse, Triangle
Frequency: 0.1 Hz - 2.0 MHz
Frequency accuracy: 2%
Output voltage: $0 - 30V$
Output Impedance: 50 Ohm
Sweep Modes: continuous, Linear, Single

1 Current transducer, ref LA 25-NP/SP11

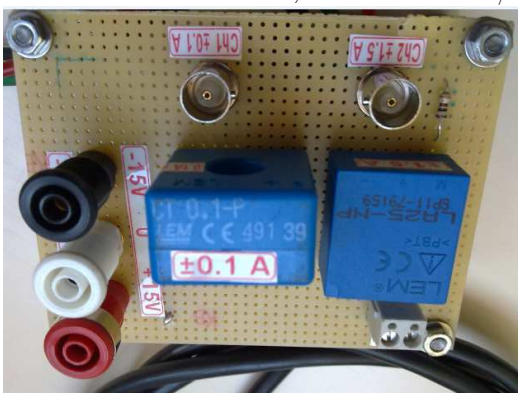

Measuring range: $\pm 1.5A$
Accuracy: $\pm 0.5\%$ at $1A$
Linearity: 0.2%
Current offset: $\pm 0.15mA$
Response time: $1\mu s$
Frequency bandwidth ($-1db$): DC to 150 kHz

NI CDAQ-9172 support, Input: NI-9215 and NI-9233, Output: NI-9263

Analog channels: 4 for each card
Simultaneous sampling
Output resolution: 16-bit
Input resolution: 24-bit
Sampling rate: 50-120 kHz

C.2 Pre-loading system

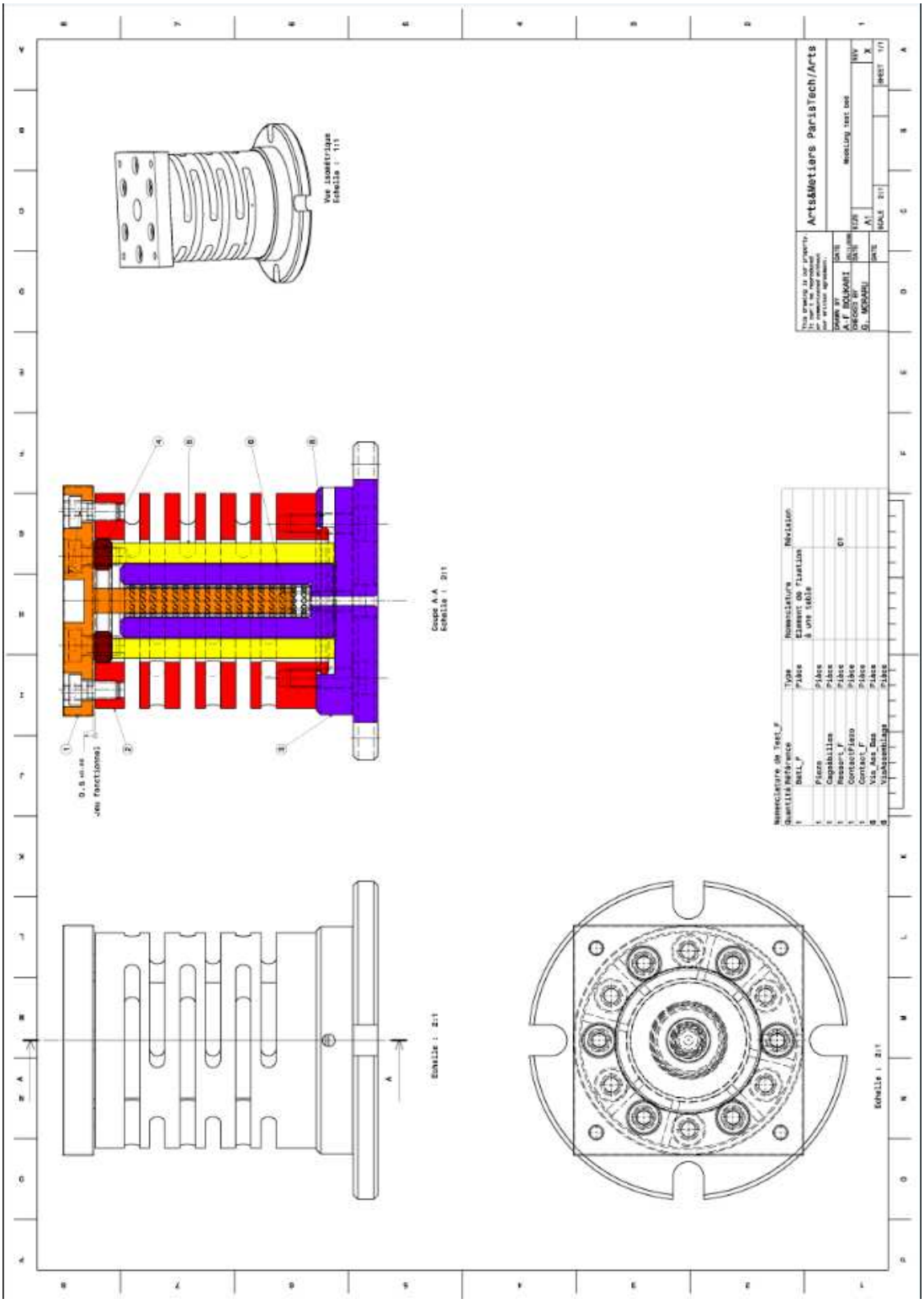

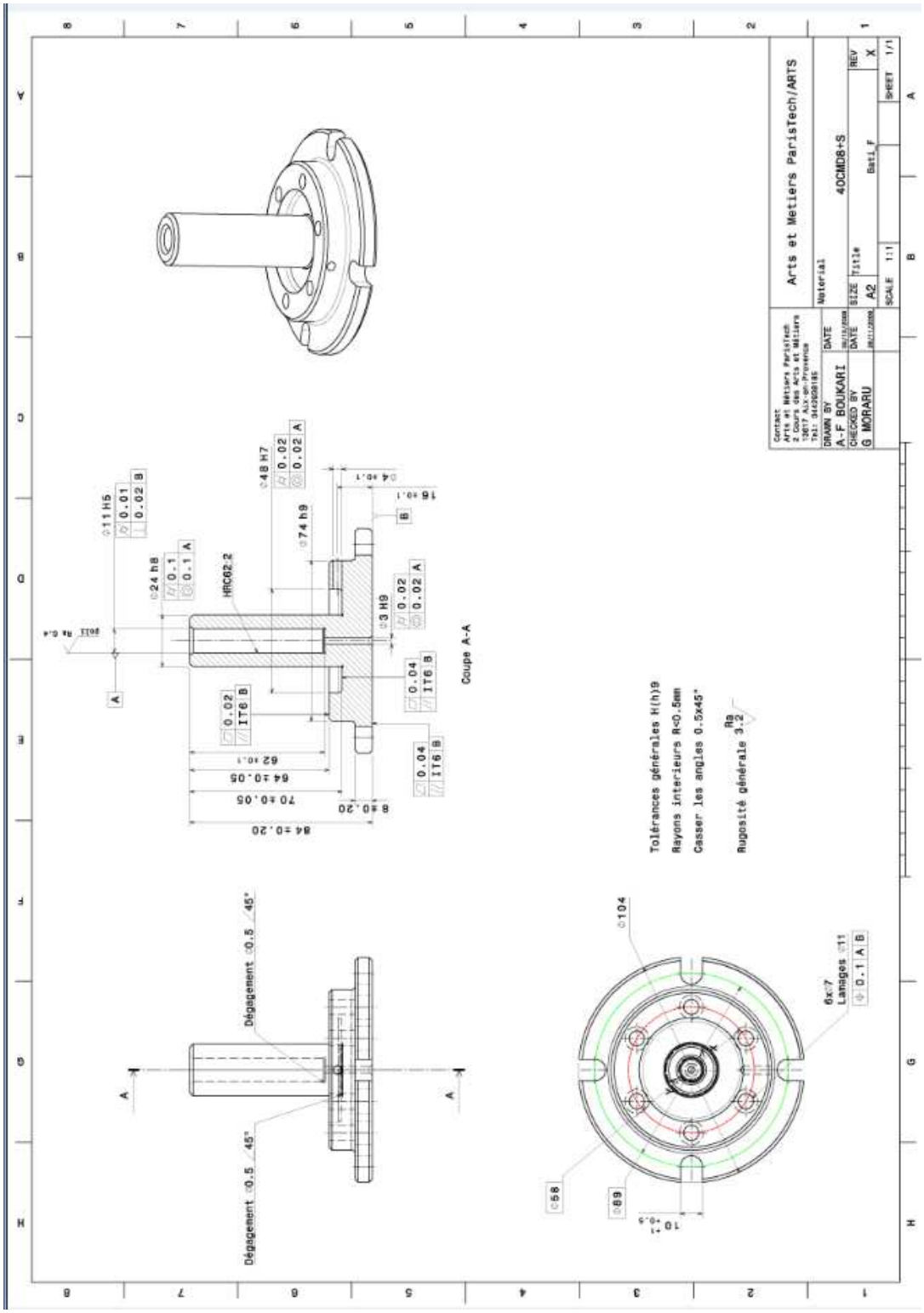
Arts et Metiers ParisTech/ARTS
40CMD8+S
Coupe A-A
Tolérances générales H(h)9
Rayons intérieurs R<0.5mm
Casser les angles 0.5x45°
Rugosité générale Ra 3.2
Dégagement 0.5 45°
Dégagement 0.5 45°
6x⌀7
Lamages ⌀11
⌀104
⌀58
⌀89
⌀48 H7
⌀74 h9
⌀24 h8
⌀11 H5
⌀3 H9
HRC62.2
84 ±0.20
70 ±0.05
64 ±0.05
62 ±0.1
8 ±0.20
16 ±0.1
4 ±0.1
10 +0.1 +0.5

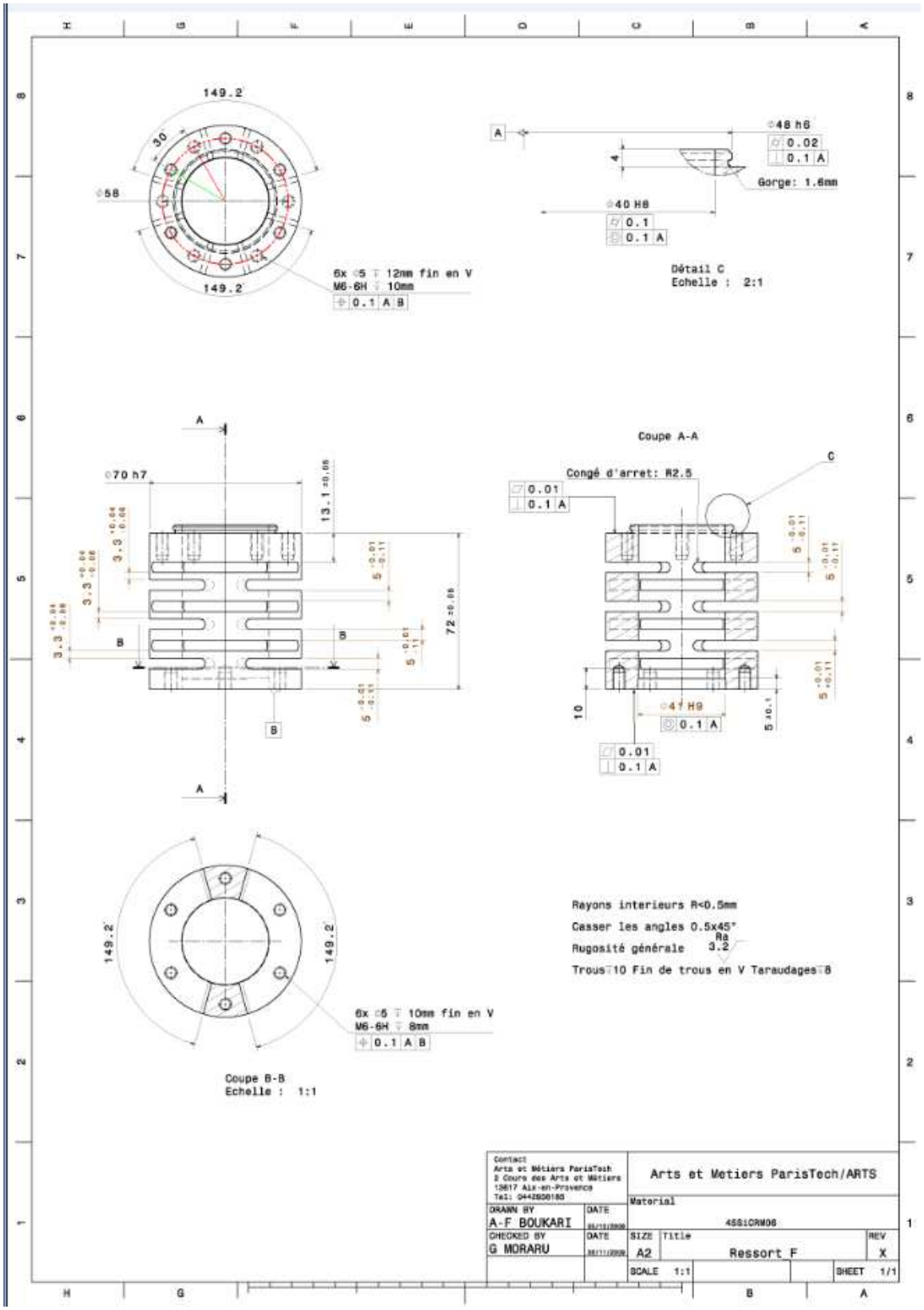
149.2
30
58
149.2
6x ⌀5 ↧ 12mm fin en V
M6-6H ↧ 10mm
0.1 A B
A
⌀48 h6
0.02
0.1 A
4
Gorge: 1.6mm
⌀40 H8
0.1
0.1 A
Détail C
Echelle : 2:1
Coupe A-A
Congé d'arret: R2.5
0.01
0.1 A
C
⌀70 h7
13.1 ±0.05
72 ±0.05
5 +0.01 -0.11
3.3 +0.04 -0.06
B
⌀47 H9
0.1 A
10
5 ±0.1
0.01
0.1 A
Rayons interieurs R<0.5mm
Casser les angles 0.5x45°
Rugosité générale Ra 3.2
Trous⌀10 Fin de trous en V Taraudages⌀8
6x ⌀5 ↧ 10mm fin en V
M6-6H ↧ 8mm
0.1 A B
Coupe B-B
Echelle : 1:1
Contact
Arts et Métiers ParisTech
2 Cours des Arts et Métiers
13617 Aix-en-Provence
Tel: 0442609160
Arts et Metiers ParisTech/ARTS
DRAWN BY
A-F BOUKARI
DATE
CHECKED BY
G MORARU
DATE
Material
45SiCrMo6
SIZE
A2
Title
Ressort F
REV
X
SCALE 1:1
SHEET 1/1

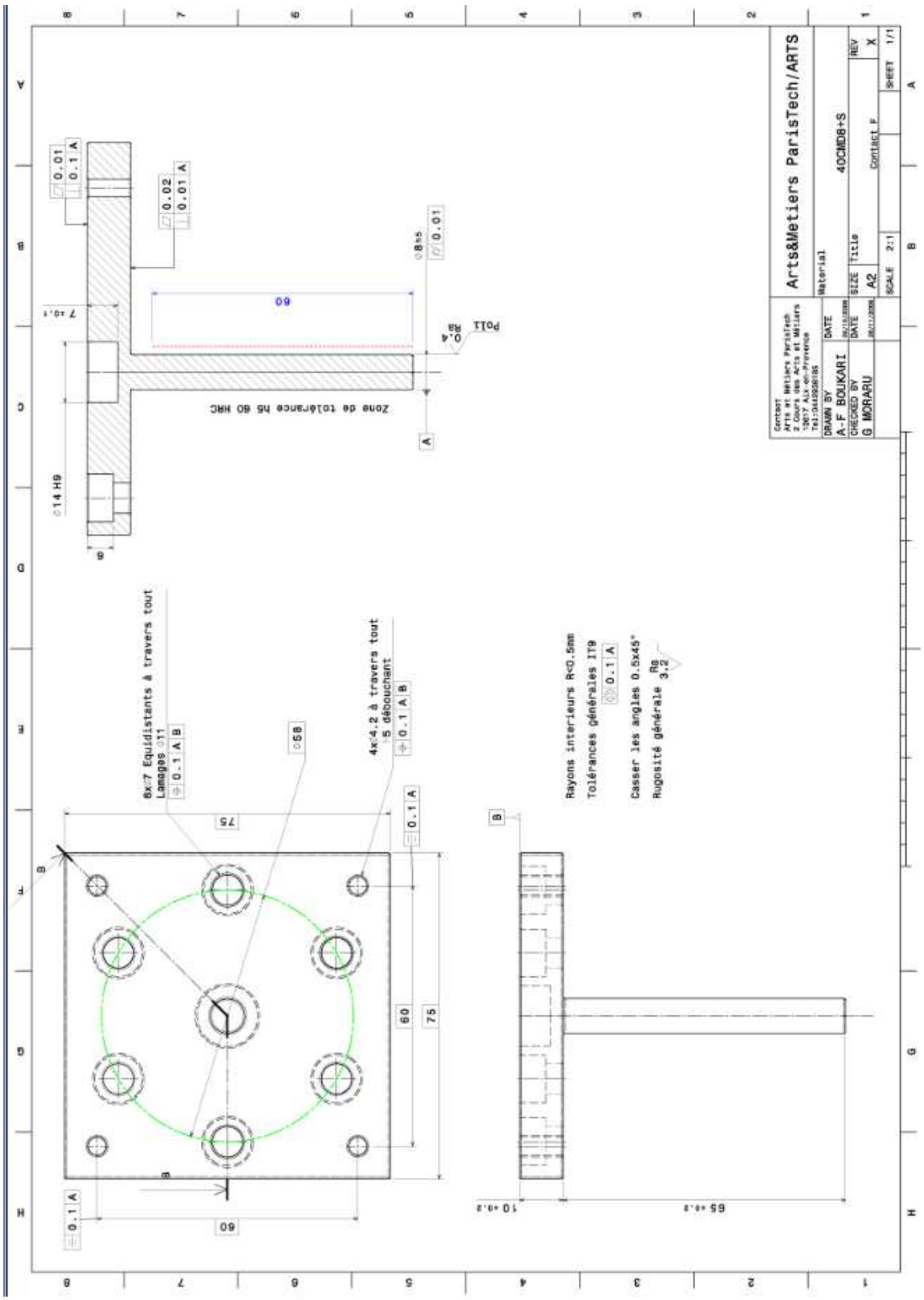
Arts&Metiers ParisTech/ARTS
40CMD8+S
Material
Contact_F
SIZE A2
SCALE 2:1
REV X
SHEET 1/1
DRAWN BY A-F BOUKARI
CHECKED BY G MORARU
Zone de tolérance h5 60 HRC
6x⌀7 Equidistants à travers tout
Lamages ⌀11
4x⌀4.2 à travers tout
⌀5 débouchant
Rayons intérieurs R<0.5mm
Tolérances générales IT9
Casser les angles 0.5x45°
Rugosité générale Ra 3.2
⌀14 H9
⌀58
75
60
65 +0.2
10 +0.2

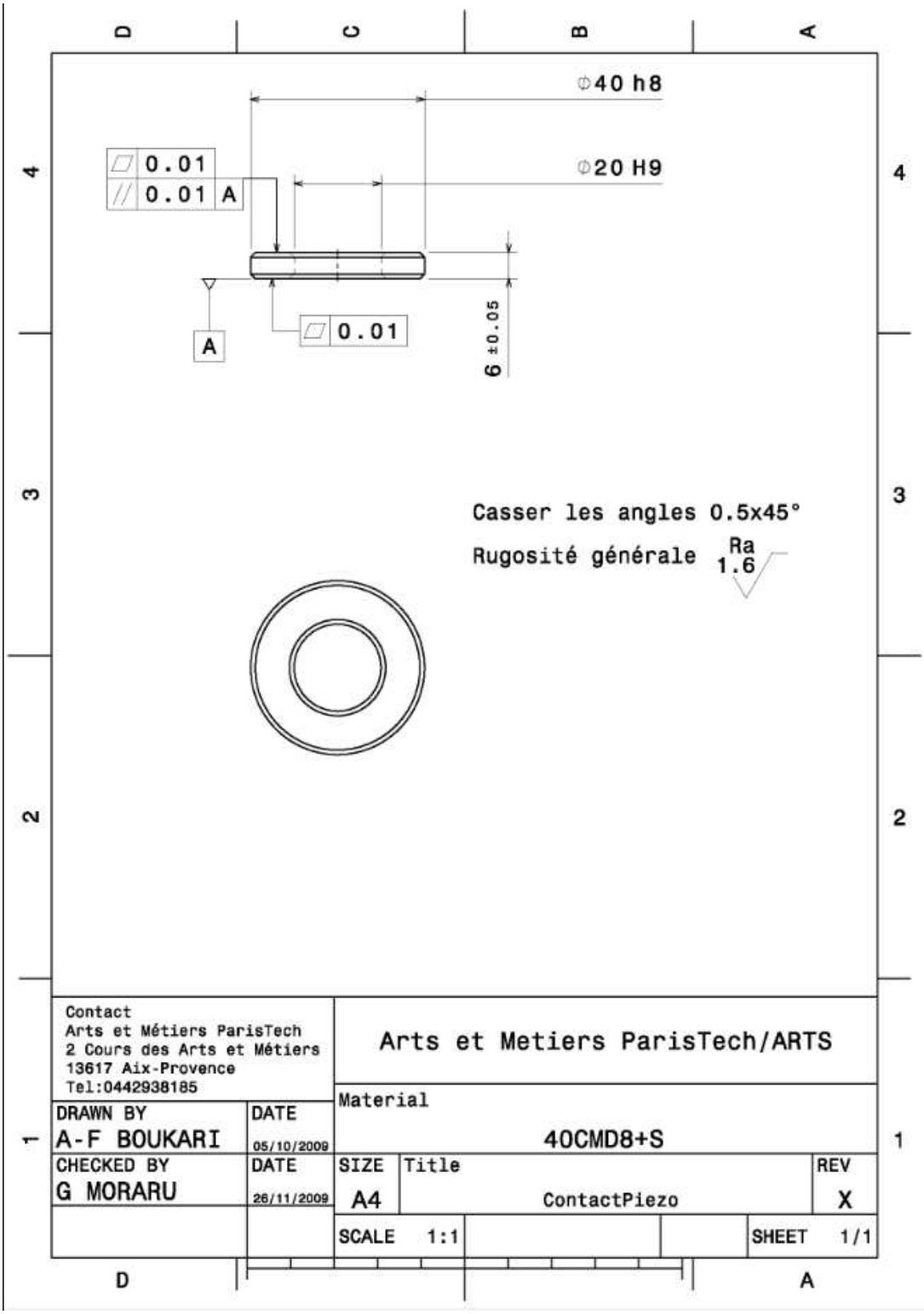
Φ40 h8
Φ20 H9
0.01
0.01 A
A
0.01
6 ±0.05
Casser les angles 0.5x45°
Rugosité générale Ra 1.6
Contact
Arts et Métiers ParisTech
2 Cours des Arts et Métiers
13617 Aix-Provence
Tel:0442938185
Arts et Metiers ParisTech/ARTS
DRAWN BY
A-F BOUKARI
DATE
05/10/2009
Material
40CMD8+S
CHECKED BY
G MORARU
DATE
26/11/2009
SIZE
A4
Title
ContactPiezo
REV
X
SCALE 1:1
SHEET 1/1

Vue de face
Echelle : 1:1

A fabriquer sur clinquant

10 pièces d'épaisseur 50µm
05 pièces d'épaisseur 100µm

Bibliography

[1] http://www.sterlinggundrills.com/index.shtml.

[2] http://www.goldengoose.tw/front/bin/ptdetail.phtml?Part=RGC.

[3] George Moraru. *Etude du comportement du système Pièce-Outil-Machine en régime de coupe vibratoire*. Mechanics, Arts et Metiers ParisTech CER Aix-en-Provence and Université Politehnica de Bucarest, 2002.

[4] A-F. Boukari, G. Moraru, J C. Carmona, and F. Malburet. Useur-oriented simulation models of piezo-bar actuators part i and part ii. In *Proceedings of IDETC/CIE 2009, ASME 2009 International Design Engineering Technical Conferences & International Conference on Mechatronic and Embedded Systems and Applications*, San Diego (USA) 2009.

[5] *LMS Imagine Software, http://www.lmsintl.com/imagine-amesim-suite.*

[6] *Controllab Products B.V 2008, Version number 4.0.1.5, P.O. Box 217, 7522 NB, Enschede, The Netherlands, http://www.20sim.com/.*

[7] Eric M. Flint, Jorg Melcher, and Holger Hanselka. The promise of smart materials for small satellites. *Acta Astronautic*, 39:809–814, 1996.

[8] Georges Akhras. Smart materials and smart systems for the future. *Canadian Military Journal*, pages 25–32, 2000.

[9] S. Mondal. Phase change materials for smart textiles Ű an overview. *Applied Thermal Engineering*, 28:1536–1550, 2007.

[10] W.R. Cook B. Jaffe and H. Jaffe. Piezoelectric ceramics. *Academic Press London*, 1971.

[11] *Shape Memory Alloys.*

[12] Dag Lukkassen and Annette Meidell. *Advanced Materials and Structures and their Fabrication Process*. Narvik University College, HiN, 2007.

[13] Sparkler Ceramics PVT. LTD, J-508, MIDC, BHOSARI, PUNE - 411 026 India. *Measuring Properties of Piezoelectric Ceramics.*

[14] A. Preumont, B. de Marneffe, A. Deraemaeker, and F. Bossens. The damping of a truss structure with a piezoelectric transducer. *Computers and Structures*, 86:227–239, 2008.

[15] *ETREMA Products Inc, <http://www.etrema-usa.com>.*

[16] A.B. Flatau and K.P. Chong. Dynamic smart material and structural systems. *Engineering Structures*, 24:261–270, 2002.

[17] National Science Foundation. *Civil infrastrucutre systems research: strategic issues.* NSF 93-5. Arlington (VA): NSF, 1993.

[18] Sanjivg Tewani, Keith E. Rouch, and Bruce L. Walcott. A study of cutting process stability of a boring bar with active dynamic absorber. *Int. I. Mach. Tools Manufact*, 35-1:91–108, 1995.

[19] Christer Richt. Minimizing vibration tendencies in machining. *Metalworking World,Sandvik Coromant, Sandviken, Sweden.*

[20] Abdelmjid Benayad, Diouma Kobor, Laurent Lebrun, Benoit Guiffard, and Daniel Guyomar. Characteristics of $pb[(zn_{1/3}nb_{2/3})_{0.955}ti_{0.045}]o_3$ single crystals versus growth method. *Journal of Crystal Growth*, 270:137Ũ144, 2004.

[21] Shujun Zhang, Ru Xia, Laurent Lebrun, Dean Anderson, and Thomas R. Shrout. Piezoelectric materials for high power, high temperature applications. *Materials Letters*, 59:3471 Ũ 3475, 2005.

[22] Marc Kamlah and Charalampos Tsakmakis. Phenomenological modeling of the non!linear electromechanical coupling in ferroelectrics. *International Journal of Solids and Structures*, 36:558–584, 1999.

[23] Marisol Delgado and Cesar Pichardo. Use of matlab and 20-sim to simulate a flash separator. *Simulation Practice and Theory*, 7:515–530, 1999.

[24] Sefer Avdiaj, Janez Setina, and Naim Syla. Modeling of the piezoelectric effect using the finite element method (fem). *Materials and technology*, 43:283–291, 2009.

[25] Sylvain Ballandras, Mikael Wilm, Paul-Francis Edoa, Abdelaziz Soufyane, Vincent Laude, William Steichen, and Raphael Lardat. Finite-element analysis of periodic piezoelectric transducers. *Journal of Applied Physics*, 93:702–711, 2003.

[26] P. Lloyd and M. Redwood. *J. Acoust. Soc. Am.*, 39, 1966.

[27] R. Holland. *IEEE Trans. Sonics Ultrason.*, 97, 1968.

[28] H. F. Tiersten. *Proc. IEEE*, 55, 1967.

[29] E. P. Eernisse. *IEEE Trans. Sonics Ultrason.*, 14, 1967.

[30] H. Allik and T. J. R. Hugues. *Int. J. Numer. Methods Eng.*, 2, 1970.

[31] http://www.ansys.com/default.asp.

[32] Marc Kamlah, Ulrich Bohle, and Dietrich Munz. On a non-linear finite element method for piezoelectric structures made of hysteretic ferroelectric ceramics. *Computational Materials Science*, 19:81–86, 2000.

[33] V. Streeter. *Handbook of Fluid Dynamics*. McGraw-Hill, 1961.

[34] J. Wolf and A. Paronesso. Lumped-parameter model and recursive evaluation of interaction forces of semi-infinite uniform fluid channel for time-domain dam-reservoir analysis. *Earthquake Engineering and Structural Dynamics*, 21:811–831, 1992.

[35] Z. Wang and S. Tan. Coupled analysis of fluid transients and structural dynamic responses of a pipeline system. *Journal of Hydraulic Research*, 35-1:119–132, 1997.

[36] Leo Donald. Energy analysis of piezoelectric-actuated structure driven by linear amplifier. *Journal of Intelligent Material Systems and Structure*, 10:36–45, 1999.

[37] Donald Leo and Khalil Nasser. Eficiency of frequency-rectifieed piezohydraulic and piezopneumatic actuation. In *Proceedings of the ASME Adaptive Structures and Materials Symposium*, volume 60, pages 485–497, 2000.

[38] L. Mauck and C. Lynch. Piezoelectric hydraulic pump. *SPIE Proceedings*, 3668, 1999.

[39] Gianluca Piazza and Albert P. Pisano. Two-port stacked piezoelectric aluminum nitirde contour-mode resonant mems. *Sensors and Actuators A*, 136:638–645, 2007.

[40] Gianluca Piazza, Philip J. Stephanou, and Albert P. Pisano. One and two port piezoelectric higher order contour-mode mems resonators for mechanical signal processing. *Solid-State Electronics*, 51:1596–1608, 2007.

[41] Hoonbum Shin, Hyungkeun Ahn, and Deuk-Young Han. Modeling and analysis of multilayer piezoelectric transformer. *Materials Chemistry and Physics*, 92:616–620, 2005.

[42] Khalil M. Nasser. Development and analysis of the lumped parameter model of a piezohydraulic actuator. Master's thesis, Virginia Polytechnic Institute and State University, 2000.

[43] IEEE Standards Association. *ANSI IEEE Standard on Piezoelectricity*, number Std 176-1987, 345 East 47th St, New York, NY 10017, 1987.

[44] A-F. Boukari, G. Moraru, J C. Carmona, and F. Malburet. Pont entre le domaine des experts des matériaux et celui de l'ingénieur en vue de l'utilisation généralisée des actionneurs piézoélectriques. In *Proceedings of CONFERE*, Marrakech (Morocco) 2009.

[45] C. Boller. Composites for sensors and actuators. In *Encyclopedia of Materials: Science and Technology*, pages 1376–82. Elsevier Science Ltd, 2001.

[46] M.V. Gandhi and B.S. Thomsom. Smart materials and structures. *Chapman and Hall*, 1992.

[47] Z.L. Wang and Z.C. Kang. *Functional and smart materials- Structural evolution and structure analysis*.

[48] Guy Grellet and Guy Clerc. *Actionneurs électriques - Principes / Modèles / Commande*. Eyrolles.

[49] T. Takagi, P.F. Gobin, and J. Tatibouet. Proceedings of the third international conference on intelligent materials and third european conference on smart structures and materials. volume 2779, pages 2–15, 1996.

[50] V. Michaud. Can shape memory alloy composites be smart? *Scripta Materiala*, 50:249–253, 2004.

[51] C.A. Rogers and V. Giurgiutiu. pages 13–34. Springer, 1999.

[52] B. Culshaw. pages 401–418. Springer, 1999.

[53] Vinod K. Wadhawan, Pragya Pandit, and Surya M. Gupta. PmnŰpt based relaxor ferroelectrics as very smart materials. *Materials Science and Engineering B*, 120:199–205, 2005.

[54] S. Hurlebaus and L. Gaul. Smart structure dynamics. *Mechanical Systems and Signal Processing*, 20:255–281, 2006.

[55] The British (U.K.) Office of Science and Technology Foresight.

[56] The Institute of Materials and Mining.

[57] Y.W. Yang, S. Bhalla, C. Wang, C.K. Soh, and J. Zhao. Monitoring of rocks using smart sensors. *Tunnelling and Underground Space Technology*, 22:206–221, 2007.

[58] Ying, Y.L. Kwok, Y. Li, Q.Y. Zhu, and C.Y. Yeung. Assessing the performance of textiles incorporating phase change materials. *Polymer Testing*, 23:541–549, 2004.

[59] Michel Brissaud. *Matériaux piézoélectriques: Caracterisation, modelisation et vibration*. Presses Polytechniques et universitaires romandes, 2007.

[60] Frederik Giraud. *Modélisation Causal et Commande d'un Actionneur piézoélectrique à Onde Progressive*. Electrics, Université de Lille I, 2002.

[61] Jean-Marie Hausonne, James L. Barton, Paul Bowen, and Claude Paul Carry. *Céramiques Et Verres : Principes Et Techniques D'élaboration*, volume 16. Presses Polytechniques et Universités Romandes, 2005.

[62] www.physikinstrumente.com. *Physiks Instrument Inc.*

[63] A.G. Olabi and A. Grunwald. Design and application of magnetostrictive materials. *Materials and Design*, 2007.

[64] Carl M. Lampert. Chromogenic smart materials. *Materials Today*.

[65] A-F. Boukari. Contribution à la modélisation d'une démarche mécatronique chez schlumberger, clamart. Master's thesis, Arts et Metiers ParisTech, CER Aix-en-Provence, 2007.

[66] F. Claeyssen, N. Lhermet, and T. Maillard. Magnetostrictive actuators compared to piezoelectric actuators. *Cedrat Technologies S.A. Ű 10 chemin de Pré Carré -ZIRST - 38240 Meylan -France: www.cedrat.com*, 2002.

[67] W. P. MASON and H. JAFFE. Methods for measuring piezoelectric, elastic, and dielectric coefficients of crystals and ceramics. In *Proceeding of the IRE*, number 42, pages 921–930, 1954.

[68] K. W. KWOK, H. L. CHAN, and C. L. CHOY. Evaluation of the material parameters of piezoelectric materials by various methods. *IEEE Trans. On Ultrasonics, Ferroelectrics and Frequency Control*, 44(4):733–742, 1997.

[69] Institue of Electrical and Electronic Engineers. *IEEE Standard Definitions and Methods of Measurement for Piezoelectric Vibrators (IEEE St 177-1966)*, number Std 177-1966, 345 East 47th St, New York, NY 10017, 1966.

[70] T.L. Jordan and Z. Ounaies. Piezoelectric ceramics characterization. Technical Report ICASE Report No.2001-28, ICASE NASA Langley Research Center, Hampton, Virginia 23681-2199, September 2001.

[71] www.piezomechanik.com. *Piezomechanik GmbH Inc.*

[72] Laurent Lebrun. *Etude de moteurs piézoélectriques ultrasonores.* Ferroelectrics, INSA de Lyon, Villeurbanne, FRANCE, 1995.

[73] J. Lemaitre and J.L. Chaboche. *Mécanique des matériaux solides*, volume 2. 2001.

[74] Nathalie Aurelle. *Non linéarités dans les céramiques piézoélectriques: Application aux transducteurs acoustiques de puissance.* PhD thesis, Institut National des Sciences Appliquées de Lyon, 1996.

[75] *National Instruments product: Labview 2009, http://www.ni.com/labview.*

[76] Dominique Scaravetti. *Formalisation préalable d'un problème de conception pour l'aide à la décision en conception préliminaire.* PhD thesis, Arts et Metiers ParisTech, CER Bordeaux, 2004.

[77] A. Buchacz and A. Wrobel. Piezoelectric layer modelling by equivalent circuite and graph method. *Journal of Achievement in Materials and Manufacturing Engineering*, 20 Issues 1-2, 2007.

[78] H.M. Saoull and R. Ben Mrad. Modeling piezoceramic actuators for smart applications. In *IFAC Mechatronic Systems*, volume 2, 2002.

[79] S. Behrens, S.O.R. Moheimani, and A.J. Fleming. Multiple mode passive piezoelectric shunt dampener. In *IFAC Mechatronic Systems*, volume 2, 2002.

[80] Mason. 1948.

[81] Guo-Qing Li, Chen Chuan-Yao, and Hu Yuan-Tai. Equivalent electric circuits of thin plates with two-dimensional piezoelectric actuators. *Journal of Sound and Vibration*, 286:145–165, 2005.

[82] J.D. Achenbach. *Wave propagation in elastic solids*, volume 12. 1975.

[83] Emmanuel de Langre et Antoine Chaigne. *Dynamique et vibrations.* 2008.

[84] Lee Davison. *Fundamentals of Shock Wave Propagation in Solids*. Springer, 2008.

[85] G.W. Taylor, J.J. Gagnepain, T.R. Meeker, T. Nakamura, and L.A. Shuvalov. *Piezoelectricity: Ferroelectricity and related phenomena*, volume 4. Gordon and Breach Science Publishers, 2008.

[86] Roger Temam and Alain Miranville. *Modélisation mathématique et mécanique des milieux continus*, volume 18. Springer, 2002.

[87] Eugene Hecht, Tamer Becherrawy, and Joel Martin. *Physique générale*. 1948.

[88] Antonio Arnau. *Piezoelectric transducers and applications*, volume 2. Springer, 2008.

[89] J. Honcu and al. Piezo-elements and damping of mechanical vibrations. *Buletinul Institului Politehnic*, Fasc.5A:76–82, 1999.

[90] A-F. Boukari, G. Moraru, J C. Carmona, and F. Malburet. Discussion des hypotheses de modélisation d'un actionneur piézoélectrique. In *Majestics*, Marseille (France) 2008.

[91] 20-Sim Inc. *http://www.20sim.com/webhelp/editor/compiling/algebraicloops.htm*.

[92] R. Paparella A. Bosotti and F. Puricelli. Pi piezolifetime test report. *INFN Milan Internal Report*.

[93] Uri M. Ascher and Linda Ruth Petzold. *Computer methods for ordinary differential equations and differential-algebraic equations*, volume 61. 1998.

[94] Mark Zachary Jacobson. *Fundamentals of atmospheric modeling*. Cambridge Univerity Press, 1998.

[95] Olivier GUILLON. *Caractérisation électromécanique et modélisation des céramiques ferroélectriques de type PZT*. Ph.d thesis, Université de Franche-Comté, 2003.

[96] H. Richter, E.A. Misawa, D.A. Lucca, and H. Lu. Modeling nonlinear behavior in a piezoelectric actuator. *Precision engineering*, 25:128–137, 2001.

[97] S. Joshi. Non-linear constitutive relations for piezoceramics materials. *Smart Materials and Structures*, 1:80–83, 1992.

[98] A. Tsoularis and J. Wallace. Analysis of logistic growth models. *Mathematical Biosciences*, 179:21–55, 2002.

[99] Richards FJ. A flexible growth function for empirical use. *Journal of Experimental botany*, 10:1980–1990, 1959.

[100] Colin P.D. Birch. A new generalized logistic sigmoid growth equation compared with the richards growth equation. *Annals of Botany*, 83:713–723, 1999.

[101] F. Preisach. Uber die mognetidche nachwirkung. *Z. Phys*, 94:277–302, 1935.

[102] Ralph C. Smith. *Smart material systems: model development*, volume 32. SIAM, 2005.

[103] Giorgio Bertoti and I.D. Mayergoyz. *The science of hysteresis: Mathematical modeling and applications*. Elsevier, 2006.

[104] Zs. Szabo, I. Tugyi, Gy. Kadar, and J. Fuzi. Identification procedures for scallar preisach model. *Physica B*, 343:142–147, 2004.

[105] I.D. Mayergozy. Dynamic preisach models of hysteresi. *IEEE Transactions on Magnetics*, 6:2925–2927, 1988.

[106] I.D. Mayergozy. Mathematical modelling of hysteresis. *Springer*, page 1991, 1991.

[107] G. Bertotti. Dynamic generalization of the scalar preisach model of hysteresis. *IEEE Transactions on Magnetics*, 28:2599–2601, 1992.

[108] Yunhe Yu, Zenngchu Xiao, Nagi G. Naganathan, and Rao V. Dukkipati. Dynamic preisach modelling of hysteresis for the piezoceramic actuator system. *Mechanism and machine theory*, 37:75–89, 2002.

[109] Vijay K. Varadan, K.J. Vinoy, and S. Gopalakrishnan. *Smart Material Systems and MEMS: Design and development Methodologies*. John Wiley and Sons Ltd, 2006.

[110] A. M. Gonzalez, J. De Frutos, and C. Duro. Changes in the piezoelectric parameters of pzt ceramics durng the poling process. *Ferroelectrics*, 208-209:449–457, 1988.

[111] S. Lengagne, N. Ramdani, and P. Fraisse. Methode pour la planification de trajectoires garanties. *Journees Francophones de Planification, Decision et apprentissage pour la conduite de systemes*, Octobre 2008.

[112] John A. Nelder and R. Mead. A simplex method for function minimization. *Ferroelectrics*, 7:308Ũ313, 1965.

[113] Marco A. Luersen and Rodolphe Le Rich. Globalized nelder-mead method for engineering optimization. *Computers and Structures*, 82:2251–2260, 2004.

[114] Qiang Xiong and Arthur Jutan. Continuous optimization using a dynamic simplex method. *Chemical Engineering Science*, 58:3817–3828, 2003.

[115] F.H. Walters, L.R.Jr. Parker, S.L. Morgan, and S.N. Deming. Sequential simplex optimization. *Boca Raton FL: CRC Press*, 58:3817–3828, 1991.

[116] *Wolfram Mathematica software, Version number 7.0.0, Platform: Microsoft Windows.*

[117] DA. Ratkowsky. Nonlinear regression modeling. *New York: Marcel Dekker Inc*, 1993.

[118] Yunhe Yu, Nagi Naganathan, and Rao Dukkipati. Preisach modeling of hysteresis for piezoceramic actuator system. *Mechanism and Machnie Theory*, 37:49–59, 2002.

[119] M. Goldfard and N. Celanovic. Modeling piezoelectric stack actuators for control of micromanipulation. *IEEE Con Syst Mag*, 17:69–79, 1997.

[120] L.E. Goodman. *HARRIS' Shock and vibration handbook - Chapter 36 :Material damping and slip damping.*

[121] J. Marin. *Mechanical behavior of engineering materials*. Prentice-Hall, 1962.

[122] J. Takacs. *Mathematics of hysteresis phenomena: the T(x) model for the description of hysteresis*. Wiley-VCH, 2003.

[123] B. Azzerboni, E. Cardelli, and G. Finocchio. A comparative study of preisach scalar hysteresis models. *Physica B*, 343:164–170, 2004.

[124] *Matlab Simulink software*.

[125] Vincent Walter. *Caractérisation et modélisation électromécanique de dépôts de couches épaisses PZT sérigraphiées sur substrat d'alumine : Application au contrôle de forme et l'amortissement actif d'un bimorphe*. Ph.d thesis, Université de Franche-Comté, 2001.

[126] M. KAMLAH and C. TSAKMAKIS. Phenomenological modeling of non-linear electromechanical coupling in ferroelectrics. *International Journal of Solids and Structures*, 36:669–695, 1999.

[127] T.-J. YEH, Shin-Wen Lu, and Ting-Ying Wu. Modeling and identification of hysteresis in piezoelectric actuators. *ASME J. Dyn. Syst. Measure. Control*, 128:189–196, 2006.

[128] T.-J. YEH, Ruo-Feng Hung, and Shin-Wen Lu. An integrate physical model that characterizes creep and hysteresis in piezoelectric actuators. *Simulation Modeling Practice and Theory*, 16:93–110, 2008.

[129] Riccardo Marino. Adaptive control of nonlinear systems: Basic results and applications. *Annual Reviews in Control*, 21:55–66, 1997.

[130] D. W. Clarke. Adaptive predictive control. *Annual Reviews in Control*, 20:83–94, 1996.

[131] B. H. Krogh. State feedback control of condition/event systems. *Mathl. Comput Modelling*, 23:161–173, 1996.

[132] G. Grelet and G. Clerc. *Actionneurs électriques, principes, modèles, commandes*. 1997.

[133] Katsuhisa Furuta. Sliding mode control of a discrete system. *Systems and Control Letters*, 14:145–152, 1989.

[134] F. Gouaisbaut, M. Dambrine, and J. P. Richard. Robust control of delay systems: a sliding mode control design via lmi. *Systems and Control Letters*, 23:219–230, 2002.

[135] S. Gentil and E. Zamai. Principes des chaines de régulation. In *Techniques de l'ingénieur, traité Automatique*, volume S7090, pages 1–22. Paris, 2003.

[136] Jing Zhou, Changyun Wen, and Wei Wang. Adaptive backstepping control of uncertain systems with unknown input time-delay. *Automatica*, 45:1415–1422, 2009.

[137] Pierre-Jean Barre, Alain Bouscayrol, Philippe Delarue, Eric Dumetz, Freqeric Giraud, Jean-Paul Hautie, Xavier Kestelyn Betty Lemaire-Semail, and Eric Semail. Commande par inversion pour entrainements electromecaniques, principes et applications.

[138] Oliver M. Fein. A model for piezo-resistive damping of two-dimensional structures. *Journal of Sound and Vibration*, 310:865–880, 2008.

[139] A. Preumont. Mechatronics: dynamics of electromechanical and piezoelectric systems. *Springer*, 2006.

[140] Behrens S., Fleming A.J., and Moheimani S.O.R. A broadband controller for shunt piezoelectric damping of structural vibration. *Smart Materials and Structures*, 12:18–28, 2003.

[141] L.A.L. Almeida, G.S. Deep, A.M.N. Lima, and H. Neff. Modeling a magnetostrictive transducer using genetic algorithm. *Journal of Magnetism and Magnetic Materials*, 266:1262–1264, 2001.

[142] A. Cavallob, D. Davinoa, G. De Mariab, S. Pirozzib C. Nataleb, and C. Visone. Hysteresis compensation of smart actuators under variable stress conditions. *Physica B*, 403:261–165, 2008.

[143] D. Davinoa, C. Nataleb, S. Pirozzib, and C. Visone. Phenomenological dynamic model of a magnetostrictive actuator. *Physica B*, 343:112–116, 2004.

[144] Kyoung Kwan Ahn and Nguyen Bao Kha. Modeling and control of shape memory alloy actuators using preisach model, genetic algorithm and fuzzy logic. *Mechatronics*, 18:141–152, 2008.

[145] K. Linnemann, S. Klinkel, and W. Wagner. A constitutive model for magnetostrictive and piezoelectric materials. *International Journal of Solids and Structures*, 2008.

[146] Byung-Hyun Kima Seok-Jun Moona, Chae-Wook Limb and Youngjin Park. Structural vibration control using linear magnetostrictive actuators. *Journal of Sound and Vibration*, 302:875–891, 2007.

[147] Y.W. Parka, Y.T. Seoka, H.J. Parka, and J.Y. Chung. Hysteresis modeling based on saturation operator without constraints. *Journal of Magnetism and Magnetic Materials*, 310:2647–2649, 2007.

[148] Xiaobo Tana and John S. Barasa. Modeling and control of hysteresis in magnetostrictive actuators. *Automatica*, 40:1469–1480, 2004.

[149] R. Smith and J.C. Doyle. Model validation: a connection between robust control and identification. *IEEE Tran. Autom. Control*, AC-37:942–952, 1992.

[150] S. Sen Roy and S. Guria. Estimation of regression parameters in the presence of outliers in the response. *Statistics*, 00:1–9, 2009.

[151] T.K. Gustafsson and P.M. Makila. Modelling of uncertain systems via linear programming. *Automatica*, 32-3:319–335, 1996.

[152] P.J. Huber. *Robust statistics*. 1981.

[153] L. Ljung. *System identification: theory for the user*. 1999.

[154] X.W. Chang and Y. Guo. Huber's m-estimation in gps positionning:computational aspects. In *Proc. Of ION NTM, San Diego, CA*, pages 829–839, 2004.

[155] C. Corbier, J.C. Carmona, and V. Alvarado. $l_1 - l_2$ robust estimation in prediction error system identification. In *CINVESTAV IEEE Congress, Toluca, Mexico*, pages 829–839, 2009.

[156] D.Braess. *Nonlinear Approximation Theory*, volume 7. 1980.

[157] I.D. Landau. *Identification des systemes*. 1998.

[158] 787; June 1979 Forward RL. US patent 4, 158.

[159] Park CH and Baz A. Vibration control of beams with negative capacitive shunting of interdigital electrode piezoceramics. *Journal of Vibration Control*, 11:331–346, 2005.

[160] N. Hagood and A. von Flotow. Damping of structural vibrations with piezoelectric materials and a passive electrical network. *Journal of Sound and Vibration*, 146:1243–268, 1991.

[161] Sung I. Kim, Robert G. Landers, and A. Galip Ulsoy. Robust machining force control with process compensation. *Journal of Manufacturing Science and Engineering*, 125:423–430, 2003.

[162] www.kistler.com. *Kistler Inc.*

[163] Marko Budimir. *Piezoelectric anisotropy and free energy instability in classic perovskites*. Materiaux, Ecole Polytechnique Fédérale de Lausane, 2006.

MODELISATION DES ACTIONNEURS PIEZOELECTRIQUES POUR LE CONTROLE DES SYSTEMES COMPLEXES

RESUME : Les récentes découvertes et avancées technologiques dans la compréhension des matériaux ainsi que l'essor des outils informatiques d'aide au calcul ont contribué à la prolifération de matériaux intelligents avec un champ d'applications très large. Cette thèse s'inscrit dans le contexte d'utilisation des actionneurs piézoélectriques plutôt qu'une vision purement matériau. Le but est d'enrichir les bibliothèques de modèles de ces types d'actionneurs afin de faciliter leur prise en compte dans les phases de conception des systèmes complexes les intégrant. Le cahier des charges est que ces modèles incluent le plus possible les non-linéarités tout en restant aisés d'utilisation. Pour atteindre ces objectifs, nous proposons de faire un pont entre le domaine des experts des matériaux et celui de l'ingénieur en suivant une méthodologie claire. Dans un premier temps nous passons en revue les approches existantes dans la littérature ainsi que les solutions offertes par certains logiciels commerciaux. Une analyse des équations constitutives de la piézoélectricité associées aux conditions de fonctionnement de l'actionneur nous permet d'en déduire un premier modèle analogique. Ce dernier est ensuite traduit en bond graph pour en déduire des modèles blocs-diagramme. En plus de cet effort de formalisation, ces premiers modèles se distinguent de ceux proposés par les logiciels commerciaux en prenant mieux en compte la dynamique propre à l'actionneur. Nous proposons deux types de modèles. L'un rend uniquement compte du premier mode de résonance alors que le second rend compte de deux modes de résonance. Ensuite nous proposons des modèles prenant en compte les non-linéarités : l'approche de Preisach pour la modélisation de l'hystérésis statique et l'approche de Voigt dans le cas dynamique. Ces deux approches sont ensuite fusionnées dans le but d'avoir un model plus complet.

Mots clés : Piézoélectricité, Magnétostriction, Approche des paramètres concentrés, Non-linéarités, Hystérésis, Modèles utilisateur, Systèmes complexes et intelligents.

PIEZOELECTRIC ACTUATORS MODELING FOR COMPLEX SYSTEMS CONTROL

ABSTRACT: The last discoveries and technology advances in understanding materials and in computation have contributed in the proliferation of the so-called smart materials with a wide applications scope. This thesis enrolls in the frame of piezoelectric actuators rather than pure material considerations. We aim to enhance their models' libraries in order to ease their integration in complex systems design. These models should take into account as more as possible the nonlinear effects (such as hysteresis) while remaining easy to handle. For this purpose we make a link between materials specialists and the field of engineers. We firstly analyze the constitutive equations of piezoelectricity with respect to operating conditions. This allows us to deduce a first analog model. This is then translated into bond graph. The obtained models are translated in block-diagrams. The established models in this step differ from those proposed by commercial package in such a way that they better integrate the dynamic nature of the actuator independently of the other parts of the structure. In fact we proposed two types of models. The first one only takes into account the first resonance mode while the second one takes into account two resonances. Thereafter, we suggested models taking into account nonlinearities and hysteresis. The Preisach approach was adopted for static hysteresis. Then we adapted Voigt approach in order to account for dynamic hysteresis. The two approaches were then merged in order to have a complete model.

Keywords : Piezoelectricity, Magnetostriction, Lumped-parameters approach, Nonlinearities, Hysteresis, User oriented models, Complex and smart systems.

ARTS ET MÉTIERS ParisTech

ParisTech
INSTITUT DES SCIENCES ET TECHNOLOGIES
PARIS INSTITUTE OF TECHNOLOGY